SPECTROSCOPIC STUDIES OF PROTEINS AND AZO DYES : PROTEIN SECONDARY STRUCTURE, STRUCTURAL CHANGES IN DYES AND DYE-PROTEIN INTERACTIONS

BISWAJIT PAL
INSTITUTE OF SELF ORGANISING SYSTEMS AND BIOPHYSICS
NORTH-EASTERN HILL UNIVERSITY
SHILLONG - 793 022

THESIS SUBMITTED
FOR THE DEGREE OF

DOCTOR OF PHILOSOPHY

TO

THE NORTH-EASTERN HILL UNIVERSITY
SHILLONG - 793 022
INDIA

JUNE, 1997

DEDICATED
TO
MY PARENTS

पूर्वोत्तर पर्वतीय विश्वविद्यालय
पू० प० विवि० परिसर, शिलांग-७९३०२२ (मेघालय)
Phone :
Grams : NEHU

North-Eastern Hill University

NEHU Campus, Shillong - 793022 (Meghalaya)

Dr. P.K.Bajpai*
Department of Physics,
North-Eastern Hill University,
Shillong - 793 022.

CERTIFICATE

This is to certify that the thesis entitled "SPECTROSCOPIC STUDIES OF PROTEINS AND AZO DYES : PROTEIN SECONDARY STRUCTURE, STRUCTURAL CHANGES IN DYES AND DYE-PROTEIN INTERACTIONS", submitted by Mr. Biswajit Pal in fulfillment of the requirements for the degree of Doctor of Philosophy of North-Eastern Hill University, Shillong embodies the record of original research work carried out by him under my supervision. He has been duly registered and the thesis submitted is worthy of being considered for the award of the Ph.D. degree.

This work has not been submitted for any other degree to any other University or Institution.

P.K.Bajpai
Supervisor

Dr. P. K. BAJPAI
Lecturer of Physics,
North-Eastern Hill University
Shillong-793022

Dated : 9/6/97
Place : BILASPUR

*Present address:
Institute of Pure and Applied Physics,
Guru Ghasidas University,
Bilaspur - 495 009,
M.P.

पूर्वांतर पर्वतीय विश्वविद्यालय
पू० प० विवि० परिसर, शिलांग-७९३०२२ (मेघालय)
North - Eastern Hill University
NEHU Campus, Shillong - 793022 (Meghalaya)
Phone :
Grams : NEHU

INSTITUTE OF SELF ORGANISING SYSTEMS AND BIOPHYSICS

Pre - Ph.D. Course Grade Certificate

This is to certify that **Mr. Biswajit Pal** secured the grades mentioned below in the following Pre-Ph.D. courses.

COURSES OFFERED	GRADES AWARDED
1. Self Organising Systems	O
2. Methods of Science	O
3. Living State and Biophysics of Living Organisms	A
4. Condensed Matter Physics	O

RPBajpai 14.6.97

Dr . R. P. Bajpai

Professor

for Director
Institute of Self Organising Systems & Biophysics, NEHU, Shillong

ACKNOWLEDGEMENT

First and foremost I express my deepest sense of gratitude to Dr. P. K. Bajpai for introducing me to this subject and for his constant guidance, encouragement and help throughout the entire course of my Ph.D. programme.

I also take this opportunity to express my sincere thanks to Professor K.P. Sinha, Former Director, I.S.O.S.& Biophysics, for his help during his tenure. I am also grateful to Professor R.P.Bajpai, for his keen interest in the progress of the work and constant encouragement. I gratefully acknowledge Dr.V.Singh, Dr.D.Roy, Dr.Satish Kumar of I.S.O.S.& Biophysics for their kind help.

I am extremely grateful to Professor A.L.Verma, Department of Physics North-Eastern Hill University for providing the facilities at his Laser Raman Laboratory. I am also thankful to Professor D. T. Khathing, Head, Regional Sophisticated Instrumentation Centre, North-Eastern Hill University for providing me IR and FT-IR spectral facilities.

I gratefully acknowledge Professor C. S. Shastry, Head, Department of Physics and Professor K. Kumar, former Head, Department of Physics, North-Eastern Hill University for their help. I an also grateful to Dr. P. Nongkinrih for her very helping nature.

I sincerely thank Dr.T.S.Basu Baul for his extremely valuable help and advice throughout the tenure of the work and also for helping me in the synthesis of the azo dye.

My heartfelt thanks are due to Dr.Tapos Chakravorty for many critical discussions during the entire period of my work. He also provided me the Lorentzian curvefitting programme, developed by him, for spectral data analysis.

I express my indebtedness to Professor R.K.Singh, Vice-Chancellor, Guru Ghasidas University for allowing me to work in the University. I also thank Professor V.K.Mishra, Dr.G.D.Varma, Dr.H.S.Tiwari and Dr.M.C.Mahato of School of Pure and Applied Physics, Guru Ghasidas University. Mr. Ajay Verma, Assistant Registrar, Guru Ghasidas University, is also gratefully acknowledged for his manifold help.

I am indebted to Dr. D. Sengupta and other faculty members of the Department of Biochemistry, University of Calcutta, for their help and encouragement during my M.Sc. and Ph.D.programmes.

My thanks are due to Mr.A.K.Rathore, who took the pain to record all my Raman spectra.

I also thank my fellow scholars like Dr. Jayati Sengupta, Dr.Vijay Sharma, Dr.A.K.Mavila, Ms.Bijoyalakshmi, Mr.Amarendra, Ms.Bakordor, Ms.Priyoasha and Mr.Sivadasan of the I.S.O.S.& Biophysics, North-Eastern Hill University, Mr. A. Khashkalam, Mr. A. Srivastava, Mr. V. Shalke, Research Scholars of the School of Pure and Applied Physics, Guru Ghasidas University, for their help and cooperation. I also thank Dr. L. Santra of Union Christian College, Barapani, for the help she extended to me.

I am thankful to Mr.N.Bhattyacharya, Mr.T.Rakshit, Bah.Warjri, Bah.Nongkinrih and Kong Melina of I.S.O.S. & Biophysics for their help and cooperation.

I take this opportunity to thank Dr.V.R.Rao, St. Edmund's College, Shillong, for his encouragement and help and everything what he did for me. I also thank Mr. Sanjeev Singh for his help.

I am grateful to many of my friends. Among them Mr. K. Nandagopal needs a special mention. Besides, Mr. Abhijit Ghosh, Mr. L. Kole and others in their laboratory at Indian Institute of Chemical Biology, Calcutta, also helped me personally in many occasions.

I pay my heartfelt gratitude to Mr. Moloy Kr. Dhar, Professor Rotheen Mukherjee and my uncle Mr.Gopinath Pal. Without their contribution I could not have come to pursue my research.

I also thank Mrs. Joyti Bajpai for her kind help and affection during my stay at Shillong as well as at Bilaspur.

This column remains incomplete if I forget to acknowledge my parents, Ms.Shyamali and other family members. It is their encouragement and sacrifice, which made me optimistic about my career.

Finally, I am extremely grateful to the Council of Scientific and Industrial Research, New Delhi, and also to North-Eastern Hill University for providing me fellowship (UGC).

Biswajit Pal

Biswajit Pal

Abbreviations

BSA	Bovine Serum Albumin
CHT	α-Chymotrypsin
CHTGA	α-Chymotrypsinogen-A
CMPAQ	5-(2′-carbomethoxyphenyl)azoquinolin-8-ol
CPAQ	5-(2′-carboxyphenyl)azoquinolin-8-ol
DRIFT	Diffused Reflectance Infrared Fourire Transform
FT-IR	Fourire Transform Infrared
FWHMI	Full Width at Half Maximum Intensity
HAB	*p*-Hydroxyazobenzene
HABA	2-(4′-hydroxybenzeneazo)benzoic acid
HMPAB	(2-hydroxy-5-methylphenylazo)benzene
HMPACB	(2-hydroxy-5-methylphenylazo)chlorobenzene
HMPAMB	(2-hydroxy-5-methylphenylazo)methoxybenzene
HNAB	(2-hydroxynaphthylazo)benzene
HNACB	(2-hydroxynaphthylazo)chlorobenzene
HNAMB	(2-hydroxynaphthylazo)methoxybenzene
IR	Infrared
$I_g G$	Immunoglobulin G
LC-SPDP	N-Succinimidyl 6-[3′-(2-pyridyldithio)propionamido] hexanoate
PAQ	5-(phenyl)azoquinolin-8-ol
RB	Rose Bengal
RIP	Ribosome Inactivating Protein
RP-HPLC	Reverse Phase High Performance Liquid Chromatography
SDS-PAGE	Sodium dodecile sulfate - polyacrileamide gel electrophoresis
SPDP	N-Succinimidyl 3-(2-pyridyldithio)propionate
UV	Ultraviolet
RR	Resonance Raman

CONTENTS

SYNOPSIS

SYNOPSIS

Vibrational spectroscopy (such as laser Raman scattering, Infrared spectroscopy etc.) have widely been used to elucidate the structural aspects of different chemical and biological molecules as also their binding properties [1-6].

The function and activity of proteins are generally dependent upon their characteristic folding and on specific interactions of the adjacent polypeptide chains. The functional behavior of the proteins are primarily governed by its active site conformation i.e. the biochemical properties at the site where the enzymatic action or ligand binding occurs, while the change in activity is generally correlated with the change in conformation. The knowledge of the secondary structure of a protein and its binding properties (number and nature of binding sites) are a priori to understand its biological activity.

Proteins are in general difficult to crystallize and thus the determination of its structure using X-ray crystallography is not easy, particularly for proteins which are yet to be crystallized. Raman and Infrared (especially Fourier Transform Infrared, FT-IR) techniques provide an alternate in this regard. A sizable amount of work have been carried out on the field [7-10]. Besides, FT-IR in transmission and absorption mode, particularly with the use of diffused reflectance spectroscopy

gives comparable and complimentary information, due to large enhancement in S/N ratio and fourier deconvolution with much better resolution, as that obtained form Raman spectra [11].

Similarly, resonance Raman technique along with electronic spectroscopy can lead to several structural details of ligand molecule and their tautomeric equilibria in solution [12-14].

On the other hand, spectroscopic methods (especially electronic absorption spectroscopy) are largely in use for investigating the binding properties of various ligand with proteins [15-16]. These studies coupled with resonance Raman results, can lead to deduce the changes in the conformation due to binding [17].

We have therefore undertaken a systematic study of some proteins. Proteins include Bovine Serum Albumin (BSA) in which structural and binding properties are well established. Another protein is a Ribosome Inactivating Protein, Gelonin, isolated from *Gelonium multifluorum*. It is a single chain RIP and has got RNA glycosidase activity. Thus it cleaves the glycosidic bond at a unique adenine base in the 28S rRNA, thereby inactivating protein synthesis [18]. The protein has large clinical potential as its conjugates with antibody, modified through crosslinking agents (such as SPDP and LC-SPDP) could be targeted to specifically destroy a cell [19].

Ligand molecules selected for the present work are

azo-phenols, azo-naphthols and azo-quinolinols. These dyes were not very well characterized for their structures and tautomeric equilibria in varied pH solutions. However, these were selected since the binding of similar type of dyes with BSA are well known [20]. Also these are biologically very important as their complexes possess carcinogenic properties [21]. Moreover, they absorbs in the visible region with significant difference in the absorption spectra in azo and hydrazone form, an important requirement for resonance Raman work.

This thesis describes systematic Raman, Infrared and Fourier Transform Infrared studies on proteins, Raman, resonance Raman, FT-IR studies of azo dyes in free form and electronic absorption studies of dye-protein interactions, as well as the resonance Raman study of bound azo dyes. We have estimated the secondary structural content of BSA and Gelonin and studied thermal denaturation of Gelonin. Laser Raman and Infrared studies on crosslinkers N-Succinimidyl 3-(2-pyridyldithio)propionate (SPDP) and N-Succinimidyl 6-[3'-(2-pyridyldithio)propionamido] hexanoate (LC-SPDP) are also included. Structures of few azodyes, namely (2-hydroxy-5-methylphenylazo)benzene, (HMPAB); (2-hydroxy-5-methyl-phenylazo)methoxybenzene, (HMPAMB); (2-hydroxy-5-methyl-phenylazo)chlorobenzene,(HMPACB); (2-hydroxynaphthylazo)benzene, (HNAB); (2-hydroxynaphthylazo)methoxybenzene, (HNAMB); (2-hydroxynaphthylazo)chlorobenzene, (HNACB); 5-(phenyl)azo-

quinolin-8-ol, (PAQ); 5-(2'-carboxyphenyl)azoquinolin-8-ol, (CPAQ) and 5-(2'-carbomethoxyphenyl)azoquinolin-8-ol, (CMPAQ) are deduced at solid state. Tautomeric equilibria of PAQ, CPAQ and CMPAQ have also been investigated. Interaction of CPAQ with BSA has been studied to determine the the number of binding sites and binding constants. Also the structure of bound CPAQ has been deduced. Further, binding of another dye, Rose Bengal (RB), with BSA as well as with Gelonin has been studied to determine number of binding sites and the binding constant.

The thesis is divided into six chapters.

In Chapter I, we have presented an overall introduction of the subject. A brief review of protein structures, structures of dyes and dye protein interactions is also presented in this chapter.

In Chapter II, we have presented relevant theoretical background of the Raman, resonance Raman, Infrared, Fourier Transform Infrared and absorption spectroscopy. Details of different experimental techniques used and the sample preparation required for various measurements along with the different accessories used are also included in this chapter.

In Chapter III, we present detailed spectroscopic studies of proteins and crosslinkers. Methods of isolation and purification of Gelonin are also described. Experimentally observed Raman and

IR spectra of proteins as well as of crosslinkers are assigned. Secondary structural contents of these proteins by two independent methods using spectral data are presented. One is William and Dunker method [22]. In this method, secondary structures were determined using Raman intensity of amide-I mode. The broad amide-I band of proteins is resolved into five components representing di-hydrogen bonded or ordered helix, mono-hydrogen bonded or disordered helix, anti-parallel β-sheet, parallel β-sheet and reverse turn and disordered structure. Normalized reference Raman spectra which represented the amide -I band of a polypeptide with 100% of single type of structure were computed from the solvent subtracted spectra of proteins and polypeptides using least square solution of overdetermined equations. Each amide-I spectrum was computed at 15 equally spaced wavenumbers between 1700-1630 cm^{-1}. Normalized intensity at any wave number is written in terms of five parameters

$I = f_1.I_1 + f_2.I_2 + f_3.I_3 + f_4.I_4 + f_5.I_5$ where f_i defines for corresponding fractional secondary structure of di-hydrogen bonded or ordered helix, mono-hydrogen bonded or disordered helix, anti-parallel β-sheet, parallel β-sheet and turn and disordered structure, respectively. Using reference data for the corresponding proteins, the values of I,s at each wave number were calculated by solving the homogeneous equations of the type

$$I = f_i \cdot I_i$$

Using the reference values of I_i and experimental values of I, the coefficients were calculated using linear regression.

The other method used is curvefitting. In this method, the intensity and the half widths of the curvefitted bands are used for the quantitative determination of the secondary structure of the proteins.

Estimated results obtained from both the methods matches well with reported results. It is found that Gelonin is having mainly α-helix and β-sheet structure with some turn and disordered structure. The estimated percentage structures being $\approx$32% α-helix, $\approx$20% β-sheet, $\approx$26% turn and $\approx$22% disorder.

Thermal denaturation of Gelonin has also been presented. Denaturation temperature has been deduced from the IR results. Study reveals thermal stability of Gelonin, with denaturation temperature around 60^{o}C. It is also found that disordered contribution increases with heating.

Chapter further includes the spectroscopic studies of two crosslinkers (SPDP and LC-SPDP) used for conjugate preparation. A comparison of C-S and S-S stretching modes suggest that the geometry in the disulfide region is different for the two compounds and LC-SPDP experiences less torsion. The results are in good agreement with the MNDO calculations performed independently.

Chapter IV includes the synthesis and spectroscopic

characterization of the azo dyes. Structures of these dyes in solid state have been deduced. pH dependent equilibria and tautomeric structures of PAQ, CPAQ and CMPAQ have also been presented in this chapter. It has been shown that even in the solid state the hydroxy group of *o*-hydroxyphenylazo dyes form an intra-molecular hydrogen bond with the distant nitrogen of the azo group to form a stable six membered ring. However, the structure is totally different for the *o*-hydroxy naphthylazo dyes. These compounds do not form hydrogen band. Instead, they dominate in hydrazone form giving rise to a quinonoid type of structure in solid state.

PAQ exist mainly in azo form in solid state. Even in solutions, it exists predominantly in azo form in acidic as well as in alkaline pH. Hydroxyl group forms hydrogen bond with the ring nitrogen giving a predominant azo structure. CPAQ exists mainly as hydrazone tautomer in solid state. In highly acidic solution it exists predominantly as hydrazone form whereas, at pH above 8 it exists as azo tautomer. CMPAQ is dominantly azoic in solid state as also in alkaline pH. As the pH goes down, equilibrium shifts towards hydrazone form and in highly acidic solution CMPAQ exists mainly in hydrazone tautomer. For both CPAQ and CMPAQ intra-molecular hydrogen bonding involving the hydroxy group and carboxy (CPAQ) or carbomethoxy (CMPAQ) stabilizes the structures. Copper complexes of both PAQ and CMPAQ exist in azo

form.

Chapter V deals with the interactions of some of these dyes with proteins. It has been shown that BSA binds with PAQ and CPAQ, however, it does not bind with CMPAQ. None of these three dyes bind with Gelonin. On the contrary, Rose Bengal (RB) binds with Gelonin as well as with BSA. It is shown that one BSA binds six CPAQ molecules and the association constant is 6.2×10^3. Number of bound RB per BSA molecule could not be estimated precisely, apparently it has three binding sites. In case of Gelonin, it has been shown that Gelonin has got two different types of binding sites for RB. There are 12 low affinity binding sites with binding constants of $\approx 8.9 \times 10^4$. On the other hand, there are only 2 high affinity binding sites per Gelonin molecule for which the binding constant is estimated to be 2.99×10^6.

Resonance Raman study of bound CPAQ has also been presented in this chapter. It has been shown that bound CPAQ exits exclusively in hydrazone form. Binding site of CPAQ has been proposed to be the nitrogen atom of the azo group, adjacent to the phenyl ring.

Chapter VI presents the main conclusions drawn from studies described in this thesis.

References

1. G.Thomas,Jr.in "*Biological Applications of Raman Spectroscopy: Raman Spectra and Conformations of Biological Macromolecules*" Edited by T.G.Spiro, John Willey & Sons, pp.135 (1987).

2. F.Ni and T.M.Cotton, *J.Raman Spectrosc.*, 19, 429 (1988).

3. J.A.Fox, A.T.Yu, V.J.Hruby and H.I.Mosberg, *Arch. Biochem. Biophys.* 211, 628 (1981).

4. W.L.Peticolas, *Biochimie*, 57, 417 (1975).

5. K. Machida, *Vibr. Spectra Struct.* 17A, 421 (1989).

6. K.Kumar and P.R.Carey, *Can.J.Chem.* 55, 1444 (1977).

7. J.R.Thomas,Jr., B.Prescott, R.Love and R.M.Stroud, *Spectrochim. Acta*, 42A, 215 (1986).

8. J.Bandekar and S.Krimm, *Proc.Natl.Acad.Sci.USA*, 76, 774 (1979).

9. J.Castresana, A.Muga, and J.L.R.Arrondo, *Biochem. Biophys. Res. Commun.* 152, 69 (1988).

10. J.M.Hadden, M.Bloemendal, P.I.Harris, S.K.S.Srai amd D. Chapman, *Biochim. Biophys. Acta* 1205, 59 (1994).

11. R.J.Jakobsen and F.M.Wasacz, *Appl. Spectrosc.* 44, 1478 (1990).

12. P. Jaques, *J. Raman Spectrosc.* 12, 102 (1982).

13. P.K.Bajpai, B.Pal and T.S.Basu Baul, *J.Raman Spectrosc.* 26, 351 (1995).

14. A.J.Barnes, M.A.Majid, M.A.Stukey, P.Gregory, and C.V.Stead, *Spectrochim. Acta* 41A, 629 (1985).

15. A Galat, *Spectrochim. Acta* 42A, 199 (1986).

16. I.M.Klotz, in *Protein Function: A Practical Approach*, Edited by T.E.Creighton, IRL Press, New York, (1990).

17. K.Kumar, R.W.King and P.R.Carey, *Biochemistry* 15, 2195 (1976).

18. Endo, Y., Mitsui, K., Motizuki, M. and Tsurugi, K. *J. Biol. Chem.* 262, 5908 (1987)

19. E.S.Vitteta R.J.Fulton, R.D.May, M.Till and J.W.Uhr, Science, 238, 1098 (1987).

20. C.J.Bowmer and W.E.Lindup, *Biochim.Biophys.Acta* 624, 260 (1980).

21. T.S.Basu Baul, *Ph.D Thesis*, University of North Bengal, India, (1986)

22. R.W.Williams and A.K.Dunker, *J.Mol.Biol.* 152, 783 (1981).

CHAPTER - I

GENERAL INTRODUCTION AND THE CURRENT STATUS OF RESEARCH IN THE FIELD OF INVESTIGATION

This chapter presents a brief introduction of the work. A brief review on the progress made in the field of protein spectroscopy using Raman and FT-IR techniques and in probing the ligand structures and tautomerism is presented. Quantitative methods for protein secondary structure estimation and for analyzing dye - protein interactions through spectroscopy are also reviewed.

1.0 INTRODUCTION

Study of protein conformation along with the elucidation of active site is one of the key challenges in molecular biochemistry due to its importance in understanding the functional behavior and the structure-functional correlation. The active site - ligand interactions are also important along with the structural characterization of the ligands for the same reason. Studies on protein/peptide conformations have grown and matured during last few decades. Though, the knowledge of structural aspects of these systems was largely restricted to molecular structure and dynamic aspects *in vivo* are generally left out due to measurement limitations of the techniques used for direct structure determination. Therefore, the need of some simple experimental methods was always felt which could give not only reliable results but probe the structural changes in dynamic situations.

X-ray diffraction has been one of the most widely used methods [1-2] in solving protein conformation as the three dimensional structure is almost directly obtained from the diffraction pattern (as the fourier transform of density distribution) and molecular structure factor. Further, due to technological advancement, the technique has become somewhat easy to handle and undoubtedly most reliable because of its undeniable advantages such as refinements in structures with increased

number of reflections and with sophisticated computer programs. However, there are some unavoidable factors which make X-ray crystallography difficult. The problem lies more with the nature of the samples than in technique *viz.* difficulty or inability to cryatallize certain proteins, the limitations in studying the modification in protein environment e.g. pH. Other limitations include the problems of translating the static information obtained into dynamic properties and the ever intriguing differences that may exist between the protein in solution and in a crystal.

Spectroscopic techniques such as Nuclear Magnetic Resonance (NMR), Electron Spin Resonance(ESR), Fluorescence, Circular Dichroism (CD) have also been used to study protein conformation [3-7]. NMR is recently being used in protein chemistry as it is possible to study protein in solution using two-dimensional NMR. However, at least in its present state, it is limited to low molecular weight proteins. Other methods may either need an external probe [5] or optical interference may occur [6].

Vibrational spectroscopy viz. Raman scattering and Infrared absorption, provides an alternate in this respect to elucidate the structural aspects of various proteins, their binding with ligand molecules and conformational changes in them [8-13]. From last three decades efforts were on to understand the

spectra- structural correlations in proteins and a large number of correlation tables have been published [14-15]. Spectrophotometric methods are largely in use for investigating the binding properties of various ligands with proteins. Resonance Raman technique when used along with electronic spectroscopy can lead to several structural details of ligand as well as protein conformation. These studies if coupled with non-resonance results, can lead to deduce the changes in the conformation of the macromolecule with binding as well as changes in the binding site along with the change in the ligand. Similarly, Fourier Transform-Infrared (FT-IR) in transmission and absorption mode, particularly with the use of Diffuse reflectance spectroscopy gives comparable and complementary information, due to large enhancement in S/N ratio and fourier deconvolution with much better resolution as that obtained from Raman spectra [16].

In order to further strengthen the claim of vibrational techniques becoming the reliable alternate of structural techniques, we have attempted a systematic study of some proteins mainly through vibrational spectroscopy. This includes Bovine Serum Albumin (BSA) in which structural and binding properties are well established [17-20] and a relatively new protein - single chain ribosome inactivating protein Gelonin [21]. Gelonin was selected for two reasons. Firstly, it has got an immense clinical potential as it arrests protein synthesis in eukaryotic

cells. Secondly, the structure and the mechanism of action of this protein was unknown. Binding properties were important in Gelonin. Thus, the spectroscopic studies of ligand-protein binding were also planned.

Ligand dyes selected for our work are azo-phenols, azo-naphthols and azo-quinolinols. These are not very well characterized for their structural changes and tautomeric equilibria. However, they were selected since the binding of these type of systems with BSA is well known [19] and they are biologically very important as their complex possesses carcinogenic properties [22]. Moreover, their salts are water soluble and absorbs in visible region with significant differences in the absorption spectra in azo and hydrazone form, an important requirement for Resonance Raman work. We have, therefore, characterized these dyes and deduced their structure in solid and solution state as well as change in the tautomeric equilibria with change in pH. Binding of these dyes with protein are also studied. In the following section a brief review of the present status of the research concerning the topic selected are presented.

1.1 PRESENT STATUS OF THE WORK

1.1.1 Vibrational Spectroscopy of Proteins

The use of the vibrational spectroscopy in the characterization of macromolecules e.g. proteins and the determination of molecular structures goes well into the first half of this century. After the discovery of Raman effect, first Raman spectra of amino acids and related compounds were recorded by Edsall [23] and the same group reported the first Raman spectra of a protein, lysozyme [24]. Even though a number of Raman spectra of proteins were recorded during that period, there was no consistent theoretical basis for the assignments of the recorded spectra. Side by side studies of model compound viz. polypeptides were also persuaded; reports on poly(L-lysine) revealed that it could be folded into α-helix, β-sheet and random coil structures by varying pH, temperature, and salt concentrations [25]. Many other studies have further suggested that the spectroscopic changes have correlations with external environmental change in the systems [14-15]. Miyazawa et.al. [26] calculated normal modes of amide I and amide III vibrations (different types of amide modes are illustrated in Figure-1.1) of *N*-methylacetamide and developed the basic approach to account for the observed splitting in the amide modes based on perturbation theory [27]. Miyazawa's analysis assumes that the summation of an unperturbed frequency and the contribution of inter and intra

molecular interactions could give the observed frequencies. It was shown later [28] that the physical origin of the perturbation lies in the coupling of amide groups transition dipole. Due to the partial double bond nature of the peptide (-CO-NH-) moiety, it assumes a planer conformation, thus allowing for the possibility of obtaining a *trans* or *cis*- configuration. This conformation then determines the backbone structure of the polypeptide and is reflected in characteristic Raman and IR active bands and in their relative intensities. The direction of dipole moment is shown in Figure-1.2.

While Raman spectra can be used to distinguish between the ordered structures (e.g. α-helix, β-sheet) and the disordered random coil; it is difficult to resolve α-helical and disordered polypeptide regions using IR-spectroscopy. However, in many cases IR-spectroscopy has been used to monitor parallel and anti-parallel β-sheet conformations [29]. Thus, a large number of correlation tables have been published for spectra-structural correlations in model polypeptides and proteins in different amide regions [30-32]. Thus the assignments became easier. One of the recent correlation table is shown in Table-1.1. Lord et.al reported Raman spectra of number of proteins using laser as the excitation source [17,33-35]. Besides, a sizable amount of work have been carried out in the field [36-39]. Attempts were also made to assign the observed protein spectra in terms of the sum

of the amino acid residues through mathematical manipulation, however, with partial success.

Along with the Raman spectroscopy of the proteins, Infrared (IR) studies were also carried out. Elliot and Ambrose [40] correlated different IR bands to various protein conformations. However, progress was tardy due to unavoidable obstacles in obtaining the IR spectra of proteins. The main difficulty was to extract information from the bands due to the intrinsic broad band width of the component bands. On the other hand, strong absorption of water, made it very difficult for extracting solution spectra of proteins. Therefore, the interest on this method was decreasing gradually till the major breakthrough came with the introduction of the Fourier-Transform IR instruments. Instruments were designed based on Michelson interferometer [41] and microcomputers were used along with the application of fast fourier transform algorithm [42]. Thus, the introduction of Fourier transform instruments and fast technological development in accessories like Attenuated total reflection (ATR), Cylindrical Internal Reflection (CIR), Diffused Reflectance Infrared Fourier Transform (DRIFT) etc. made it possible to use IR method extensively. IR method thus emerged as an undeniable technique and a number of qualitative as well as quantitative works are being reported [43-45] and the trend is increasing everyday.

For the quantitative estimation of protein secondary structure, amide III and amide I bands were generally taken. Initially, the amide III band intensity was taken by Pézolet and co-workers to estimate β-sheet structure [44]. They used the 1450 cm^{-1} band (CH_2 bending mode) as an internal intensity standard. Using the relative intensity of the 1240 cm^{-1} (amide III) band, they calculated the β-sheet structure.

In another method [47] the CH_2 bending vibration (1450 cm^{-1}) was again used as an internal standard. However, poly-L-lysine was used to standardize the spectral intensities for α-helical, β-sheet and random coil structure in amide III region in H_2O. Poly-L-lysine, lysozyme and ribonuclease-A were used to standardize intensities of these conformations at 1632 cm^{-1} and 1660 cm^{-1} in the amide I region in D_2O. The percentage secondary structures were calculated from the fractions f_α, f_β, and f_r for α-helix, β-sheet and random coil, respectively, from the following equations:

$$C^{Prot}I^{Prot}_{1240} = f_\alpha I^{\alpha}_{1240} + f_\beta I^{\beta}_{1240} + f_r I^{r}_{1240} \quad (1.1)$$

$$C^{Prot}I^{Prot}_{1632} = f_\alpha I^{\alpha}_{1632} + f_\beta I^{\beta}_{1632} + f_r I^{r}_{1632} \quad (1.2)$$

$$C^{Prot}I^{Prot}_{1660} = f_\alpha I^{\alpha}_{1660} + f_\beta I^{\beta}_{1660} + f_r I^{r}_{1660} \quad (1.3)$$

$$1.0 = f_\alpha + f_\beta + f_r \quad (1.4)$$

Here, I_i^{Prot} is the height of the protein Raman band at the respective wavenumbers in water relative to the band height of the methylene bending mode at 1450 cm^{-1}; I_i^j is the standard value

for 100% j-type structure. f_j are the fraction of the j-type structure in a particular protein. This method could successfully quantify the structural contents of some proteins. However, it failed for the proteins having more than the mentioned three types of structural elements.

William and Dunker [48-49] proposed a method for the determination of secondary structures using Raman intensity of amide I mode. In their approach, the broad amide I band of proteins is resolved into six components representing the following types of secondary structure; di-hydrogen bonded or ordered helix, mono-hydrogen bonded or disordered helix, anti-parallel and parallel β-sheet, reverse turn and disordered structure. Normalized reference Raman spectra which represented the amide I band of a polypeptide with 100% of single type of structure were computed from the solvent subtracted spectra of proteins and polypeptides using least square solution of overdetermined equations. Each amide I spectrum was computed at 15 equally spaced wavenumbers between 1700-1630 cm^{-1}. Normalized intensity (I) at any wavenumber is written in terms of six parameters

$$I = f_1.I_1 + f_2.I_2 + f_3.I_3 + f_4.I_4 + f_5.I_5 + f_6.I_6 \qquad (1.5)$$

where f_i defines for corresponding fractional secondary structure of di-hydrogen bonded or ordered helix, mono-hydrogen bonded or disordered helix, anti-parallel β-sheet, parallel β-sheet, turn

and disordered structure, respectively. Using X-ray crystallographic data for the corresponding proteins, the values of I_i at each wave number were calculated by solving the homogeneous equations of the type

$$I = f_i \cdot I_i \qquad (1.6)$$

Using the reference values of I_i and experimental values of I, the coefficients were calculated using linear regression.

Another method based on multiparameter analysis is proposed by Alix et.al. [50-51]. In their method the percentage of different secondary structural forms in a protein are expressed in terms of some parameters of the amide I band. The parameters are the wavenumber of the peak (ν_{max}), left half width (ν_{left}) and right half width (ν_{right}) at half height. The % secondary structure is calculated from the equation:

$$\% \text{ secondary structure} = a_o + a_1 \nu_{max} + a_2 \nu_{left} + a_3 \nu_{right} \qquad (1.7)$$

where, the constants a_o, a_1, a_2 and a_3 are calculated for each type of structure from the large set of proteins of known structure.

Among the above methods William and Dunker method [48-49] have been found most reliable on statistical tests. But, like the other methods, which have been described above, this method also needs reference data and thus it is based on crystallographic results. In search of an independent method from

the Raman data, different mathematical manipulations have been adopted. Among these methods curve-fitting [52] could be used as an convenient and powerful technique.

1.1.2 Azo Dyes : Characteristic Properties and Vibrational Spectra

Azo dyes possess their color characteristics due to an intense electronic transition that produces a broad absorption spectrum in the visible region. The position of the absorption maximum is sensitive to substituents that donate or withdraw electrons from the *trans* azo benzene backbone [53] indicating that charge transfer process plays an important role in shifting the intensity into the visible region, away from strong UV $\pi \rightarrow \pi^*$ transition present in *trans*-azobenzene [54].

These dyes are used for different purposes. This include acid-base indicators and as probe molecules in protein chemistry. These dyes have been studied extensively, mainly by absorption spectroscopy, and different ionic equilibria were established [55-58]. It has been shown that these dyes exist in different tautomeric structures varying from protonated to neutral to deprotonated form, depending on the pH of the solution. With the use of the laser Raman and Infrared spectroscopy in routined manner, new horizons were opened to study the tautomeric structures of these dyes [59-61].

Especially, the advent of dye lasers, tunable at different excitation line along with the use of isotopic substitution [62], assignments of observed dyes spectra became reliable and easy. Similarly, the structural changes could also be followed.

Different derivatives of azo dyes are used for a number of purposes. Among a wide variety, hydroxy azo dyes and amino azo dyes are most common. When the neutral solution of an amino azo dye is acidified to pH below the color change interval, the azo type basic form is protonated at the azo group and is transformed into the quinoid type acid form [63]. This transformation gives rise to the replacement of azo bands by quinoid bands in RR spectra along with the red shift of λ_{max} in visible absorption spectra. On the contrary, the color change of hydroxy azo type indicators occur mostly in the basic pH region in such a way that λ_{max} shifts to red on addition of alkali to the neutral solution [63]. Further, in the hydroxy azo dyes if the hydroxy group is in *o*-position with respect to the azo group, then the hydroxy group may participate in the formation of five or six membered ring via hydrogen bonding.

The structure of these dyes are of much interest. These have been studied using resonance Raman (RR) and Infrared techniques. RR study of *o*-hydroxy azo dyes have been concerned mainly with the tautomeric equilibria in solution [63-68]. Reports in solid state for these compounds are scanty. In one

report solution state (in CCl_4) results were used for analyzing the solid state spectrum [66] leading to an incorrect assignment of the vibrational modes. Recent reports also did not deal with the structural details [69-70]. Further, the reports lacks a complete assignment of the bands and the role of the effect of substituents.

It is reported that the simple azo dye *p*-hydroxy azo benzene (HAB) exist mainly as azo tautomer in aqueous solution irrespective of the pH of the solution [64]. Whereas (2-hydroxy-5-methylphenylazo)benzene (HMPAB) exists in azo form and (2-hydroxynaphthylazo)benzene (HNAB) in hydrazone form exclusively [71-72]. The RR spectra of HMPAB reported earlier suggest azo structure of the compound [73]. In solution, tautomerism has been proposed but in another report the azo structure is said to be dominant [74]. From solid state studies it has been said that tautomerism is not possible [65]. However, these results do not contribute much to the structural details. Similarly, for HNAB and its derivatives, RR reports are available which deal mainly with the acid base equilibria and formation of likely species in solution [61, 63-64, 66-68, 75-77].

Information regarding the vibrational spectra of azo dyes of the 5-(aryl)azoquinolin-8-ol type is sporadic (68,79-80), and gives little insight regarding the structural details. It is also reported that the copper complexes of these compounds exist

in azo form [79].

The electronic transition involving the hydrazone form in general appear at higher wavelengths than those due to azo form [53]. Bathochromic shift with increasing pH has also been reported for number of azo dyes and support the azo-hydrazone equilibria [80]. It may be noted that acid-base transformations in solutions lead to change in the electronic spectra of azoquinolinols and a number of equilibria have been investigated and characterized as mono-, di- and deprotonated species [80-81]. Information regarding protonation can be derived from electronic spectra in the light of CNDO/2 results [79]. The current progress in the field of vibrational spectroscopy of azo dyes is shown in tabular form in Table-1.2.

1.1.3. Ligand - Protein Interactions

Binding of an effector molecule to a biological macromolecule is the primary step in most of the biological reactions. Thus, binding of a ligand molecule to a receptor molecules such as enzyme-substrate, antigen-antibody, or antibody-hapten reactions or the binding of drugs to the plasma protein have been studied extensively [82-85].

It is reported that albumin group of proteins bind with several drugs and the number of ligand molecules vary; number of diflunisal molecules bind per protein molecule exceeds 10 [86],

for medium and long-chain fatty acids, it is 10 to 15 [87] and in most of the cases, the binding of ligand does not show a tendency of saturation [89]. Number of 2-(4'-hydroxybenzeneazo)benzoic acid (HABA) molecule bound per molecule of human serum albumin varies from 1 to 5 depending on the concentration of protein [19].

For the quantitative study of dye protein interactions, there are two main procedures : (i) equilibrium dialysis and (ii) titration. Both methods deal with the determination of free ligand concentration. This could be done indirectly through a number of spectroscopic techniques; either estimating the spectroscopic changes of bound ligand molecule or from the change in property of the receptors viz. protein. Spectroscopic methods have got some advantages to detect the perturbation on ligand, once it is bound. Colored ligands absorb in the visible region. Thus, it becomes easier to detect the change in property of these ligand molecules. The position of absorption maxima or its intensity or both may change due to binding.

Utilization of spectroscopic changes as a measure of the extent of interaction is based on the explicit assumption that the fractional saturation of binding sites by ligand is linearly proportional to the fraction change in the spectroscopic signal. These indirect methods of monitoring ligand protein interaction determine binding constant and stoichiometry.

Binding of ligand to a protein may result in a change in the environment surrounding either the ligand or amino-acid residues in the protein. Such a change may perturb the electronic interactions of the ligand or the residues in the protein producing a shift in the absorbance spectrum [69]. The difference between the unperturbed and perturbed spectrum is termed as the difference spectrum which can be calculated according to the following equation [90]:

$$A_\lambda(P+L) - A_\lambda(PL) = \Delta A_\lambda \qquad (1.8)$$

where A_λ is the absorbance at wavelength λ, (P+L) indicating protein and ligand absorbances added separately; while (PL) indicates that mixing and presumably binding has taken place. ΔA_λ is the difference in the absorbance of the two solutions at wavelength λ.

Perturbation of the protein can most readily be detected in the 250-300 nm range for phenylalanine, tyrosine and tryptophan. These residues when perturbed have different spectra which are easily recognized. The spectral shifts may be a result of direct interaction of the ligand in or around the binding site or it may be due to conformational change away from binding sites. Association or dissociation of protein may also produce a spectral shift, but the binding of the ligand would have to be linked to the association or dissociation to affect a change that is ligand concentration dependent.

The spectrum of the ligand may also be perturbed since it may be shifted from an aqueous environment to a hydrophobic one upon binding to the protein. Interaction of the ligand might also change the degree of ionization and thereby shifts the spectrum. Thus an observed spectral change may be caused due to a wide variety of perturbation.

A general theory of changes due to perturbation on the electronic states of free molecule can be used to understand the effect of various types of agents on the ligand and protein state. The general perturbation treatment on electronic levels are discussed at length in a number of reviews and the change in the spectral parameters as a result of perturbation due to interactions are deduced in detail [89].

Experimentally, one can design a number of schemes to analyze the spectroscopic changes. One way of doing this, is to find out the wavelength (λ) at which ΔA_λ is maximum. The observed difference spectrum should reveal it. This wavelength will provide the maximum intensity in the observation of the change; hence it should be used in the studies to determine the effect of ligand concentration, [L], on the spectral change. The maximum change in absorbance can then be determined by plotting $1/\Delta A_\lambda$ versus 1/[L] and extrapolating it to infinite ligand concentration. The y-intercept will yield the maximum absorbance change, $\Delta A_{\lambda_{max}}$. The fractional change in the absorbance

$\Delta A_\lambda / \Delta A_{\lambda_{max}}$ can be assumed, to a good approximation, to be linearly proportional to the fractional saturation of binding sites.

Thus, $$\Delta A_\lambda / \Delta A_{\lambda_{max}} = r/n \qquad (1.9)$$

where, r is the number of moles of ligand bound per mole of protein and n the number of binding sites.

Another way of determining n is by measuring $\Delta\varepsilon$, where, $\Delta\varepsilon = [\varepsilon(\text{bound}) - \varepsilon(\text{free})]$, i.e. the difference in the molar extinction coefficient due to binding. The increment in $\Delta\varepsilon$ of ligand can be measured by extrapolating the result of a titration of ligand solution of finite concentration with excess protein. The aliquots of a protein solution are titrated with known total concentration of ligands. The bound ligand concentration, $[L]_b$, can be determined as $\Delta A_\lambda / \Delta\varepsilon$ and free ligand concentration, $[L]_f$, estimated from the difference.

The binding isotherm can be expressed as

$$r = \frac{n[L]_f}{K_d + [L]_f} \qquad (1.10)$$

where K_d is dissociation constant.

This equation (1.10) was originally proposed by Scatchard [90]. From a set of experiments, it is possible to find the number of binding sites and/or the binding constant from the rearranged form of equation (1.10) :

$$r/[L] = n/K_d + r/K_d \qquad (1.11)$$

The degree of cooperativity can also be estimated, if the change ($\Delta A_\lambda / \Delta A_{\lambda_{max}}$) is non-linear, by

$$r = \frac{n\,([L]_f)^h}{K_d + ([L]_f)^h} \qquad (1.12)$$

h being Hill coefficient [91], an indication of cooperativity in ligand binding.

If we consider equation (1.11) and plot r/[L] versus r, gives us Scatchard plot. In a simple system having identical binding sites, the plot will be linear with slope of $-1/K_d$. r/[L] intercept will give the value of the n/K_d and the r intercept giving the value of n, i.e. the number of binding sites.

The concave curvature of Scatchard plot is ascribed to 'negative cooperativity'. It is argued that in such cases receptor molecule has at least two (or more) types of binding sites. Such types of curves are fitted into two (for two independent sites) straight lines, one attributed to 'high affinity' (steeper line) and the other to 'low affinity' (less steep).

Interpretation of this type of graph gives spurious results if not used very carefully [92]. Even, it has also been suggested that the second type of representation may be totally wrong in some cases though it has been used widely.

On the other hand, association constant K_a could be found directly from the equation of Klotz [93-94]:

$$\frac{1}{r} = \frac{1}{nK_a(1-\alpha)[L]_T} + \frac{1}{n} \qquad (1.13)$$

where, $[L]_T$= total dye concentration,

and α = fraction of bound dye, which could be calculated from the following equation [92]:

$$A = \alpha A_b + (1-\alpha)A_f \qquad (1.14)$$

where, A = absorbance

A_b = absorbance at fully bound condition,

A_f = absorbance of free ligand

From the plot of 1/r versus $1/(1-\alpha)[L]_T$ one gets slope as 1/nk and an intercept of 1/n.

On the other hand, concentration of the bound dye, $[L]_B$ could be expressed as

$$[L]_B = \frac{A_{Cal} - A_{Obs}}{\varepsilon_{free} - \varepsilon_{Obs}}, \qquad (1.15)$$

where, A_{Cal} and A_{Obs} are the absorption maxima for free and bound dye at the λ_{max} of free form and ε_{free} and ε_{Obs} are the molar extinction coefficient of free and bound dye at λ_{max}. From, $[L]_B$ and C_p, protein concentration, r could be found.

References

1. K.R.Acharya and A.R.Rees, in *Molecular Biology and Biotechnology A Comprehensive Desk Reference*, Edited by R A Meyers, VCH Publicers Inc. (1995).

2. R.J.Read, *Structure* 4, 11 (1996).

3. K.Wüthrich, *Science* 243, 45 (1989).

4. G.K.Radda, *Biochem. J.* 122, 385 (1971).

5. L.D.Weber, A.Tulinsky, J.D.Johnson and M.A.El-Bayoumi, *Bichemistry* 18, 1297 (1979).

6. N. Greenfield and G. D. Fasman, *Biochemistry* 8, 4108 (1969).

7. P.Carmona, A.Lasagabaster and M.Molina, *Biochim. Biophys. Acta* 1246, 128 (1995).

8. J.Bandekar and S.Krimm, *Proc.Natl.Acad.Sci.USA*, 76, 774 (1979).

9. C.H.Chou and G.D.Fasman, *J.Mol.Biol.* 115, 135 (1977).

10. J.A.Fox, A.T.Yu, V.J.Hruby and H.I.Mosberg, *Arch. Biochem. Biophys.* 211, 628 (1981).

11. W.L.Peticolas, *Biochimie*, 57, 417 (1975).

12. G. Thomas, Jr. in *Biological Applications of Raman Spectroscopy: Raman Spectra and Conformations of Biological Macromolecules*, Edited by T.G.Spiro, John Willey & Sons, (1987).

13. F.Ni and T.M.Cotton, *J.Raman Spectrosc.*, 19, 429 (1988).

14. Y. Sugawara, J. Harada, H. Malsura and T. Shimanouchi, *Biopolymer* 17, 1405 (1978).

15. B.G.Frushour, P.C.Painter and J.L.Koenig, *J. Macromol. Sci.* C15, 29 (1976).

16. R.J.Jakobsen and F.M.Wasacz, *Appl. Spectrosc.* 44, 1478 (1990).

17. M.C.Chen and R.C.Lord, *J.Am.Chem.Soc.USA*, 98, 990 (1976).

18. R.J.Jakobsen and D.G.Cornell, *Appl. Spectrosc.* 40, 318 (1986).

19. C.J.Bowmer and W.E.Lindup, *Biochim.Biophys.Acta* 624, 260 (1980).

20. S.Kishore and M.Maruthamuthu, *Proc. Indian Acad. Sci. (Chem.Sci.)* 105, 279 (1993).

21. F.Stripe, S.Olsnes and A.Phil, *J.Biol.Chem.* 255, 6947 (1980).

22. T.S.Basu Baul, *Ph.D. Thesis*, University of North Bengal, India (1986).

23. J.T.Edsall, *J.Chem.Phys.* 4, 1 (1936).

24. J.T.Edsall, R.B.Martin and B.R.Hollingworth, *Proc. Natl. Acad. Sci. USA* 44, 505 (1958).

25. B.Davidson and G.D.Fasman, *Biochemistry* 6, 1616 (1967).

26. T.Miyazawa, T.Shimanouchi and S.Mizushima *J.Chem.Phys.* 29, 611 (1958).

27. T.Miyazawa, *J.Chem.Phys.* 32, 1647 (1960).

28. J.Bandekar and S.Krimm, *Proc. Natl. Acad. Sci. USA* 76, 774 (1979).

29. Z. Iqbal and E. Weidekamm, in *Vibrational Spectroscopy of Phase Transitions* Edited by Z.Iqbal and F.J.Owens, Academic Press, (1984).

30. W.H.Moore and S.Krimm, *Biopolymers* 15, 2465 (1976).

31. M.D.Baron, G.DeLoze, T.Toniolo and G.D.Fashman, *Biopolymers*, 18 411 (1979).

32. J.R.Thomas,Jr., B.Prescott, R.Love and R.M.Stroud, *Spectrochim. Acta*, 42A, 215 (1986).

33. R.C.Lord and N.-T.Yu, *J.Mol.Biol.* 50, 509 (1970).

34. M.C.Chen and R.C.Lord, *Biochemistry* 15, 1889 (1976).

35. M.C.Chen and R.C.Lord, *J.Am.Chem.Soc.USA*, 96, 4750 (1974).

36. W.L.Peticolas, *Methods in Enzymology* 246, 389 (1995).

37. P.S.Belton and A.M.Gil, *Biopolymer* 34, 957 (1994).

38. D.Aslanian, P Grof, F.Renault and P.Masson, *Biochim. Biophys. Acta* 1249, 37 (1995).

39. G.J.Thomas,Jr. and D.A.Agard, *Biophys. J.* 46, 763 (1984).

40. A.Elliot and E.J.Ambrose, *Nature*, 165, 921 (1950).

41. A.A.Michelson, *Phil. Mag.*, 31, 256 (1891).

42. J.W.Cooley and J.W.Tukey, *Math. Comput.*, 19, 297 (1965).

43. J.Castresana, A.Muga, and J.L.R.Arrondo, *Biochem. Biophys. Res. Commun.* 152, 69 (1988).

44. J.M.Hadden, M.Bloemendal, P.I.Harris, S.K.S.Srai amd D. Chapman, *Biochim. Biophys. Acta* 1205, 59 (1994).

45. D.J.Hodges, D.C.Lee, C.J.Slater, D.G.Reid, G.P.Herper and T.E.Cawston, *Biochim. Biophys. Acta* 1208, 94 (1994).

46. M.Pézolet, M.Pigeon-Gosselin and L.Coulombe, *Biochim. Biophys. Acta* 453, 502 (1976).

47. J.L.Lippert, D.Tyminski and P.J.Desmeules, *J.Am.Chem.Soc.*, 98, 7075 (1976).

48. R.W.Williams and A.K.Dunker, *J.Mol.Biol.* 152, 783 (1981).

49. R.B.Honzatko and R.W.Williams, *Biochemistry*, 21, 6201 (1982).

50. A.J.P.Alix, G.Pedanou and M.Berjot, *J. Mol. Struct.* 174 (1988).

51. A.J.P.Alix and G.Pedanou, in *Proceedings of the Fourteenth International Conference on Raman Spectroscopy, 22-24 August, 1994, Hong Kong,* Edited by N.-T.Yu and X.Y.Li, Wiley, Chichester (1994).

52. H.Susi and M.Byler, *Appl. Spectrosc.* 42, 819 (1988).

53. J.Griffiths, *Colour and Constitution of Organic Molecules.* Academic Press, New York (1976).

54. R.H.Dyck and D.S.McClure, *J. Am. Chem. Soc.* 88, 1948 (1966).

55. G.E.Lewis, *Tetrahedron*, 10, 129 (1960).

56. E.Sawicki, *J.Org.Chem.*, 22, 365 (1957).

57. M.Isaks and H.H.Jaffe, *J.Am.Chem.Soc*, 86, 2209 (1964).

58. Y.Tanizaki, T.Kobayashi and T.Hoshi, *Bull.Chem.Soc. Jpn.*, 39, 558 (1966).

59. D.Hadzi, *J. Chem. Soc.*, 2143 (1963).

60. P.Bassignana and C.Cogrossi, *Tetrahedron*, 20, 2361 (1964).

61. H.Hacker, *Spectrochim. Acta*, 21, 1989 (1965).

62. R.Kübler, W.Lüttke and S.Weckherlin, *Z. Electrochem.*, 64, 650 (1960).

63. Y.Saito, B.K.Kim, K.Machida and T.Uno, *Bull. Chem. Soc. Jpn.* 47, 2111 (1974).

64. K. Machida, *Vibr. Spectra Struct.* 17A, 421 (1989).

65. P. Jaques, *J. Raman Spectrosc.* 12, 102 (1982).

66. A.J.Barnes, M.A.Majid, M.A.Stukey, P.Gregory, and C.V.Stead, *Spectrochim. Acta* 41A, 629 (1985).

67. J.Keleman, S.Moss, H.Santer and T.Winkler, *Dye Pigments* 3, 27 (1982).

68. P.J.Trotler, *Appl. Spectrosc.*, 31, 30 (1977).

69. G.G.Siu and Z.L.Chen, *J.Raman Spectrosc.*, 24, 173 (1993).

70. S. Chattopadhyay, G. S. Kastha and S. K. Brahma, *J. Raman Spectrosc.*, 22, 449 (1991).

71. S.Basu Baul, T.S.Basu Baul and M.Gielen, *Synth.React. Inorg. Met.-Org. Chem.*, 22, 107 (1992).

72. A.Lycka, D.Snobl, V.Machacek and M.Vecera, *Org.Magn.Reson.*, 15, 390 (1981).

73. J.Socha, J.Schreiber and R.Rotscheen, *Collect. Czech. Chem. Commun.*, 35, 857 (1970).

74. G.Gabor, Y.Frei, D.Genjou, K.Kaganowitch and E.Fischer, *Isr. J. Chem.*, 5, 195 (1982).

75. P.M.Drozdzewski, *Spectrochim.Acta*, 41A, 1035 (1985).

76. R.K.Scheule, H.E.Vanwart, B.L.Vallee and H.A.Scheraga, *Proc. Natl. Acad. Sci. USA*, 74, 3273 (1980).

77. P.R.Carey and R.W.King, *Biochemistry*, 18, 2834 (1979).

78. T.S.Basu Baul, T.K.Chattopadhyay and B.Majee, *Polyhedron*, 2, 635 (1983).

79. T.S.Basu Baul, T.K.Chattopadhyay and B.Majee, *Indian J. Chem.*, 23A, 470 (1984).

80. I.S.Mustafin and O.S.Sivanova, *Tr. Kom. Anal. Khim., Akad. Nauk SSSR*, 17, 133 (1969).

81. V.M.Ivanov and T.F.Rudometkina, *Zh. Anal. Khim.*, 33, 2426 (1978).

82. R.N.Smith and C.Hansch, *Biochemistry*, 12, 4924 (1973).

83. H.Vorum, K.Fisker and R.Brodersen, *Biochim. Biophys. Acta*, 1205, 178 (1994).

84. L.D.Faller and R.E.LaFond, *Biochemistry*, 10, 1033 (1971).

85. A.Froese, A.H.Sehon and M.Eigen, *Canadian J. Chem.*, 40, 1786 (1962).

86. B.Honore and R Brodersen, *Mol. Pharmacol.*, 25, 137 (1984).

87. A.O.Pedersen, B.Hust, S.Andersen, F.Nielsen and R.Brodersen, *Eur. J. Biochem.*, 154, 545 (1986).

88. R. Brodersen, B. Honore and F.G.Larsen *Acta. Pharmacol. Toxicol.*, 54, 129 (1984).

89. R.W.Oberfelder and J.C.Lee, *Methods in Enzymology* 117, 381 (1985).

90. G.Scatchard, *Ann. N.Y. Acad. Sci.*, 51, 660 (1949).

91. A.V.Hill, *J. Physiol., (London)* 40, 190 (1910).

92. I.M.Klotz, in *Protein Function: A Practical Approach*, Edited by T.E.Creighton, IRL Press, New York, (1990).

93. I.M.Klotz, F.M.Walker and R.G.Bivan, *J.Am.Chem.Soc.USA* 68, 1486 (1946).

94. S.T.Christian and R.Janetzko, *Arch.Biochem.Biophys.* 145, 169 (1971).

Table-1.1A: Assigned Amide I and Amide III modes of Proteins in Raman and Infrared spectra[a]

Protein	Structural Element	Assigned Bands (cm^{-1})	
		Amide I	Amide III
Tropomysin	α-helix	1655	1200-1270
Myosin	α-helix	1650	1304/1265
Concanavalin	β-sheet	1672	1242
Human I_gG	β-sheet	1673	1239
Bence-Jones Protein	β-sheet	1670-1675	1242-1246
Bovine Serum Albumin	α-helix	1652	1272
	random	1665	1248
Glucagon	α-helix	1658	1266
	random/turn	1685	1235,1248
Insulin	β-sheet	1672	1232
	α-helix	1662	1303,1284,1269
	random/turn	1685	1240

[a]For reference please see P.R.Carey in *Biochemical Applications of Raman and Resonance Raman Sectroscopies*, Chapter 4, (1982) Academic Press, New York and refences cited therein.

Table 1.1B General Assignment of Protein Amide I and Amide III Modes[b]

Type	Conformation	Band Positions(cm^{-1}) Raman	Infrared
Amide 1	Turn	1680-1695	1677-1685
Amide I	Antiparallel β-sheet	1672-1677	1685-1689
Amide I	Random	1660-1670	1642-1647
Amide I	α-helix	1645-1657	1650-1655
Amide I	Parallel β-sheet	1630-1635	1630-1638
Amide III	α-helix	1270-1300	-
Amide III	Random	1243-1253	-
Amide III	β-sheet	1229-1235	-

[b]For reference please see R. Sanches, in *Spectroscopy*, H4.SMR/916 - 10, (notes provided in *Seventh College on Biophysics: Structure and Function of Biopolymers: Experimental and Theoretical Techniques)*, ICTP, Trieste, Italy (1996) and references cited therein.

Table 1.2 Some of the azo dyes for which Resonance Raman spectra are reported. General Structure considered is $Ar^1-N=N-Ar^2$ (a)

No.	Type of the dye	Ar^1	Substituent on Ar^1	Ar^2	Substituent on Ar^2
1.	Amino	Phenyl	4-NH_2	Phenyl	-
2.		Phenyl	4-NH_2,D_4	Phenyl	D_5
3.		Phenyl	4-NH_2	Phenyl	4-SO_2NH_2
4.		Phenyl	4-NH_2	Phenyl	4-COOH
5.		Phenyl	4-NH_2	Phenyl	4-SO_3^-
6.		Phenyl	4-NH_2	Phenyl	4-AsO_3^{2-}
7.		Phenyl	4-$N(CH_3)_2$	Phenyl	-
8.		Phenyl	4-$N(CH_3)_2$	Phenyl	D_5
9.		Phenyl	4-$N(CH_3)_2$	Phenyl	4-SO_3^-
10.		Phenyl	4-$N(CH_3)_2$	Phenyl	2-COOH
11.		Phenyl	4-$N(CH_3)_2$	Phenyl	4-NH_2
12.		Phenyl	4-$N(CH_3)_2$	Phenyl	4-$C(NH_2)_2^+$
13.		Phenyl	4-$N(CH_3)_2$	Phenyl	4-SO_2NH_2
14.		Phenyl	4-$N(C_2H_5)_2$	Phenyl	2-NO_2
15.		Phenyl	4-$N(C_2H_5)_2$	Phenyl	3-NO_2
16.		Phenyl	4-$N(C_2H_5)_2$	Phenyl	4-NO_2
17.	Hydroxy	Phenyl	4-OH	Phenyl	-
18.		Phenyl	4-OH	Phenyl	D_5
19.		Phenyl	4-OH,D_4	Phenyl	
20.		Phenyl	4-OH,D_4	Phenyl	D_5
21.		Phenyl	4-OH	Phenyl	4-SO_3^-
22.		Phenyl	4-OH	Phenyl	4-NO_2
23.		Phenyl	3-COOH 2,4-diOH	Phenyl	4-SO_3^-
24.		Phenyl	4-OH	Phenyl	4-SO_2NH_2
25.		Phenyl	4-OH	Phenyl	2-COOH

Continued

26.	Phenyl	4-OH, D_4	Phenyl	2-COOH
27.	Phenyl	4-OH	Phenyl	2-COOH, 4-Cl
28.	Phenyl	4-OH	Phenyl	2-COOH, 5-NO_2
29.	Phenyl	4-OH	Phenyl	2-COOH, 4-CH_3
30.	Phenyl	2-OH 3-CH_3	Phenyl	2-COOH
31.	Phenyl	2-OH 3-OCH_3	Phenyl	2-COOH
32.	Phenyl	4-OH 3-CH_3	Phenyl	2-COOH
33.	Phenyl	4-OH 3,5-diCH_3	Phenyl	2-COOH
34.	Phenyl	4-OH 3,5-diCH_3	Phenyl	2-COOH, 4-CH_3
35.	Phenyl	2,4-diOH	2-Pyridyl	-
36.	Phenyl	2-OH 4-CH_3	5-Tetrazolyl	-
37.	Phenyl	2-OH 5-OCH_3	2-Benzo-thiazolyl	-
38.	Phenyl	2-OH 5-OCH_3	2-Benzo-thiazolyl	-
39.	Naphthyl	2-OH	Phenyl	-
40.	Naphthyl	2-OH	Phenyl	4-SO_3^-
41.	Naphthyl	4-OH	Phenyl	4-SO_3^-
42.	Naphthyl	2-OH	2-Pyridyl	-
43.	Naphthyl	2-OH	Phenyl	4-NO_2
44.	Naphthyl	2-OH	4-Benzo-thiazolyl	-
45.	Phenyl	2-OH	2-Benzo-thiazolyl	-
46.	Quinolyl	8-OH	Phenyl	4-SO_2NH_2

For reference please see K. Machida, *Vibr. Spectra Struct.* 17A, 421 (1989); R.S. Cataliotti et. al. *J. Raman Spectrosc.* 20, 601 (1989); S. Chattopadhya et.al. *J. Raman Spectrosc.* 22, 449 (1991); G.G.Siu et. al. *J. Raman Spectrosc.*, 24, 173 (1993).

a D_n represent the number of H atoms substituted by D atoms

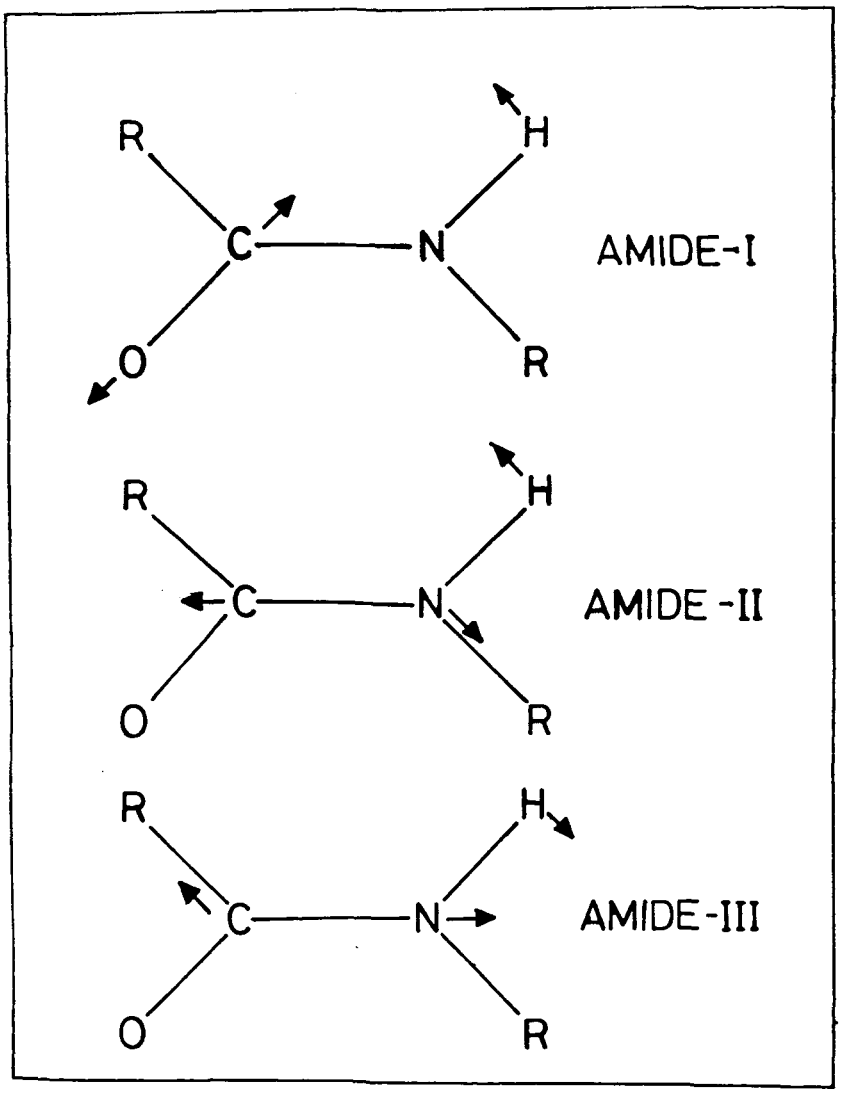

Figure - 1.1: Different types of amide modes:

Amide I $\nu_{C=O} + \nu_{C-N} + \delta_{C-C-N}$

Amide II $\delta_{C-N-H} + \nu_{C-N} + \delta_{O-C-N} + \nu_{C-C} + \nu_{C-N}$

Amide III $\delta_{C-N-H} + \nu_{C-N} + \nu_{C-C} + \delta_{O-C-H}$

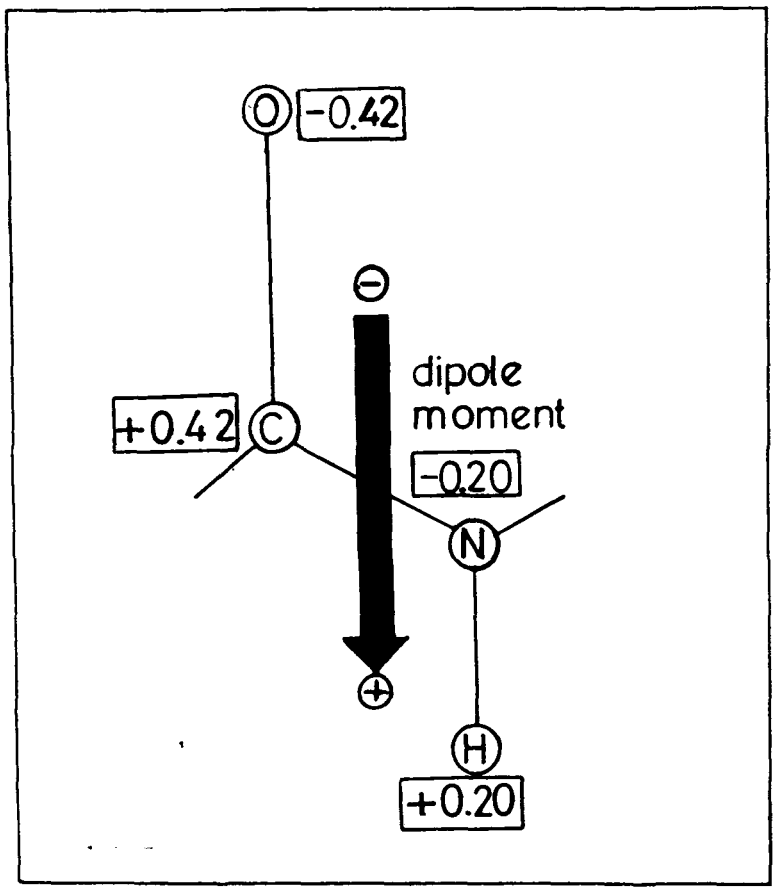

Figure - 2.2: Direction of amide dipole in a peptide unit

CHAPTER - II

VIBRATIONAL AND ELECTRONIC SPECTROSCOPY : THEORETICAL CONSIDERATIONS AND INSTRUMENTATION

This chapter presents the basic theoretical framework for Raman, Resonance Raman, Infrared, Fourier Transform Infrared and Electronic spectroscopy used as experimental techniques in the present work. Instrumentation details of the techniques used are summarized. Mathematical data handling and manipulation techniques such as Difference spectroscopy, Deconvolution, Curvefitting etc. are also presented briefly.

2.0 INTRODUCTION

Vibrational spectroscopy dealing with absorption and inelastic scattering of photons has contributed significantly in understanding the complex structure and molecular dynamics of polyatomic systems. It provides valuable information pertaining to the nature as well as the magnitude of several physical parameters (such as intra- and inter-molecular forces, bond length, bond angle, identification of functional groups in compounds etc.) and thermodynamic properties. Spectroscopic studies on large molecules, particularly on biomolecules such as peptides, proteins, nucleic acids etc. has also been followed rigorously. In this chapter, we briefly present the basic concepts of vibrational and electronic absorption spectroscopy including the experimental details and theoretical considerations used.

2.1 THEORETICAL BACKGROUND

2.1.1 Raman Scattering

If the exciting frequency of the electromagnetic radiation is in the visible or ultraviolet (UV) range, molecules sometimes fall to a different excited vibrational or rotational energy level of the electronic ground state giving rise to secondary emission of different frequency - this phenomenon is called Raman effect. During the process of Raman scattering,

photons of exciting radiation interact with the molecules of the medium. The energies of the inelastically scattered photons may either be increased or decreased relative to the exciting photon energy by quantized increments corresponding to the vibrational or rotational energy levels [1]. The molecule in the ground state may be momentarily raised to a higher excited state due to interaction with the incident photon, which in turn comes back to the ground vibrational state or to an excited vibrational state which correspond to Rayleigh and Stokes Raman scattering, respectively. On the other hand, if the exciting photon interacts with a molecule in the excited vibrational state, it may return to the ground vibrational state via a higher unstable state giving rise to anti-Stokes Raman scattering.

The fraction of the incident photons scattered during Raman process is always very small, and thereby Raman lines or shifts are of extremely weak intensity. Intense monochromatic laser is, therefore, used as excitation source to obtain good quality Raman spectra. In normal Raman scattering, the excitation frequency of radiation is far away from the stationary energy states of the system, i.e., the intermediate state is not associated with any particular molecular eigen state as such and is considered to be a statistical superposition / summation of a large number of excited electronic states of the system. When the incident light approaches an electronic absorption band the

intermediate state assumes more importance and summation term is dominated by this electronic state. This is called pre-resonance Raman scattering. Resonance Raman (RR) scattering is obtained by tuning the excitation wavelength through the electronic absorption band.

In Resonance Raman scattering, the intermediate state is dominated by a few vibronic levels in the vicinity of the incident light frequency. Finally, the resonance fluorescence limit is reached when the incident light coincides with a single sharp level of the electronic state. Though both, resonance Raman and resonance fluorescence involve excitation and emission in the electronic absorption band. However, there is very precise demarcation between these two processes. In case of resonant scattering, the process depends not only on the energy difference between the molecule and the photon state, but also on the line shapes associated with them. In the resonant fluorescence case, the molecular state is much sharper than the photon state and is thus completely in resonance with the incident beam. The scattering may then be described as a rapid decay of population of the excited state followed by a slow decay characteristic of the life time of this state. In the resonance Raman limit, the photon state is much sharper than the molecular state and in resonance with only a small part of it. In this case, the two emission processes are involved; a fast one with life time of the

incident photon state and a slower one with the excited state life time. The former part represents the resonant contribution, while the later represents the non-resonant part of the scattering.

2.1.2 Resonance Raman Scattering and Band Intensity

If a molecule is considered at the origin of a space fixed coordinate system which interacts with an incident plane wave of light with electric vector represented as

$$\bar{E}_\sigma = \bar{E}^o_\sigma \exp(i\bar{k}.r - i\omega t) \qquad (2.1)$$

propagating along $\bar{k}$ with angular frequency ω, the oscillating electric dipole moment induced in the molecule is given by

$$(\bar{\mu}_\sigma)_{mn} = (\tilde{\tilde{\sigma}}_{\rho\sigma})_{mn} \bar{E}_\sigma \qquad (2.2)$$

where $(\bar{\mu}_\sigma)_{mn} = \langle \Psi_m | e\bar{\rho} | \Psi_n \rangle$ is the amplitude of the transition moment and Ψ_m and Ψ_n are the time dependent wave functions of the initial and final states, respectively; $(\tilde{\tilde{\sigma}}_{\rho\sigma})_{mn}$ is the polarizability tensor for the transitions from m to n and $\bar{\rho}$ and $\bar{\sigma}$ are molecular cartesian axes of the scattering tensor $(\tilde{\tilde{\sigma}}_{\rho\sigma})$.

The intensity of the scattered light I_{mn} in terms of photons per molecule per second in 4π solid angle, after averaging over all orientations of the molecule is given by [2,3],

$$I_{mn} = 128\pi^5/9c^4(\nu_o \pm \nu_{mn})^4 I_o \sum_{\rho,\sigma} |(\alpha_{\rho\sigma})_{mn}|^2 \qquad (2.3)$$

where ν_o is the frequency of incident light, I_o its intensity, $(\nu_o \pm \nu_{mn})$ is the frequency of the scattered light, c is the

velocity of the light and sum goes over ρ,σ=x,y,z.

Thus, the intensity of the scattered radiation depends upon the frequency of the incident radiation, and more critically on $|(\alpha_{\rho\sigma})_{mn}|^2$ when the exciting radiation approaches an electronic absorption band in the resonance Raman effect.

The $(\rho\sigma)^{th}$ component of the matrix element of the polarizability tensor for the transition from vibronic state $|m\rangle$ to $|n\rangle$ is given by the second order perturbation theory as calculated by Kramer-Heisenberg-Dirac [4].

$$(\alpha_{\rho\sigma})_{mn} = 1/h \sum_e \frac{\langle n|\mu_\sigma|e\rangle\langle e|\mu_\sigma|m\rangle}{\nu_{em}-\nu_o+ i\Gamma e} + \frac{\langle n|\mu_\sigma|e\rangle\langle e|\mu_\sigma|m\rangle}{\nu_{en}+\nu_o+ i\Gamma e} \qquad (2.4)$$

and the sum goes over the excited vibronic states, e, of the molecule.

When $\langle e|\mu|m\rangle$ is finite for a real state $|e\rangle$, the transition from $|m\rangle$ to $|e\rangle$ is accompanied by light absorption which would have the center of frequency at ν_{em} and full width at half maximum of $2\Gamma e$, and the absorption intensity would be proportional to $|\langle e|\mu|m\rangle|^2$. If the photon energy of Raman excitation ($=h\nu_o$) were close to the energy of the electronic transition, the first term of $(\alpha_{\rho\sigma})_{mn}$ and thus I_{mn} would be remarkably large. This is called resonance Raman scattering. The vibrational modes which gain resonance enhancement in intensity are limited to the vibrations involved in the chromophore responsible for the absorption band.

In Born-Oppenheimer adiabatic approximation [5] the main term contributing to the polarizability tensor of equation (2.4) under resonance with a particular electronic state, $|r\rangle$, are the following:

$$(\alpha_{\rho\sigma})^{r}_{ij} = (A_{\rho\sigma})^{r}_{ij} + (B_{\rho\sigma})^{r}_{ij} \tag{2.5}$$

where

$$(A_{\rho\sigma})^{r}_{ij} = \frac{M_{\sigma}^{gr} M_{\rho}^{gr}}{h} \sum \frac{\langle j|v\rangle\langle v|i\rangle}{\nu_{rg}+(v-i)\Delta\nu_{a}-\nu_{o}+ i\Gamma r} \tag{2.6}$$

and

$$(B_{\rho\sigma})^{r}_{ij} = \frac{M_{\sigma}^{gr} h_{a}^{rs} M_{\rho}^{sg}}{h^{2}(\nu_{r}-\nu_{s})} \sum_{v} \frac{\langle j|q_{a}|v\rangle\langle v|i\rangle}{\nu_{rg}+(v-i)\Delta\nu_{a}-\nu_{o}+ i\Gamma r} +$$

$$\frac{M_{\sigma}^{gs} h_{a}^{sr} M_{\rho}^{rg}}{h^{2}(\nu_{r}-\nu_{s})} \sum_{v} \frac{\langle j|q_{a}|v\rangle\langle v|i\rangle}{\nu_{rg}+(v-i)\Delta\nu_{a}-\nu_{o}+ i\Gamma r} \tag{2.7}$$

where $M_{\sigma}^{gr} = \langle g^{o}|\mu_{\sigma}|r^{o}\rangle$, $h\nu_{rg}$ is the energy separation between $|r\rangle$ and $|g\rangle$, $\Delta\nu_{a}$ is the frequency of the normal mode with coordinates q_{a} and h_{a} is a vibronic coupling operator $(\frac{\delta H}{\delta q_{a}})$ for a normal mode q_{a}.

Thus when Raman spectra are obtained with excitation in the region of an electronic absorption band, the vibrational modes which are expected to show enhancement are the ones which contribute intensity to the electronic spectrum, i.e., they are vibronically active modes. These are of two types: (i) modes which connect the ground state to the excited state involved in the resonance through the Franck-Condon (FC) overlap (A-term);

(ii) modes which mix the resonant electronic state to another one of higher energy (B-term).

Since A-term is the leading term, it is generally the dominant contribution to RR intensity.

Non-totally symmetric modes, however, can gain intensity via the B-term because of Q-dependent vibrational integrals.

2.1.3 Infrared Absorption

The Infrared (IR) absorption to a first order approximation, arises due to change in electric dipole moment ($\vec{\mu}$) of the molecular unit during its excitation to a higher energy state. It may, however, also arise due to change in electric moments of higher order, magnetic moments etc., but the absorption induced by such interactions is negligibly weak. For example, if a typical transition induced by the electric dipole moment is assumed to take place at a rate of 10^{8} sec^{-1}, the transitions induced by magnetic dipole and electric quadrupole moments are expected to take place at a rate 10^{3} and 1 sec^{-1}, respectively [6]. The spectrum is obtained by dispersing the radiation using a prism or grating and analyzing each frequency sequentially, and using a narrow exit slit to prevent all the other frequencies from reaching the detector. There is, however, another method by which each frequency in the spectrum can be

distinguished. This is done by the use of a interferometer i.e. Fourier Transform Infrared (FT-IR) spectroscopy.

FT-IR spectroscopy is based on the interferometric pattern of the IR radiation which is developed recently as a routine vibrational technique after the development of high speed computers. The spectra of broad band sources could not be accurately derived from the interference pattern or interferogram, since the two are related by a complex numerical operation known as the Fourier transform. FT-IR instruments are based on Michelson interferometer.

In Michelson interferometer (Figure-2.1) a beam is divided into two parts with the aid of a beam splitter. Then the splitted beams are again reconstructed after the introduction of a path difference using a movable mirror giving an optical path difference (distance travelled by the movable mirror) of $\lambda/4$ to $\lambda/2$. When the distance of the movable mirror and the fixed mirror (Figure-2.1) are equal, the situation is termed as Zero-Path-Difference (ZPD) and the sinusoidal wave is expressed by

$$f = v/\lambda = v\nu \qquad (2.8)$$

where, v is the constant velocity of the movable mirror and ν is the wavenumber of the monochromatic radiation.

In case of a polychromatic source, all the frequencies will be in-phase at ZPD and will produce a varying degree of destructive interference at all other distances. Thus, the

intensity of the cosine waves will be a function of the distance, d, travelled by the movable mirror and $I(d)$ will be proportional to $\cos(2\pi\nu d)$. This is called an interferogram. The interferogram resulting from one stroke movement of the movable mirror will be proportional to the sum of the cosine waves:

$$I(d) = \sum_i A_i \cos(2\pi\nu_i d) \qquad (2.9)$$

where, A_i is the maximum amplitude for each ν_i. Maximum amplitude of the interferogram will be obtained at d=0. This is an ideal situation with 100% efficiency (of the beam splitter etc.). In practice, A_i is substituted by $B(\nu)$, which depends on the instrumental characteristics, and the equation becomes

$$I(d) = \int_{-\infty}^{\infty} B(\nu) \cos(2\pi\nu d).\, d\nu \qquad (2.10)$$

Then the interferometric data is fourier transformed (F-T) into frequency,

$$I(d) \overset{F\text{-}T}{\Rightarrow} I(\nu)$$

and the equation (2.10) becomes

$$I(\nu) = \int_{-\infty}^{\infty} B(d) \cos(2\pi\nu d).\, dd \qquad (2.11)$$

From $I(\nu)$ and $I_o(\nu)$, values I_o/I is obtained and absorbance, A, is plotted as $\log(I_o/I)$. Resolution is determined by the distance by which the mirror moves.

2.1.4 IR Band Intensity

The intrinsic absorption corresponding to a transition between $|f\rangle$ and $|i\rangle$ state is given by

$$dI(\nu) = -hc\nu I(\nu)\, B_{fi}\, (N_i - N_f)dl \qquad (2.12)$$

where, B_{fi} is the Einstein co-efficient related with the transition moment as

$$B_{fi} = \left(\frac{8\pi^3}{3ch^2}\right) \left|\langle f|\vec{\mu}_\rho|i\rangle\right|^2 \qquad (2.13)$$

$\nu = \nu_{fi} = (E_f - E_i)/hc$, N_i and N_f are the number of molecules per unit volume in the initial and final stage, respectively, $I(\nu)$ is the intensity of light beam at frequency after traversing a distance dl in the absorbing medium and $dI(\nu)$ is the absorbed intensity at the same frequency.

Since, the population of excited centers N_f can be considered to be negligibly small compared to N_i, equation (2.12) can be recast as

$$dI(\nu) = -hc\nu I(\nu)\, B_{fi}\, N_i\, dl \qquad (2.14)$$

Moreover, equation (2.14) can also be expressed in terms of absorption coefficient a_ν at frequency ν as

$$dI(\nu) = -I(\nu)\, a_\nu\, dl \qquad (2.15)$$

comparing equation (2.14) and (2.15) a_ν can be written as

$$a_\nu = -\frac{1}{I(\nu)}\frac{dI(\nu)}{dl} = hc\nu B_{fi}.N_i \qquad (2.16)$$

On integration, equation (2.15) becomes

$$I(\nu) = I_o(\nu)\ \mathrm{Exp}\ (-a_\nu l) \qquad (2.17)$$

where, $I_o(\nu)$ is the total incident intensity at frequency ν. The equation (2.17) is known as Beer-Lambert Law. From the equation (2.16) we have

$$a_\nu = \frac{1}{l} \log_e \frac{I_o(\nu)}{I(\nu)} = \frac{2.303}{l} \log_{10} \frac{I_o(\nu)}{I(\nu)} \qquad (2.18)$$

and

$$A_\nu = \log_{10} \frac{I_o(\nu)}{I(\nu)} = \frac{1}{2.303} a_\nu . l = k . l \qquad (2.19)$$

where A_ν is absorbance and k is Bunsen-Rascoe extinction coefficient.

In developing equation (2.18), it was assumed that the absorption due to the transition i→f gives rise to an infinitely sharp spectral line. However, a spectral line is always broadened due to uncertainty, the Doppler effect, and the influence of intermolecular forces. Hence, every transition is having some finite width and the integrated absorption over the full band has more significance than the peak absorption. Consequently, the absorption coefficient, a_ν is usually integrated over the full absorption band and expressed in absolute unit as

$$\begin{aligned} a_{int} &= \int_{band} a_\nu \, d\nu \\ &= \frac{2.303}{l} \int_{band} \log_{10} \frac{I_o(\nu)}{I(\nu)} \, d\nu \\ &= \frac{2.303}{l} A_{int} \end{aligned} \qquad (2.20)$$

where, $A_{int} = \int A_\nu \, d\nu$

Most of the commercially available double beam IR

spectrophotometers measure the quantity $I(\nu)$ (c.f. equation no. 2.17), except some spectrometers which measure the quantity A_ν (c.f. equation 2.19). The computation of A_{int} from spectra obtained on either type of the spectrometers become complicated because of the difficulties encountered in measurements of $I_o(\nu)$ and/or 1. However, A_{int} can easily be deduced from the spectra recorded on the later type of spectrometers. A_{int} is only of relative importance. Its approximate value can be found by multiplying peak absorptivity with full width at half maximum intensity (FWHMI).

2.1.5 Band Shapes

For bands well isolated from their neighboring bands, most commonly used functions for describing band shapes are Gaussian i.e.

$$I(\nu) = I(\nu_o)\mathrm{Exp}\left[-\left\{\frac{(\nu-\nu_o)^2}{\underline{a}}\right\}\right] \qquad (2.21)$$

or Lorentzian, i.e.

$$I(\nu) = I(\nu_o)\frac{\underline{b}^2}{\underline{b}^2 + (\nu-\nu_o)^2} \qquad (2.22)$$

These functions are symmetrical around ν_o of the band peak. $I(\nu_o)$ is the maximum intensity at (ν_o), and $\underline{a}$ and $\underline{b}$ are adjustable parameters. For Gaussian band the full width at half maximum intensity is $2\underline{a}\log_e 2$ while that for Lorentzian is $2\underline{b}$.

2.1.6 Electronic Absorption Spectra

The absorbance of light energy by any compound in the visible / ultraviolet region involves promotion of electrons in σ, π and n- orbitals from the ground state to the higher energy antibonding orbitals e.g. σ^*, π^*. As the n electrons can not form bonds, corresponding antibonding orbitals are not there.

The electronic transitions ($\rightarrow$) that are involved in the ultraviolet and visible region are of the following types: $\sigma \rightarrow \sigma^*$, $n \rightarrow \sigma^*$, $n \rightarrow \pi^*$ and $\pi \rightarrow \pi^*$. The energy required for $\sigma \rightarrow \sigma^*$ transitions are very high and $n \rightarrow \pi^*$ are very low whereas $\pi \rightarrow \pi^*$ are of intermediate energy. High energy transitions ($\sigma \rightarrow \sigma^*$) occur at shorter wavelength and the low-energy transitions ($n \rightarrow \pi^*$) occur at longer wavelength.

Most of the recording spectrophotometers record wavelength versus absorbance. The absorbance A or 'optical density' is given by

$$A = \log(I_o/I) \qquad (2.23)$$

where I_o is the intensity of the incident light and I is the intensity of transmitted light. A is also expressed by the equation

$$\varepsilon = A/cl \qquad (2.24)$$

where ε is the molar extinction coefficient, c is the molar concentration, and l is the path length in centimeters.

When the molecular weight of a substance is unknown,

the intensity of absorption is conveniently expressed as the $E^{1\%}_{1cm}$ (or $A^{1\%}_{1cm}$) value, the absorbance of a 1% solution of the substance in 1.0 cm cell. This value is easily related to the molar extinction coefficient by expression

$$10\varepsilon = E^{1\%}_{1cm} \text{ x mol.wt.} \qquad (2.25)$$

2.2 INSTRUMENTATION

2.2.1 Raman Measurement Setup

A set of instruments are used for recording the Raman spectra. These consist of Laser (with power supply), Monochromators, Photomultiplier tube, Spectrophotometer control etc. besides accessories like plasma filter etc.

2.2.1.1 Laser

The Argon ion laser used (Spectra-Physics Model 165-09 Argon Ion Laser) is a CW laser and consists of the laser head and model 265 Exciter.

The laser head consists of a beryllium oxide (BeO) plasma tube terminated at each end by fused-silica Brewster's angle windows, a solenoid for providing necessary magnetic field and an optical resonator. The plasma tube is mounted in an optical cavity resonator formed by spherical reflector at the output and a prism and flat mirror assembly at the high reflector end. The whole assembly of the resonator is held solidly against

quartz rods with springs to minimize microphonic frequency shifts. The plasma tube is supported on a kinematically adjustable mount and is adjusted in such a way that the plasma tube is exactly centered. Wavelength selections are achieved by rotating a thumb wheel control on the rear side of the laser head.

The (spectra physics model 265) exciter is fully equipped with the necessary electric and electronic circuit to achieve regulated ion discharge current in the plasma tube and thereby control the output power from the laser by simultaneously regulating the solenoid circuit. The 265 Exciter is fed with stabilized three phase 230 V (phase to phase) power line. This unit requires cooling of the transistor pass bank in the exciter, the solenoid and BeO plasma tube which is achieved by circulating distilled and deionized water at $15^{o}C$ at 40 PSI from water chiller plant (from Neslab Model HX 500).

2.2.1.2 Spectrophotometer and Photomultiplier Tube

Raman spectra of different samples were recorded in a 90^{o} scattering geometry with SPEX Ramalog 1403 double monochromator (Figure-2.2 represents the optical diagram of the instrument) equipped with a thermoelectrically cooled RCA 31034 photomultiplier tube and a photon counting arrangement. The spectrometer control and data processing were achieved with the

help of a microprocessor based SPEX DATAMATE and also by computer using DM3000 software. Excitation lines were also obtained from Linconix Model 4240 He-Cd laser apart form Spectra Physics Model 165-09 argon ion laser described above.

The spectrophotometer is a f/7.8 instrument with spectral coverage from 31000 cm^{-1} to 11000 cm^{-1} with an accuracy of $\pm 1 cm^{-1}$ in the 10000 cm^{-1} range. Spectral repeatability is ± 0.2 cm^{-1} and the resolution is 0.15 cm^{-1} at 5719 Å (Hg line, FWHM). The gratings used are holographic type having rulings with 1800 grooves/mm and blazed at 5000 Å. The gratings are mounted on a modified Czerny-Turner mount.

For recording the Raman spectra, the laser beam is passed through the (SPEX Model 1459) UVISIR illumination after being filtered from "Lasermate" (SPEX Model 1460), a small unit consists of grating having 1200 lines/mm blazed at 5000Åand a mirror assembly to isolate the spurious plasma lines. The filtered laser beam from the lasermate is then deflected upward (90^{o}) by mirror and focused on to the sample by the fused silica condensing lens. The scattered radiation is then collected by an elliptical mirror (f/1.4) and focused onto the entrance slit (S_3)(Figure-2.2) of the spectrometer after deflecting from the mirror (M_7) and passing through a polarization scrambler. The polarization scrambler converts plane-polarized scattered radiation to circularly polarized radiation before it reaches the

spectrometer and thus cancels variations in spectrometer response that result from polarization dependent efficiencies. The polychromatic scattered radiation focused onto the entrance slit gets dispersed by the 1800 lines/mm holographic gratings (G_2 and G_3). Thus finally nearly monochromatic light signal of frequency cm^{-1} selected by spectrometer control reaches the exit slit (S_7) of the double monochromator.

2.2.1.3 Spectrometer Control and Data Processing

The spectrometer control (frequency scanning) and data processing were carried out through a 8-bit dedicated microcomputer SPEX "DATAMATE" with the help of the in built software, it is possible to manipulate the spectral data for background subtraction, integration, addition, division, frequency range and intensity range expansion/reduction, differentiation etc., whenever necessary. The incoming spectral data as well as the manipulated data array could be stored in the 4K data point storage in any of the eight variable length files. The stored data could be plotted on a strip chart recorder or transferred to external peripherals, e.g., floppy discs or to a PC through the standard RS 232 port for further manipulation of data. The unavoidable wavelength dependent distortions to the spectral data from the spectrometer optics could be erased by applying the radiometric corrections from the in built 1K EAROM.

Using the programming option, the entire spectrometer control as well as data collection and manipulation could be completely automated. The data storing facility could be bypassed and real time spectra could be recorded in the strip chart recorder. Some of the spectra were recorded using a PC having a software DM3000. This software is capable of manipulations of data e.g. addition, subtraction, etc. In this case it was possible to copy the spectral data in a floppy disk.

The photomultiplier tube (model RCA 31034) is a 11-stage QUANTACON photomultiplier having a gallium arsenide chip as its photo cathode, an ultraviolet transmitting glass window and an in-line copper beryllium dynode structure. This tube is cooled to $-30^{o}C$ by a thermoelectric cooling device and has a almost linear absolute response in the 3000Åto 8500Å wavelength range and operated for current gain of 10^{6} with a maximum dark pulse summation of 12 CPS (counts per second).

2.2.1.4 Scanning of Raman Spectra

There are number of difficulties associated with recording the Raman spectra of colored samples under resonance conditions. The most prominent include (a) the optimization of the concentration of the scattering species in the solution to minimize reabsorption of the scattered light by the sample and at the same time allowing the scattering to be maximum, (b) the

local heating of the sample due to absorption of exciting line which may give rise to thermal lens effect and also lead to thermal decomposition of the sample, (c) the strong background due to fluorescence from impurities in the compound or in the solvents or intrinsic fluorescence from the sample itself.

The first one can be taken care by using samples of different concentrations until a good quality spectrum is obtained. To avoid local heating effect Kiefer and Bernstein [7,8] had developed a technique which involve continuous rotation of the sample with respect to the laser beam. In this case, as the sample rotates continuously, the portion of the sample from which light scattering takes place due to laser irradiation, remains in the laser beam only for a short period of time and thereby reducing the local heating and thermal decomposition. To reduce the fluorescence background, Raman spectra could be measured in the solid form in KBr pellet. However, to obtain vibrational information from solution, it is always better to get rid of impurities from compounds and solvents that are in use by usual purification methods.

To record Raman spectrum of liquid, 2-3 ml solution of respective compound at an appropriate concentration is taken in a cylindrical cell and positioned in the proper mount. The laser beam at a selected wavelength is then made to strike the bottom edge of the cell. In this way, the self absorption of the

scattered light is minimized. The spectra were routinely calibrated with known CCl_4 lines in the lower region (100-500 cm^{-1}) and with Indene in the higher frequency region (1300-1675 cm^{-1}) and sometimes using the internal standard of the bands. Other spectral parameter such as laser power, integrating time, wave number increment, slit width etc. are adjusted time to time in order to optimize signal to noise ratio. For weak Raman signals, 3-4 spectra were averaged with the help of datamate.

2.2.2 Dispersive Infrared Instrument

A Perkin-Elmer (model 983) dispersive Infrared Instrument was used for the present work. This is a dual beam having f/4.2 monocromator with four gratings and nine filters and uses a coated CsI lens and thermocouple as the detectors. This spectrophotometer covers the 5000 to 180 cm^{-1} frequency range. The resolution used was 1-0.5 cm^{-1}. Repeated spectral data acquisition and absorbance expansion facilities are also available with the spectrometer

2.2.3 FT-IR Instrument

FT-IR instrument used was a BOMEM-DA-8. Optical diagram of the instrument is shown in Figure-2.3.

Various sources are used in this instrument for different regions. Globar is used for the range 125 to 7000 cm^{-1},

whereas, high pressure Hg lamp is used for 10 to 500 cm^{-1}.

In this instrument, interferometer uses a beam splitter for dividing the beam into two parts. A stretched Mylar pelicle of different thickness for FIR range and alkali metal halides are used for the purpose.

Room temperature DTGS is used as detector. These detectors operate at room temperature and being a thermal device, it possesses essentially flat wavelength response ranging from NIR to FIR.

Mirror alignment is an important step for the recording of spectra in FT-IR instruments. For high resolution, instruments mirrors are required to move in excess of 20 cm^{-1}, which is quite critical. In BOMEM instrument this is achieved with dynamic alignment. Here, the phase of the interference pattern at two positions are measured and whenever any disturbance is measured, an error signal is generated, which in turn is fed to the motor kinematics of the fixed mirror (Figure-2.3). The fixed mirror is then adjusted with the error signal. The process is repeated until the error signal comes to zero. This process is very fast and for working mirror velocities, are able to maintain very good alignment. Should the alignment not maintain, the scan would be aborted. Fast fourier transformation (FFT) is done through DEC 3100 work station.

2.2.4 Sample Handling Techniques for Solids Samples

There are different techniques to prepare the solid samples. Among them KBr pellets and Nujol (mineral oil) Mull techniques are the more commonly used sample preparation methods for solids. Both are used in the present work.

In KBr disc technique a very small amount of finely ground solid sample is intimately mixed with powdered KBr and then pressed in an evacuated die under high pressure. The resulting discs are transparent and yield excellent spectra.The only infrared absorption by KBr matrix is from small amount of absorbed water in the powder. However, this can be confused with the OH absorptions in the sample. Care was taken to avoid any moisture absorption during pellet preparation and the background of the pellets were recorded routinely. Similar technique using polyethylene pellets is also used for some samples, especially, in FT-IR.

Another extremely valuable technique for solid samples is the mineral oil (Nujol) mull technique. A small amount of solid sample is mulled in a mortar with small amount of Nujol to yield a paste which is then transferred to a rock salt plate or the sample may be mulled directly between the plates. The small scratches that result from this later method can be completely removed from the plate when it resurfaced.

2.2.5 Specialized IR measurement Techniques Used in the Present Work

2.2.5.1 Diffused Reflectance Infrared Fourier Transform (DRIFT)

The basic principle behind diffused reflectance spectroscopy is that light impairing on a solid or powdered surface diffusively scattered in all directions (Figure-2.4). The scattered light is collected with a proper optical setup and directed to the detector. The high sensitivity, selectivity to detect surface species, and the non-destructive sample preparation procedure used for DRIFT experiments are valuable characteristics of the technique. BARNES-SPECTRATECH make, center focus version of diffused reflectance cell was used in the present work.

2.2.5.2 Temperature Dependent Variable Cell for IR Spectra

The room temperature as well as temperature dependent spectra were recorded in PE-983 spectrophotometer using nujol mull technique and placing the slurry in CsI windows which were mounted in a specially designed cell (SPECAC). The inner window were of CsI, whereas the outer window were of NaCl type. The cell was evacuated before starting the experiment. Subsequently, the sample temperature was varied by heating the sample holder

through an electric heater. Temperature monitoring and controlling was achieved by a copper-constanton thermocouple also fixed very close to the sample.

2.2.6 Electronic Absorption Spectrophotometer

The electronic absorption spectra were recorded in a Shimadzu UV-VIS model 160A spectrophotometer. The model could be used for measuring transmittance and absorbance of liquid, solution etc. in the visible and ultraviolet region. The instrument is capable of measuring negative absorbance. Manipulation of data e.g., derivation etc. are also possible.

The optical diagram of the instrument is depicted in Figure-2.5 . The light emitted from the light source passes through grating monochromators and a filter for preparing a monochromatic beam and then split into two beams. After passing through the sample compartment, the monochromatic sample and reference beams are detected by photodiode detectors, logarithmically converted, and their difference is obtained by a differential amplifier. The signal then passes through two amplifier, 1 and 2. Amplifier 1 serves to finely adjust the signal level and amplifier 2 serves to apply a GAIN up to 10 fold to the signal. Then, after being A/D converted, the signal is read by CPU and displayed on the monitor. The plot could also be recorded on a thermosensitive chart paper. This instrument

operates between the wavelength range Of 200 to 1100 nm with ±0.5 nm wavelength accuracy (with automatic wavelength correction). Spectral band width (resolution) is 2 nm with wavelength repeatability of 0.1 nm.

2.3 DATA PROCESSING AND RESOLUTION ENHANCEMENT FOR QUANTITATIVE SPECTROSCOPY

A number of mathematical manipulations were used to obtain quantitative information from the measured spectra. These are described in brief in the section followed.

2.3.1 Frequency and Band Width Measurements

This is the first step to analyze any spectrum. For the assignments as well as for quantitative estimation for a particular sample it is of immense importance. Due to digitalization of the spectra, the data points are encoded at frequency intervals with a very highly reproducible wave number scale, regardless of the resolution. Either of two algorithms can be used for peak position determination, namely the center of gravity or the least square algorithm. Band width measurements are obtained using a relative simple algorithm which measures half-width at half-height (HWHH) or full width at half maximum intensity (FWHMI) or the width at any fraction of the peak height.

2.3.2 Difference Spectroscopy

Difference spectroscopy is used for solvent correction, especially for the studies of proteins. In case of IR (or FT-IR), because of this manipulation only protein spectra in aqueous solution could be recorded. Water is a very strong absorber and thus interferes with the protein spectrum. Therefore, subtraction must be accomplished before studying the protein spectrum. Otherwise, D_2O solution must be used. Furthermore, difference spectroscopy is very useful to study the small changes in the conformation of biological molecules.

2.3.3 Deconvolution

Amide I region of protein comprises of a broad and overlapped bands. Thus it becomes very difficult to assign different structural contributions separately. Introduction of fourier deconvolution achieves band narrowing in the spectrum at the expense of signal to noise ratio [9-11].

The basis for deconvolution [9-10] is that any recorded spectrum can be considered as a convolution of a known line shape with a true spectrum. The spectrum is then distorted by the instrumental line shape function. Molecular dynamics studies show that the true profile (of an infrared band) can be expressed as a Lorentzian (or Cauchy) function. A real spectrum also contains noise. In deconvolution, the noise will be weighed

with an exponential that increases with time. Therefore, following deconvolution the noise will be no longer random, but highly periodic and will appear across the whole spectrum. In practice, maximum band narrowing is limited by noise and instrumental resolution.

The use of fourier deconvolution of unknown samples requires only the assumption of the initial bandwidth. Underestimation of the bandwidth leads to a incomplete band separation maintaining a high degree of Lorentzian character. Overestimation yields the appearance of undesired side lobes. If the bands to be separated have the same HWHH, bandwidth is reduced until negative sidelobs appear. However, composite bands with different bandwidths in their components are commonly found. In such a situation there can be no unique set of optimal conditions but, avoiding over-deconvolution, a partial band separation can be of use to identify the overlapped components. Band height will not then be useful as a quantitative criterion in comparing the relative contribution of bands of different widths, since deconvolution will affect each component in a different way.

2.3.4 Curvefitting

Curvefitting is an useful technique to visualize the components of any broad, overlapping band. This is very much

useful for the quantitative studies of proteins, particularly the amide I band. The component bands of the amide I region are visualized by reducing their bandwidth without interfering the peak positions, although at the expense of signal to noise ratio.

The mathematical solution to amide I band curvefitting by the least squares procedure is not, in principle, unique, but restrictions can be applied because some of the solutions do not agree with the theoretical basis, i.e. bands with negative heights, widths larger than the HWHH of the amide I band, high-frequency component of β-sheet structure larger than 1/10th of the low-frequency component intensity, etc. Thus, it should be used carefully, at least for the quantitative studies.

References

1. G.Herzberg, in *Infrared and Raman Spectra of Polyatomic Molecules*, Vol.2, Van Nostrond Reinhold Co., New York, (1945).

2. J.Tang and A.C.Albrecht in *Raman Spectroscopy*, Ed. H.A. Szymanski, Vol.2, Plenum, New York, (1970).

3. D.A.Lond in *Raman Spectroscopy*,McGraw-Hill, New York (1977).

4. H.A.Kramer and W.Heisenberg, *Z. Physik.*, 31, 681 (1925).

5. G.Herzberg, in *Electronic Spectra of Polyatomic Molecules*, Van Nostrond Reinhold Co., New York, (1960).

6. C.J.H.Schutte, in *The Theory of Molecular Spectroscopy*, Vol.1, North-Holland, Amsterdam, (1976).

7. W.Kiefer and H.J.Bernstein, *J. Appl. Spectrosc.* 25, 500, (1971)

8. W.Kiefer and H.J.Bernstein,*J. Appl. Spectrosc.* 25, 609, (1971)

9. J.K.Kauppinen, D.Moffat, H.H.Mantsch and D.G.Cameron, *Appl. Spectrosc.*, 35, 271 (1981).

10. J.K.Kauppinen, D.Moffat, H.H.Mantsch and D.G.Cameron, *Anal. Chem.* 53, 1454 (1981).

11. D.G.Cameron and D.Moffat, *J. Test Eval.* 12, 78 (1984).

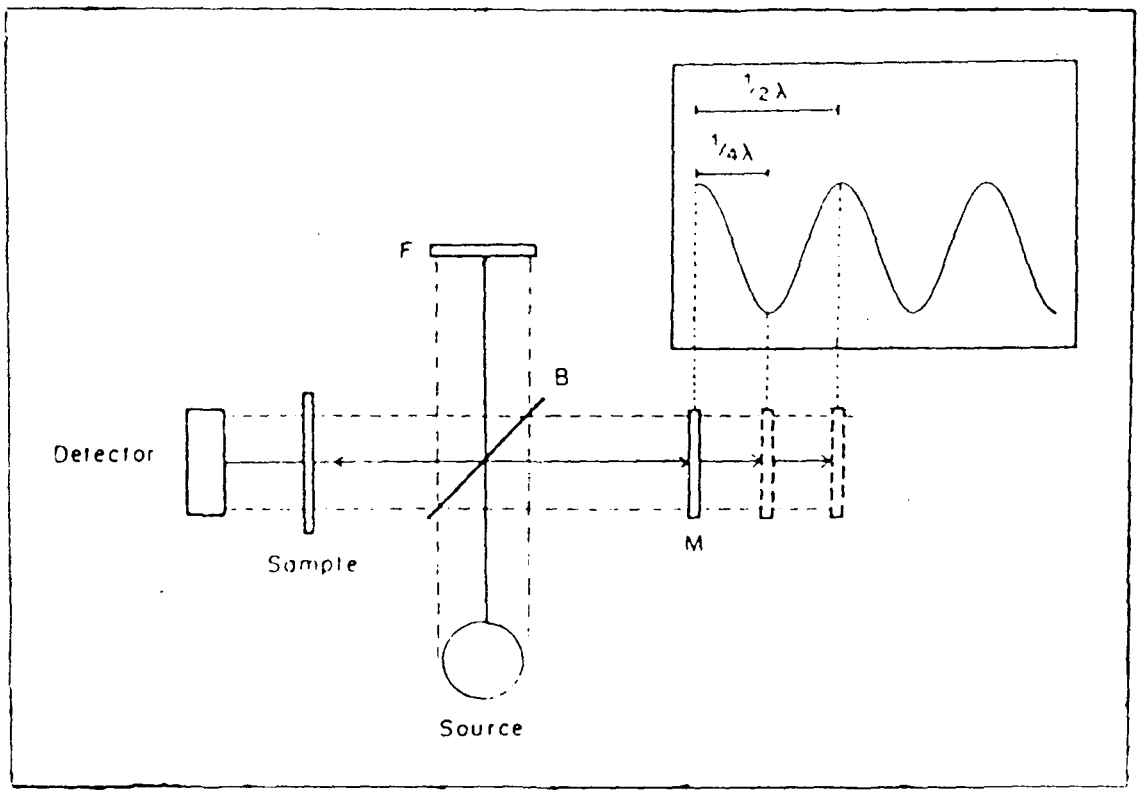

Figure-2.1 Michelson Interferrometer. B is beam splitter, F is fixed mirror and M is movable mirror.

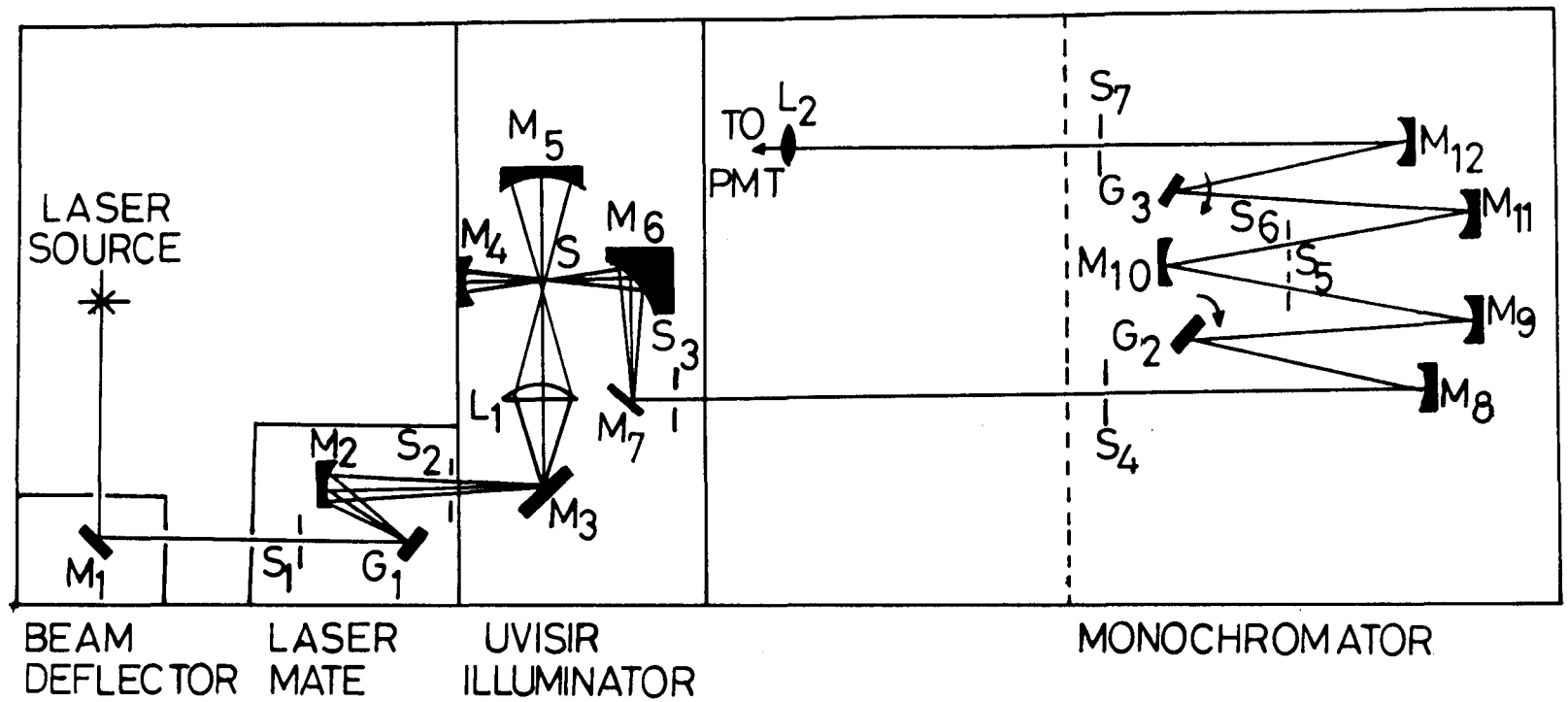

Figure-2.2 Optical Diagram of a SPEX model Ramalog 1403 laser Raman Spectrophotometer including the lasermate and UVISIR illuminator. M_1, M_3, M_7, M_{13}-M_{16} are the plane mirrors; M_2, M_4, M_5, M_8, M_9-M_{12} are concave mirrors; M_6 is elliptical mirror; S_1-S_8 are slits; L_1 is fused silica condenser lens; L_2 is field lens; S is sample; G_1-G_3 are the gratings and PMT is the photomultiplier tube.

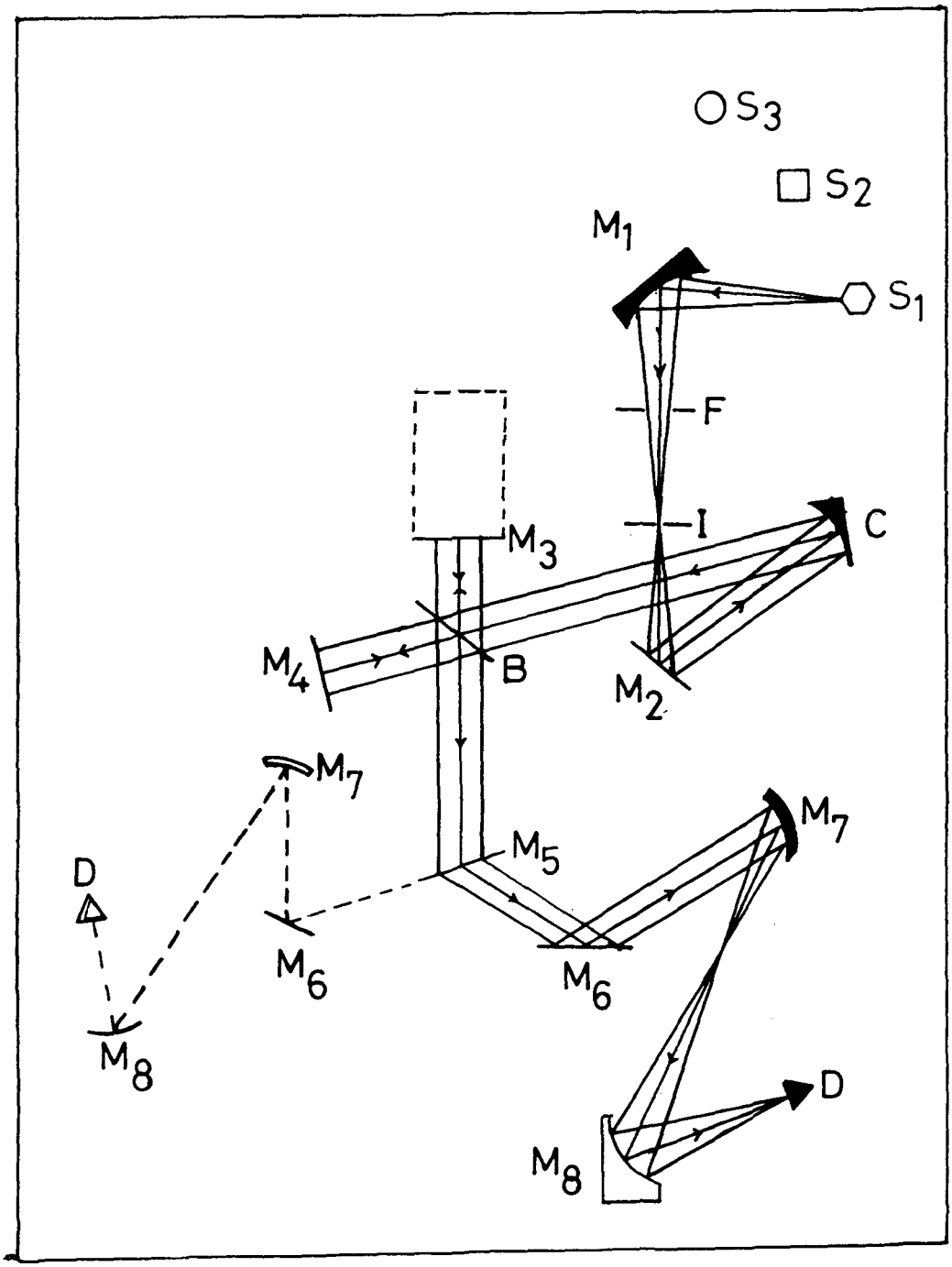

Figure-2.3 Optical Diagram of BOMEM-DA-8 FT-IR Instrument. S_1-S_3 are the sources, M_1-M_8 are the mirrors, M_3 being the movable mirror, F is filter wheel, I is iris, C is collimator, B is beam splitter and D is the detector. M_1, F, I, M_3, M_5 are controlled by computer.

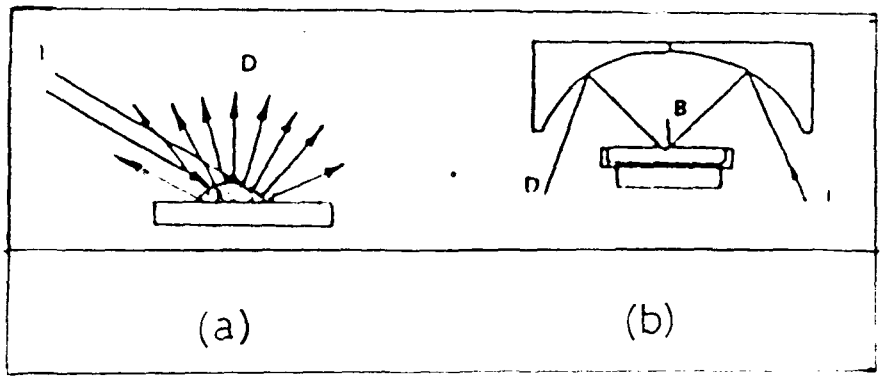

Figure-2.4 Schematics of (a) DRIFT attachment and (b) blocking device

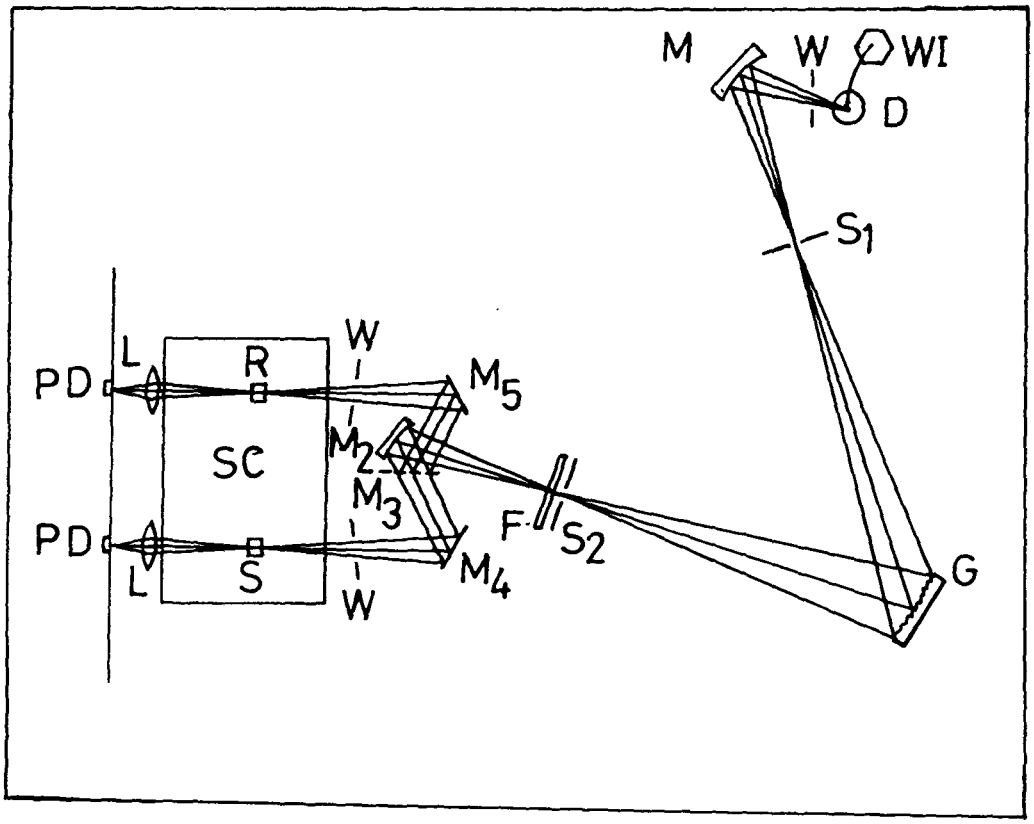

Figure-2.5 Optical Diagram of Shimadzu 160A UV-VIS Spectrometer. D is deuterium lamp, W is window plate, WI is halogen lamp, M_1-M_5 are mirrors, M_3 is a half-mirror, F is filter, L is lens, G is grating, S is Sample cell, R is reference cell, S_1 is entrance slit, S_2 is exit slit, PD is photo diode.

CHAPTER - III

RAMAN, INFRARED AND FOURIER TRANSFORM INFRARED STUDIES ON PROTEINS AND CROSSLINKERS : ISOLATION, PURIFICATION AND STRUCTURE DETERMINATION OF GELONIN

This Chapter presents the purification and spectroscopic characterization of proteins under investigation. Observed vibrational modes are assigned. Secondary structure of Gelonin and Bovine Serum Albumin (BSA) has been estimated from the Raman spectroscopic data. BSA contains nearly 50% α-helix and the remaining is due to turn and random structure. Gelonin is having mainly α-helix and β-sheet structure with some turn and disordered structure. The estimated percentage, being $\approx$ 32% α-helix, $\approx$ 20% β-sheet, $\approx$ 26% turn and $\approx$ 22% disorder type. The temperature dependent Infrared study of Gelonin reveals its thermal stability; the denaturation temperature as estimated is around 60^{o}C and disordered contribution increases with increasing temperature. Two cross-linking agents, SPDP and LC-SPDP have been studied spectroscopically and their geometry have been deduced. It has been argued that LC-SPDP has less torsion around C-S-S-C bond in comparison to SPDP.

Based on these studies, following papers have been published:

1. Vibrational studies on heterobifunctional crosslinking agents N-succinimidyl3-(2-pyridyldithio)propionate and N-succinimidyl 6-[3-(2-pyridyldithio)propionamido]hexanoate and theoretical elucidations.
   Biswajit Pal, P.K. Bajpai Jayati Sengupta and Vinod Singh
   J. Raman Spectrosc. 28 323, 1997.

2. Spectroscopic Characterization of A Protein - Gelonin: Assignments, Secondary Structure and Thermal Denaturation
   Biswajit Pal and P.K.Bajpai
   Indian J. Biochem. Biophys. (Communicated)

3.0 INTRODUCTION

Ribosome Inactivating Proteins (RIPs) are attracting considerable interest for their possible use as immunotoxins and hormonotoxins which could selectively destroy malignant cells [1-2]. RIPs effectively arrest the protein synthesis in Eukaryotic cells and are widely distributed over the plant kingdom [3]. The concentration of RIPs is highly variable from plant to plant and also among different tissues of the same plant. Also, the different tissues of RIP producing plants may vary considerably from species to species.

Two classes of RIPs exist in nature [3]. One class of RIP is having two subunits : chain A and chain B. Chain B acts as the binding subunit and it binds with the receptor for internalization and chain A acts as the toxic subunit which essentially arrests the protein synthesis. This class of RIPs is designated as type 2. On the other hand type 1 RIPs are having only one subunit which resembles the chain A of type 2. Type 1 RIPs can not enter the intact cell as they are lacking binding subunit. On the contrary, type 2 RIPs enter the cell but they are less potent to kill cells as these are non-specifically active against the whole cell. Thus the concept of conjugates viz. immunotoxins and hormonotoxins emerged.

RIPs arrest protein synthesis by damaging the larger ribosomal subunit (60S) irreversibly [3]. The effect of RIPs on

ribosomes is due to the enzymatic activity of type 1 RIPs and of A chain of type 2 RIPs, which are highly specific *N*-glycosidases and cleave the *N*-glycosidic bond of at least one particular adenine in rRNA [4-5]. As a consequence, the elongation factors cannot bind to ribosomes and this inhibit protein synthesis.

Gelonin is a type 1 RIP isolated from the seeds of a plant *Gelonium multifluorum* of *Uphorbiaceae* family. It is a glycoprotein having molecular weight of about 30 kD and is strongly basic in nature (pI ≈9.5). It lacks a binding or lectin subunit and thus is generally not highly toxic to intact cells. Like other RIPs, Gelonin is also an RNA glycosidase and cleaves the glycosidic bond at a unique adenine base in the 28S rRNA, thereby inactivating protein synthesis. Several investigators have covalently linked it with different carrier proteins and studied their specific toxicity [6-7]. However in the absence of secondary structure known, it was very difficult to understand the changes leading to varied levels of toxicity with different systems.

For the specific killing of the cells, hybrid molecules like hormonotoxins or immunotoxins were synthesized using heterobifunctional crosslinking agents [8-11]. These crosslinkers also play a novel role to induce immune response against protein/peptide [8,12]. N-Succinimidyl-3-(2-pyridyldithio) propionate (SPDP) and N-Succinimidyl-6-[3'-(2-pyridyldithio)

propionamido]hexanoate (LC-SPDP) are the most commonly used crosslinkers [Figure-3.1].

It has been reported that the bioefficacy of the conjugate molecules increases if it is modified through LC-SPDP instead of SPDP [13]. This difference in bioefficacy as a result of modification is not properly understood. The enhancement (in bioefficacy) in case of LC-SPDP is correlated with the less steric hindrance between the crosslinked proteins because of the longer spacer arm of the LC-SPDP molecule in comparison to SPDP molecule.

It is known that SH group in proteins, which binds with these agents to form conjugates, may form disulfide bridges having different conformation in different crosslinkers. This depends upon the conformation around the C-S and S-S bonds in crosslinkers. Obviously, the conformational changes may be induced in the protein as a result of its binding with crosslinker, leading to change in the bioefficacy of the same protein if the crosslinking molecule is changed. Thus the geometry around these bonds in crosslinkers may be crucial in deciding the activity of the conjugate formed. An obvious question which emerges is whether there exist any correlation between the conformational state of the conjugate molecule and its activity. This can be addressed if one starts with the study of the structure of the crosslinker in its native state and

analyses the conformational sensitivity in the region of binding.

Vibrational spectroscopic techniques provide an important tool to investigate such differences in structure. This is due to the fact that C-S and S-S moieties give rise to very strong Raman bands which are sensitive to the changes in the local environment. Comparative vibrational analysis of ν_{C-S} and ν_{S-S} may, therefore, provide some clue about the differences in the -C-S-S-C- geometry in the two systems, if any. Further, as these crosslinkers contain disulfide (pyridyl disulfide) residues, they may be used as model compounds for the study of ν_{S-S} and ν_{C-S} too.

On the other hand, function and activity of proteins are generally depend upon their characteristic folding and on specific interaction of adjacent polypeptide chains and the change in activity can be correlated with the change in conformation. The knowledge of secondary structure and the induced changes in them with pH and temperature are a priori to understand the biological activity of proteins.

In this chapter we present a systematic vibrational study of Gelonin to assign different vibrational modes and to understand the structural aspect of this protein as well as the changes in the structure/conformation with temperature. BSA has also been incorporated for comparison. The Raman intensities of amide I band profile of proteins are taken for the quantitative

estimation of the structural content using two different methods.

To establish the thermal stability of the protein, Infrared (IR) spectra of Gelonin along with the denatured analogous in a wide range of temperature (25°C to 100°C) is investigated in Nujol Mull.

To make assignments more reliable, Diffused Reflectance Infrared Fourier Transform (DRIFT) spectrum has been recorded for Gelonin and also for Bovine Serum Albumin (BSA) for comparison. Since, Gelonin and its antibody have same type of IR spectra and our main interest is on Gelonin, DRIFT spectra of antibody is not presented here. It is also noticed that DRIFT can yield better result in analyzing the secondary structure of proteins. Besides, structural changes due to the carbohydrate moiety present in Gelonin is also studied.

Besides Gelonin, vibrational studies of SPDP and LC-SPDP are also presented. These compounds could be used as models for C-S and S-S stretching vibration along with the conformational determination of C-S-S-C geometry.

3.1 EXPERIMENTAL

3.1.1 Material

3.1.1.1 Gelonin

The seeds of *Gelonium multifluorum* were purchased from M/s United Chemicals & Allied Products, Calcutta. Dry, deshelled

seeds were used for Gelonin isolation. Gelonin used in the present investigation was judged to be over 98% pure.

3.1.1.2 Bovine Serum Albumin

Bovine Serum Albumin, fraction V, both fatty acid free and with fatty acids were from Sigma Chemical Co., USA.

3.1.1.3 SPDP and LC-SPDP

Heterobifunctional crosslinking reagents, SPDP and LC-SPDP were purchased from Pierce Rockford, (IC, USA) were of highest purity grades available and were used without further purification for recording the spectra.

3.1.1.4 Reagents

All other reagents used were of analytical grade and were used without further purification. Double distilled water was used throughout the experiments.

3.1.2 Gelonin Isolation and Purification

Three different methods have been reported in the literature [14] for its isolation. Cation exchange and gel filtration chromatography (method I); salt precipitation followed by cation exchange and gel filtration chromatography (method II) and cibacron blue dye binding affinity chromatography (method III). However, reports suggest that protein isolated using various methods has almost the same physico-chemical and immunological properties. Gelonin was isolated by first two

methods (method I and method II) for our study as described bellow.

Method I

In this method, the following protocol is used as reported in literature [14]. Seeds of *Gelonium multifluorum* were deshelled and soaked overnight in sodium phosphate buffer (pH 7.2 5mM) with 0.1M NaCl in ten times volume of buffer. Soaked seeds were blended in blender with ice cold solution of the same type of fresh sodium phosphate buffer. Slurry was left stirring overnight at $4^{o}C$ and then filtered through cheese cloth/ strainer. Filtered solution was centrifuged at 8000 rpm for 10 minutes. The precipitate was reextracted with the same buffer. The supernatant of both extractions were dialyzed extensively against 0.05M sodium phosphate buffer (pH 6.5, without NaCl) and passed through CMC-52 column (3.2x40 cm). The column was extensively washed with the equilibriation buffer until eluate showed absorbance less than 0.05 at 280 nm. The bound material was then eluted by applying a linear gradient of 0-0.3 M NaCl in the same buffer at flow rate of 30 ml/hr at $4^{o}C$. The protein eluting between 0.15-0.20 M NaCl gradient was pooled, concentrated and subjected to gel-filtration chromatography on a pre-calibrated Sephadex G-100 (3.4x110cm) column. The column was washed with 0.05 M ammonium bicarbonate. The protein eluting at ~30kD was collected and lyophilized directly. The lyophilized

protein was rechromatographed on the same G-100 column.

Method II

As described above, the deshelled seeds were soaked with four times of extraction buffer (0.05M sodium phosphate buffer containing 0.01M NaCl and 0.001M EDTA) and blended in the presence of seven times more of extraction buffer. The recovery of supernatant and re-extraction were the same as described in Method I. The supernatant was precipitated with ammonium sulphate and the precipitate of 45-90% fraction was dissolved in 0.01M sodium phosphate buffer (pH 6.5) containing 0.02M NaCl and dialyzed extensively against the same buffer. The dialyzed protein was then centrifuged to remove the precipitated protein prior to its passing through CMC-52 column. Bound material was eluted by applying 0.02-0.03M NaCl gradient in the same buffer. Further purification was carried out on the gel-filtration column as described above for the method I.

SDS-PAGE pattern Gelonin isolated by two methods are shown in Figure-3.2. Two methods vary in yield and no appreciable difference is found in the spectroscopic data except for the content of carbohydrate moiety. In further studies we have therefore not distinguished among the spectra obtained from Gelonin isolated using different methods.

3.1.3 Spectroscopy

3.1.3.1 Proteins

Raman spectra in the range 1000-1700 cm^{-1} were recorded using 488.0 nm excitation line of Ar^{+} laser and the laser power was 400 mW. A plasma filter was used to screen the plasma lines. The experimental slit width was 5 cm^{-1} for all the experiments. Increment was 0.25 cm^{-1} and integration time was 2 sec. A sum of 5 to 10 scans were used. Buffer solutions of proteins were used (Phosphate buffer for pH 7.2). Protein in buffer solution was first centrifuged at 5000rpm for 15 minutes. Then it was filtered through the millipore filter. The concentration of the solutions were $\approx 10^{-4}$M. Then the solution was mounted on a rotating Raman cell and kept under laser irradiation for 10 minutes to reach the equilibrium.

IR spectra of proteins were recorded in Nujol mull from 4000-600cm^{-1} for temperature dependent study. The resolution was 2 cm^{-1}.

FT-IR spectra in the solid phase were recorded by using polyethylene pellet technique. The resolution with 25 coadded scans was 2 cm^{-1}. Hamming function was used for apodization.

3.1.3.2. Crosslinkers

IR spectra were recorded in the range 300-4000 cm^{-1} in the KBr pellet.

Solid state Raman spectra were recorded in a fused quartz capillary using Ar^+ laser with 488 nm excitation source. The laser power was 300 mW at laser head. The resolution was 2 cm^{-1}.

3.2 RESULTS AND DISCUSSIONS

3.2.1 Assignment of Proteins

Buffer subtracted baseline corrected Raman spectra of Gelonin and BSA in 1800-1200 cm^{-1} in the phosphate buffer at pH 7.2 are shown in Figure-3.3. The diffused reflactance infrared fourier transform (DRIFT) spectra for the two proteins in powder form in 1000-1750cm^{-1} range are given in Figure-3.4.

We have used DRIFT technique in addition to Raman scattering, to study the effect of artifact coming due to sample preparation, since no sample preparation is needed in DRIFT. Secondly, S/N ratio could be increased by order of magnitude. This is accompanied by the advantage of Fourier deconvolution of bands which increases the resolution of all the bands without creating asymmetry or lobs near the bands. The observed spectra of BSA matches quite well with the powder spectra and even with deconvoluted solution spectra recorded by us. Since the vibrational spectra of BSA is very well characterized [25-26], we have not attempted that. The observed modes were carefully assigned and are presented in Table-3.1. These assignments are

based on the literature results as well as the shifts due to deuteration.

The amide I (1700 - 1630 cm^{-1}) Raman spectra of Gelonin is centered around 1648 cm^{-1} and that of BSA near 1650 cm^{-1}. The assignments in amide I region is done after curvefitting since the observed spectra is not well resolved. Most of the bands observed are well characterized in the literature [25-26]. It is known that BSA contains 55% α-helix structure in solution. The remaining 45% is attributed by most of the workers as due to turn and disordered structure. Thus, in Raman spectra, 1680-1695 cm^{-1} bands are assigned to turn, whereas $\approx$1666 cm^{-1} band as disordered, $\approx$1653 cm^{-1} as α-helix and $\approx$1674 and 1634 cm^{-1} bands as β-sheet structure in Raman spectra of Gelonin. The sharp band $\approx$1620 cm^{-1} in Raman spectra is taken as Tyrosine (Tyr) side chain vibration. The band around 1600 cm^{-1} is taken for Phenylalanine (Phe). Even though both BSA and Gelonin have only one Tryptophan (Trp), the bands observed at 1550 and 1370 cm^{-1} are assigned to Trp side chain vibration. The 1550 cm^{-1} band is observed in BSA and earlier assigned to Trp residue [26]. Moreover, it is reported that the "buried" Trp residues show a sharp band at 1361 cm^{-1} [27-28]. Thus the appearance of diffuse bands at around 1371 cm^{-1} for both the proteins reflect the fact that Trp concentration is very less confirming its assignment to the "buried" Trp. Bands in 1500-1550 cm^{-1} range are associated with

amide II modes and 1230-1300 cm^{-1} due to amide III modes. The observed modes in amide III region are easily assignable to α-helix in 1275-1295 cm^{-1} region, disorder around 1260 cm^{-1} whereas the band around 1244 cm^{-1} observed only in Gelonin is assigned due to anti parallel β-sheet.

The strong band at 1005 cm^{-1} for Gelonin and 1004 cm^{-1} for BSA are assigned to Phe side chain vibrations. The band at 717 cm^{-1} and 719 cm^{-1} are assigned to ν_{C-S} for Gelonin and BSA respectively. 625 cm^{-1} and 633 cm^{-1} bands are assigned to δ_{C-C} and 520 cm^{-1} and 525 cm^{-1} bands are assigned to ν_{S-S} for these two proteins respectively.

In case of DRIFT two bands in 1678-1684 cm^{-1} region and around 1650 cm^{-1} are observed. The former are associated mainly with turn structure whereas the later as α-helix. This clearly indicate the predominant α-helix structure of Gelonin. Amide-II is split into two clear bands in Gelonin which is not the case in BSA. Splitting of amide II band suggests the presence of β-sheet structure in Gelonin. The splitting is hardly visible in BSA even in deconvoluted spectra. Further, the absence of 1674 and 1634 cm^{-1} modes in the Raman spectra of BSA also support the conclusion that β-sheet structure is absent in BSA while Gelonin has significant sheet structure. 1680 cm^{-1} band in DRIFT spectra is stronger in BSA in comparison to Gelonin, particularly, in BSA containing fatty acids impurities. Also a band around 1580 cm^{-1}

is comparatively stronger in BSA than in Gelonin. These observations suggest that 1680 cm^{-1} band may have contribution from asymmetric carbonyl stretch of fatty acid impurities in addition to arginine and asparagine side chain vibrations. 1580 cm^{-1} mode will then be the corresponding COO^- asymmetric stretch. Since the carbohydrate moiety is H-bonded in Gelonin and is part of structure, its contribution will be less.

3.2.2 Quantitative Estimation of Secondary Structure of the Proteins

The quantitative estimation of secondary structural content in both proteins is attempted by two independent methods. The first method was proposed by William & Dunker [29-30]. They presented the theoretical basis for the correlation of observed spectra with conformation. In their approach, the broad amide I band of proteins is resolved into six components representing the following types of secondary structure; mono hydrogen bonded or ordered helix, di-hydrogen bonded or disordered helix, anti-parallel and parallel sheet, reverse turn and disordered structure. Normalized reference Raman spectra which represented the amide I band of a polypeptide with 100% of single type of structure were computed from the solvent subtracted spectra of proteins and polypeptides using least square solution of overdetermined equations. Each amide I spectrum was computed at

15 equally spaced wavenumbers between 1700-1630 cm^{-1}. The statistical test show significant difference between two types of helix and sheets. However, the difference between turn and disordered structure was not significant. We have found that computing the values using linear regression for the determination of five coefficient with or without intercept changes the value of the coefficient significantly. Also, in some cases the value of a particular coefficient comes out to be negative and the error level is higher than the values. This physically signifies a situation where a particular component though not present in the system is overdetermined due to parameter fitting. William and Dunker in their original calculations used non-negativity condition ($f_i \geq 0$, where f_i is the fraction of the ith component) to avoid this situation. In such cases, the fitting with the spectra comes out to be good, however, some of the coefficients looses their interpretation and in the process other parameter are underweighed. We have also observed that curve fitting results in some situation also helps in deciding the number of coefficients to be used. In our scheme of things, we have calculated the intensity contribution of each type of structure exactly in the same way as done originally. However, the normalized intensity (I) at any wavenumber is written in terms of five parameters instead of six.

$$I = f_1 . I_1 + f_2 . I_2 + f_3 . I_3 + f_4 . I_4 + f_5 . I_5 \qquad (3.1)$$

where f_i defines one of the corresponding secondary structure, the last having the contribution from turn as well as disordered structure. Using the reference Raman spectra data of William & Dunker and X-ray crystallographic data for the corresponding proteins, the values of I,s at each wavenumber were calculated by solving the homogeneous equations of the type

$$I = f_i . I_i \qquad (3.2)$$

We have taken the reference Raman spectra data of William & Dunker [27] calculations.

Using the reference values of I_i and experimental values of I the coefficients were calculated using linear regression. In cases where negative values or error prone values of the coefficients occur, the *ab initio* regression was done to check the error in the regression. However, the negative values were found to be the effect of fitting. We then drop the corresponding term in the equation (3.1) and calculated the parameters. This procedure was followed till realistic values were achieved. The results of such calculation are given in Table-3.2. The approach is justified since the observed spectra supports the absence of such components where values are negative. For example, in case of BSA, where estimated sheet structure value is negative, no band is at all visible in the curve fitted spectral results, while 5-parameter calculation gives large contribution in this region.

In the second method, a locally developed lorentzian curvefitting program is used to resolve the bands. In this method, buffer subtracted, base line corrected Raman Spectra of proteins are curvefitted and the results of such calculations in the amide I region (1700-1630 cm^{-1}) are presented in Table-3.3. Curvefitted bands in this region can easily be assigned to various structural types. The bands in the region 1680-1695 cm^{-1} are assigned due to turns, 1675 cm^{-1} is assigned due to anti parallel β-sheet, 1666 cm^{-1} bands due to disorder structure, 1644-1660 cm^{-1} is assigned due to α-helix, while that at 1634-36 cm^{-1} is assigned due to parallel β-sheet structure. These assignments are quite general and match with the assignment given by various workers [26, 31-33]. The c.a.1645 cm^{-1} bands may need some comments. In this region the bending mode of water molecules is generally observed in Raman spectra. We have, therefore, tried the curvefitting procedure in buffer subtracted spectra with and without a band in this region. From the results of Table-3.3 it is clear that in case of BSA summation of α-helix content due to 1645 and 1657 cm^{-1} bands are equal to the helix content due to 1651 cm^{-1} band. This result matches very well with reported results. In case of Gelonin, where crystallographic results are also published recently [34], it is found that the result matches very well if we consider the 1645 cm^{-1} band due to helix. We, therefore, consider 1645 cm^{-1} band due to helix. However, it may

be pointed out that the assignments are not simply based on the band positions. Band shapes, the corresponding IR positions and band intensity behavior are carefully analyzed. Thus the assignments are reliable to a greater extent. From the calculated band parameters, band area of each resolved component of amide I mode was calculated and this ratio was used to deduce the secondary structure (Table-3.3). These values are given in Table-3.4 along with the values of other methods.

Some interesting inferences can be deduced from the Table-3.4. It is found that these two methods, used for the estimation of secondary structure match extremely well with the reported results in case of BSA. First method also matches qualitatively with the crystallographic data for Gelonin which has been reported recently [34]. The estimated values obtained from curvefitting method seem more reliable as the estimates for BSA as well as for Gelonin match quite well with the reported results.

3.2.3 Thermal Denaturation of Gelonin

The temperature dependent IR spectra for Gelonin in wide range(4000-600 cm^{-1}) are recorded in powder form. Our attempt for investigation of the denaturation in solution phase were unsuccessful due to the fact that solution becomes turbid above temperature around 60°C because of the reduced solubility

of the denatured proteins. Moreover, the secondary structural content obtained using powder and solution state Raman spectra show no change in the percentage secondary structure of each type and IR spectra at room temperature in solid and solution phase matches quite closely. It is, therefore, expected that temperature dependent changes in in the solid state spectra will reflect the situation in the solution.

Change in the spectral pattern are found only in 700 - 1700 cm^{-1} region and are shown in Figure-3.5. We have analyzed the changes by calculating the band intensities of various modes at different temperatures. The relative band intensities normalized against the band intensities of various nujol modes are found to behave in the similar fashion. One set of data normalized against 720 cm^{-1} bands are given in the table. From the data it is clear that bands at 1580, 1170, 1150 and 1310 cm^{-1} remain almost constant with temperature. From the table it is also clear that the mode arising due to nujol show similar temperature dependence in protein spectra and their intensity remains constant. Thus, these can be used as internal standards. We have taken the 720 cm^{-1} band of nujol as internal standard. From these data it is found that the appreciable change in spectral pattern are found in 1580 cm^{-1}, 1650 cm^{-1} and in amide A and B mode. 1580 cm^{-1} band is assigned to the ν_{COO^-}. In amide A and B modes it becomes difficult to assign the denaturation. Thus

only 1650 cm^{-1} band has been considered for the purpose.

Spectra in the range 1575-1725 cm^{-1} are shown in Figure-3.6. It is seen from the spectra that the amide I band is centered around 1652 cm^{-1} in the protein. As the temperature increases amide I band becomes asymmetric and shifts to nearly 1645 cm^{-1} at temperature higher than $60^{o}C$. Amide-I band at $\sim$1650cm^{-1} is assigned to mainly α-helix structure by various workers [35-37] while the 1645 cm^{-1} band is assigned to the disordered structure [38]. Thus it is seen qualitatively that the helix structure of the protein decreases with temperature and disordered structure increases.

Peak position for the band peaking in 1642.5-1652.5 cm^{-1} range are plotted as a function of temperature and shown in Figure-3.7. From the figure it is clearly seen that $\approx$1651cm^{-1} band show discontinuity at $\approx 60^{o}C$. These changes could be correlated with the denaturation of the protein. Thus, it could be argued that for this protein the denaturation occurs at around $60^{o}C$ as revealed by the change in the frequency shift of 1651 cm^{-1} mode. It can, therefore, be argued that at around $60^{o}C$ denaturation of Gelonin occurs and with denaturation disordered structure increases.

The IR spectra of Gelonin, isolated by two different methods are identical except for the band at 1581 cm^{-1} which is absent in Gelonin isolated by method-I and for the appearance of

two bands at 1064 and 1003 cm^{-1} in the same sample. The band at 1581 cm^{-1} is assigned due to ν_{COO^-} of impurities which are in the non-hydrogen bonded form. Similarly, the other two bands which are quite weak, in all probability, are due to C-C stretch. Thus the changes may be attributed to the differing concentrations of carbohydrate moiety in two samples.

3.2.4 Assignment of SPDP and LC-SPDP

Raman and IR spectra of SPDP and LC-SPDP were recorded in solid state as attempts of recording the spectra in aqueous solution were unsuccessful due to totally insoluble nature of crosslinkers in water. We have assigned the observed spectra considering a planar geometry for rings. However, in the absence of crystal structure data for these compounds the assignments are only tentative. The probable assignments of various modes for the two systems are presented in the Table-3.5. It is based on the comparison of "frequencies" of different group vibrations as reported in the literature and their relative intensities in the IR and Raman spectra as expected from the vibrational selection rules [15-20]. Assigned "frequencies" are also compared with those of closely related systems. CH_2-vibrations were compared with those of aliphatic chains having similar environment [17], of amide from di-methylacetamide [21] and those of rings from pyridine [22] and succinimide rings [23]. The most important

spectral range from our point of view is that of 400-800 cm^{-1} where the ν_{C-S} and ν_{S-S} modes are expected. Raman spectra for this range are presented in the Figure-3.8. In this range strong bands are observed at 432, 528, 599, 622, 669, 717, 732 and 762 in the Raman spectrum of SPDP and at 422, 523, 573,619, 633, 669, 717, 736 and 764 cm^{-1} in LC-SPDP. In Infrared the corresponding bands are observed except for 523/528, and 732/736 cm^{-1}. Moreover, most of the remaining bands in IR are weak in this region except the ones around 669 and 763 cm^{-1}. The ν_{S-S} mode generally appears in the narrow range of 550-500 cm^{-1} [24]. It is strong in Raman and very weak or missing in Infrared.

The occurrence of a very strong band at 523 cm^{-1} in LC-SPDP and 528 cm^{-1} in SPDP in the Raman spectra is assigned to ν_{S-S} which is absent in IR spectra as expected. In contrast, the bands due to ν_{C-S} appear over the wider range of 800-600 cm^{-1} depending on the dihedral angle and the environment around the C-S bond a single or several bands are observed due to ν_{C-S}. In our systems two C-S bonds have different environment, therefore it is expected that they will give rise to more than one ν_{C-S} which may further be splitted due to resonance coupling. Therefore the assignment of ν_{C-S} becomes ambiguous. Still it is possible to assign the modes due to ν_{C-S} because of the fact that C-S and S-S "frequency" will be correlated. The bands around 764 and 669 cm^{-1} cannot be due to ν_{C-S} because of their strong

intensity in Infrared. For the remaining three bands the relative intensity ratio of 736 and 717 cm^{-1} bands with respect to ν_{S-S} are quite similar in both compounds while that of 619 cm^{-1} is significantly different. The two bands at 732 and 717 cm^{-1} in LC-SPDP and 736 and 717 cm^{-1} in SPDP are thus attributed to ν_{C-S}.

3.2.5 Geometry Around C-S-S-C of the Crosslinkers

The assigned ν_{S-S} as well as ν_{C-S} do not show significant change in "frequency" for the two systems ($\Delta\nu$ for ν_{S-S} is 5 cm^{-1} and for ν_{C-S} is 4 cm^{-1}). Even though the difference lies beyond experimental inaccuracy, it does not signify a totally different conformation. However, there may be minor differences in the disulfide geometry in two cases.

In order to compare the disulphide geometries in two crosslinking agents, we have calculated the band intensity ratios (I_{S-S}/I_{C-S}) which are 3.6 for I_{523}/I_{736} and 5.0 for I_{523}/I_{717} in LC-SPDP and 1.43 for I_{528}/I_{732} and 1.1 for I_{528}/I_{717} in SPDP, indicating that the relative torsion about (C-S) and (S-S) bonds in the two systems is different. This observation along with subtle difference in ν_{S-S} and ν_{C-S} indicate that even though the S-S bridge has almost same confomation in both compounds, there exist minor differences in the geometry. The ν_{S-S} and ν_{C-S} are extensively studied in various model compounds and peptides and are found to be conformation sensitive. Various correlations

[39-40] between band positions and dihedral angles are also established. The position of ν_{S-S} depends upon the dihedral angle between the adjacent C-S planes and that of ν_{C-S} on the geometry of adjacent S-S bridge. Using the well established correlations it can be deduced that C-S-S-C linkages are not linear. Also the torsional angle around S-S bond in SPDP and LC-SPDP may lie between ($85^{\circ}\pm20^{\circ}$) [30] and the torsional angle around C-S bond varies between $0-50^{\circ}$. Recently the *ab initio* scaled force field for disulphide geometry is derived from the quadratic force constants and geometry parameters of model compounds such as dimethyl disulphide etc. and is used for normal coordinate calculations in peptides and proteins [41-42]. The calculated "frequencies" for various conformations of disulphide bridge is found to be in good correlation with the observed Raman bands. It is observed that the correlation of ν_{C-S} is only suggestive.

Recently, we have performed MNDO calculations on these two and the optimized geometries of -S-S- environments for SPDP and LC-SPDP have been deduced [43]. These theoretically calculated values are considered for the validation of our spectroscopic findings. Bond length and bond order values predict that the -S-S- bond strength of these two crosslinkers are similar but the geometries around the -S-S- region are different. The results of these calculations show considerable differences in these two molecules for this particular region. The change in

the dihedral angle as predicted from spectroscopic data (ϕ_1 is $85^{\circ}\pm20^{\circ}$ and ϕ_2 is $0\text{-}50^{\circ}$) is established by theoretically determined geometry (ϕ_1^{SPDP} 94.4°, $\phi_1^{LC\text{-}SPDP}$ -94.6° and ϕ_2^{SPDP} -122.8°, $\phi_2^{LC\text{-}SPDP}$ 19.3°) too and thus can be utilized to corroborate the spectroscopical findings.

References

1. I.H.Parton, M.C.Willingham and D.J.P.Fitzgerald, *Cell*, 47, 641 (1986).

2. E.S.Vitteta R.J.Fulton, R.D.May, M.Till and J.W.Uhr, *Science*, 238, 1098 (1987).

3. F.Stirpe and L.Barbieri, *FEBS Letters*, 195, 1 (1986).

4. Endo, Y., Mitsui, K., Motizuki, M. and Tsurugi, K. *J. Biol. Chem.* 262, 5908 (1987).

5. F.Stirpe, L.Barbieri, M.G.Battelli, M.Soria, and A.Doughlas, *Biotechnology*, 10, 405 (1992).

6. V.Singh, M.R.Sairam, G.N.Bhargabhi and R.G.Akhras, *J. Biol. Chem.*, 264, 3089 (1989).

7. E.S.Vitteta and J.W.Uhr, *Annu.Rev.Immunol.*, 3, 197 (1985).

8. E.J.Wawrzynczak and P.E.Thrope, in *Immunoconjugates: Antibody conjugate in Radioimaging and Therapy of Cancer*, pp.28, Edited by C.W.Vogel, Oxford University Press, NY (1987).

9. G.Mooller, *Immunl.Rev.* 62, 1 (1982).

10. A.E.Frankel, in *Immnotoxins*, Kluwer Academic Publications, Norwell, MA (1988).

11. V.Singh, M.R.Sairam, G.N.Bhargavai and R.G.Akhras, *J. Biol. Chem.* 264, 3089 (1989).

12. J.M.Peters, T.G.Hazedonk and E.C.Beuvery, *J.Immunol. Method* 120, 133 (1989).

13. In *Pierce-Immuno Technology Catalog and Handbook*, Pierce Chemical Co., Rockford, USA (1992).

14. V.Singh and S.K.Kar, *Ind.J.Biochem.Biophys.* 29, 31 (1992).

15. L.J.Bellamy, in *The Infrared Spectra of Complex Molecules*, Chapmann and Hall, London (1975).

16. G.Varsanyi, in *Assignment of Vibrational Spectra of Benzene Derivatives*, Vol-I,Adam Hilger, London (1974).

17. F.R.Dollish, W.G.Fateley and F.F.Bentley, in *Characteristic Raman Frequencies of Organic Compounds*, John Wiley & Sons,New York (1974).

18. R.Prasad and Neelam Dube, *Ind.J.Pure & Appl.Phys.* 25, 178 (1987).

19. V.Volvsek, L.Colombo and K.Furic, *J.Raman Spectrsc.*14, 347 (1983).

20. J.A.Drager, *Spectrochim.Acta* 39A, 809 (1983).

21. I.Suzuki, *Bull.Chem.Soc.Japan* 35, 540 & 1279 (1962).

22. B.Klein and J.Berkowitz, *J.Am.Chem.Soc.* 81, 5160 (1959).

23. K.W.F.Kohlrausch, A.Pongratz and R.Seka, *Chem.Ber.* 66, 1 (1933).

24. H.Li, C.J.Wurrey and G.J.Thomas(Jr.), *J.Am.Chem.Soc.* 114, 7463 (1992).

25. M.C.Chen and R.C.Lord, *J.Am.Chem.Soc.USA*, 98, 990 (1976).

26. R.J.Jakobsen and F.M.Wasacz, *Appl. Spectrosc.* 44, 1478 (1990).

27. Yu, N.-T. *J.Am.Chem.Soc.*, 96, 4664 (1974).

28. Craig,W.S and Gaber, B.P. *J.Am.Chem.Soc.*, 99, 4130 (1977).

29. R.W.Williams and A.K.Dunker, *J.Mol.Biol.*, 152, 783(1981).

30. R.B.Honzatko and R.W.Williams, *Biochemistry*, 21, 6201 (1982)

31. M.C.Chen and R.C.Lord, *J.Am.Chem.Soc.USA*, 98, 990 (1976).

32. P.C.Painter and J.L.Koenig, *Biopolymer*, 15, 2155 (1976).

33. H.Takeuchi, I.Harada and H.Yoshida, *Biochim.Biophys.Acta*, 1078, 307 (1991).

34. M.V.Hosur, Bindu Nair, P.Satyamurthy, S.Misquith, A.Surolia, and K.K.Kannan *J.Mol.Biol.*, 250, 368 (1995).

35. P.I.Haris and D.Chapman,*Trends Biochem Sci.* 17, 328 (1992).

36. W.K.Surewiez and H.H.Mantsch, *Biochem. Biophys. Acta* 952, 115 (1988).

37. H.Susi and D.M.Byler *Methods. Enzymol.* 130, 290 (1986).

38. C.Qinglong, L.Huizhou and C.Jiayong, *Biochim. Biophys. Acta* 1026, 247 (1994).

39. H.Sugeta, A.Go and T.Miyazawa, *Bull. Chem. Soc. Japan* 46, 340 (1973).

40. H.E.VanWart and H.A.Scheraga, *J.Phys.Chem.* 80, 1812 (1976).

41. W.Zhao and S.Krimm, *J.Mol.Struct.* 224, 7 (1990).

42. W.Qian, W.Zhao and S.Krimm, *J.Mol.Struct.* 250, 89 (1991).

43. B.Pal, P.K.Bajpai, J.Sengupta and V.Singh, *J. Raman Spectrosc.* 28, (1997) (In press).

Table.3.1: Assignments of observed bands (cm^{-1}) of Gelonin and BSA

Raman		FT-IR			Assignments
BSA	Gelonin	BSA[$]	BSA	Gelonin	
		1678	1683		Amide I turn
					Am I undefined
1650	1648	1655	1650	1655	Amide I helix
					Amide I sheet
		1633			Amide I turn
1625	1615				Tyr
1590	1589	1597			Phe
		1575	1584	1580	ν_{COO^-}(asym)
1550	1558				Trp
		1547	1537	1526	Amide II
		1518			Amide II
		1499			Phe(Tyr)
		1470		1485	δ_{CH_3}
1445	1450	1447	1457	1458	$\delta_{CH_3}/\delta_{CH_2}$
		1420			
1408	1408	1398	1390	1388	ν_{COO^-}(sym)
	1371	1363			Trp
1342	1346	1344	1336	1338	δ_{CH_3}/Lys
1318	1313	1315			δ_{CH_3}
1314		1300		1305	δ_{CH_3}+Amide III
			1296		AmideIII Helix
1267		1270			Amide III
	1244	1244		1245	Amide III
			1224	1228	Amide III
1200		1213			Tyr
1167		1172	1169	1170	Leu,Lys,Tyr,Val
					C-N
	1158	1151			Glu (Asp,Phe)
1125	1125	1126	1122	1118	
		1106			Ala, Leu, Lys
	1045				
1005	1004				Phe
808	775				
717	719				ν_{C-S}
625	633				δ_{C-C}
520	525				ν_{S-S}

[$]Data taken from reference number 26 for comparison.

Table.3.2: Results of coefficients representing secondary structure(%) obtained using modified William and Dunker Method.

Protein	Segment	Parameter		
		five	three	two
BSA	a	04 ± 07	-01 ± 07	
	b	10 ± 34	50 ± 13	50 ± 12
	c	20 ± 40	-	
	d	53 ± 31	-	
	e	55 ± 16	41 ± 09	41 ± 09
Gelonin	a	22 ± 05	22 ± 05	
	b	90 ± 25	52 ± 09	
	c	-24 ± 29	-	
	d	34 ± 22	-	
	e	-20 ± 12	22 ± 07	

a- di hydrogen bonded helix; b- mono hydrogen bonded helix; c- antiparallel β sheet; d- parallel β sheet and e- turn and f- disordered structure.

Table.3.3: Curvefitting Results with Assignments and Calculated Secondary Structure

Band Position (cm^{-1})	Half Width (cm^{-1})	Intensity (Arb.Unit)	%	Assignments
		BSA		
1691.73	13.27	841.0	37.16	Turn
1667.01	9.23	442.0	13.59	Disorder
1657.17	8.95	341.9	10.19	Helix
1645.46	16.56	708.3	39.06	Helix(?)
1691.41	13.11	844.4	36.90	Turn
1665.88	9.53	399.8	12.70	Disorder
1651.13	16.79	900.5	50.40	Helix
		Gelonin		
1692.71	6.93	632.0	14.71	Turn
1683.16	5.21	656.4	11.49	Turn
1674.32	5.57	570.9	10.69	AP-β-sheet
1665.93	7.86	820.6	21.67	Disorder
1653.49	7.22	864.3	20.97	Helix
1643.24	5.84	554.8	10.88	Helix(?)
1634.31	5.06	563.2	9.58	P-β-sheet
1692.18	6.33	549.8	11.62	Turn
1684.03	6.27	502.4	10.52	Turn
1675.26	4.95	460.6	7.62	AP-β-sheet
1666.54	6.71	518.6	11.62	Disorder
1653.47	11.08	863.7	31.96	Helix
1635.39	12.01	664.4	26.65	P-β-sheet

Table.3.4: Comparison of % Secondary Structural Contents Obtained by Different Methods

Protein	Structural Type	X-Ray/Other	Deconvolution With 1645 cm^{-1} band	Deconvolution Without 1645 cm^{-1} band	William & Dunker Linear Regression
BSA	Helix 1	55-50	10.19	50.40	50 + 12
	Helix 2	-	39.06	-	
	Sheet 1	-	-	-	
	Sheet 2	-	-	-	
	Turn	45-50	37.16	36.90	41 ± 09
	Disorder		13.59	12.70	
Gelonin	Helix 1	35.50	20.97	31.96	22 ± 05
	Helix 2	2.40	10.88	-	52 ± 09
	Sheet 1	21.1	10.69	7.62	22 ± 07
	Sheet 2		9.58	26.65	
	Turn	20	26.20	22.14	
	Disorder	20	21.67	11.62	

Table 3.5 Observed frequencies(cm^{-1}) of the vibrational modes and assignments of the fundamental modes in SPDP and LC-SPDP.

SPDP		LC-SPDP		Probable Assignments
Infrared Frequency	Raman Shift	Infrared Frequency	Raman Shift	
		3343	3315	ν_{N-H}
		3248	3238	ν_{N-H}
	3127		3130	ν_{C-C} x2
3064	3064		3072	ν_{C-H}
			3050	ν_{C-H}
			3029	ν_{C-H} (Ring)
	3010	3010	3010	ν_{C-H}
	2997			ν_{C-H}
	2977		2972	ν_{C-H}
	2956		2962	ν_{C-H}(asym)
	2947		2939	ν_{C-H}(sym)
	2921		2927	ν_{C-H}(sym)
	2935		2935	ν_{C-H}(asym)
	2886		2908	ν_{C-H}(asym)
			2870	ν_{C-H}(sym)
			2849	ν_{C-H}(sym)
1809	1803	1810		$\nu_{C=O}$(ester)
1786	1787	1784	1789	$\nu_{C=O}$(ester)
		1777	1777	$\nu_{C=O}$
1728	1727	1727	1732	$\nu_{C=O}$
1713	1716			$\nu_{C=O}$

Continued

1697				
		1662	1662	Amide I
1641	1649	1641	1646	$\nu_{C=N}$
1566	1577	1570	1576	ν_{C-C}(Ring) 8a
1554	1564	1553	1549	ν_{C-C}(Ring) 8b
1534		1539		ν_{C-O}
1513		1514		ν_{C-N}
1486		1486		ν_{C-C} (Ring)
		1466	1466	CH_2 bending
1448	1449	1442	1448	CH_2 bending
	1426		1440	ν_{C-C} (Ring)
1416	1411	1415	1418	CH_2 bending
1391	1404	1397	1405	CH_2 bending
1384			1390	
1358	1361	1367	1368	ν_{C-C}
		1333	1330	CH_2 wagging
	1287	1294	1294	CH_2 wagging
1246	1254	1261	1261	CH_2 twisting
1222	1231	1239	1235	CH_2 twisting
1199	1205	1209	1212	δ_{C-H}(Ring)
1145	1150	1153	1162	δ_{C-H}(Ring)
		1137	1137	CH_2 twisting
1117	1131	1114	1124	ν_{C-C}
	1086		1100	ν_{C-C}
1077	1072	1073	1066	ν_{C-C}
1046	1053	1048		
1029	1016		1037	in-plane bending
988	995	990	989	Ring breathing
	964	933	956	γ_{C-H}

Continued

902	908	915	920	γ_{C-H}
883	887		890	CH_2Rocking
		867	863	CH_2Rocking
		831		
808	810	806		
763	762	770	764	CH_2Rocking
	732		736	ν_{C-S}
714	717	713	717	CH_2Rocking
669	669	672	669	$\delta_{O=C-O}$
647		648	633	δ_{C-C} (Ring)
623	622	621	619	δ_{C-C} (Ring)
601	599			
		570	573	
	528		523	ν_{S-S}
474	481	478	476	$\delta_{C=O}$
421	432		422	δ_{C-C-C} (Ring)
	402	391	399	δ_{C-C-C} (Ring)
375	356		370	
	332		338	
305	310	308	308	$\delta_{O=C-O-C}$
	255		250	
	210			
	198		198	Lattice modes
	176		172	
	145			
	125		130	

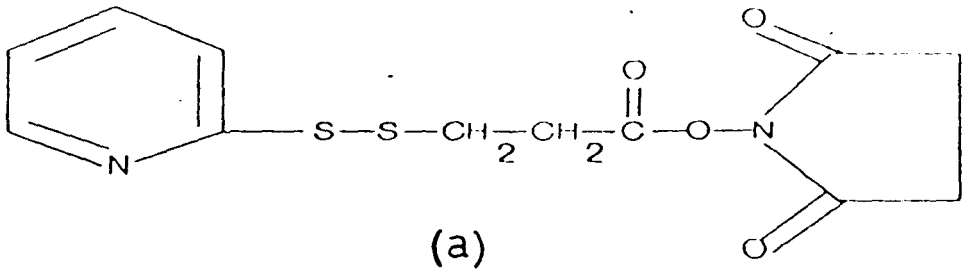

(a)

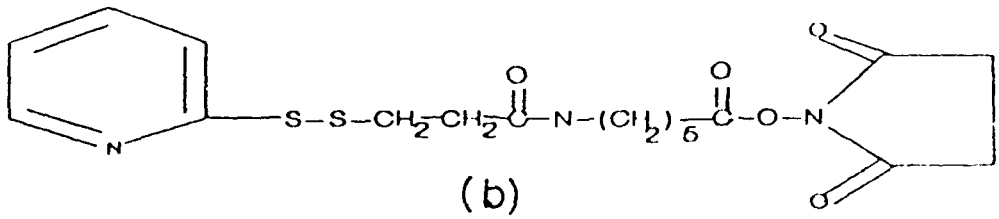

(b)

Figure-3.1 Structure of (a) SPDP and (b) LC-SPDP

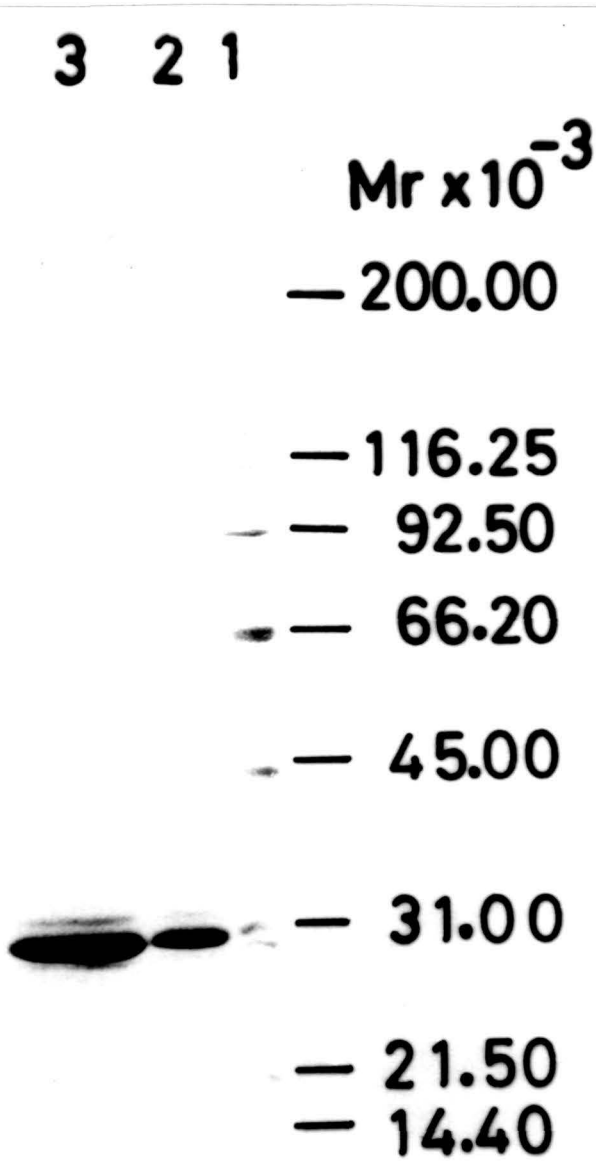

Figure-3.2 SDS-PAGE analysis of Gelonin purified by two different methods (lane 2 for method I and lane 3 for method II). A gel consisting of 5-15% (w/v) acrylamide was used. The gel was fixed in methanol-acetic acid and stained with coommasie blue and destained with methanol-acetic acid for 24 hours. Lane 1 contains molecular weight markers: myosin (200kD); β-galactosidase (116.25kD); phosphoamylase B (92.5kD); bovine serum albumin (66.2kD); ovalbumin (45kD); carbonic anhydrase (31kD); soyabin trypsin inhibitor (21.5kD); lysozyme (14.4kD).

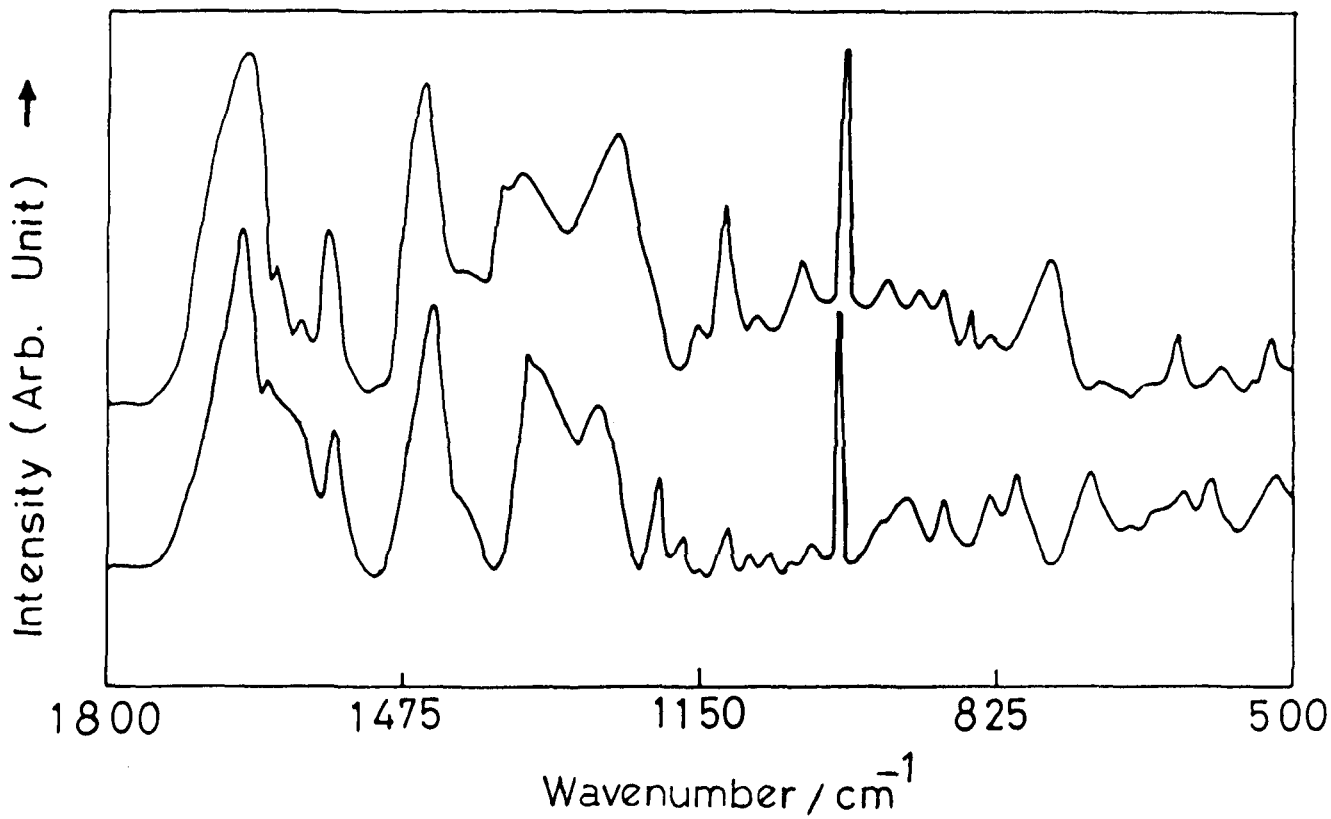

Figure-3.3 Raman Spectra of (a)Gelonin, and (b)Bovine Serum Albumin. Laser line used was 488nm and power at the laser head was 400mW

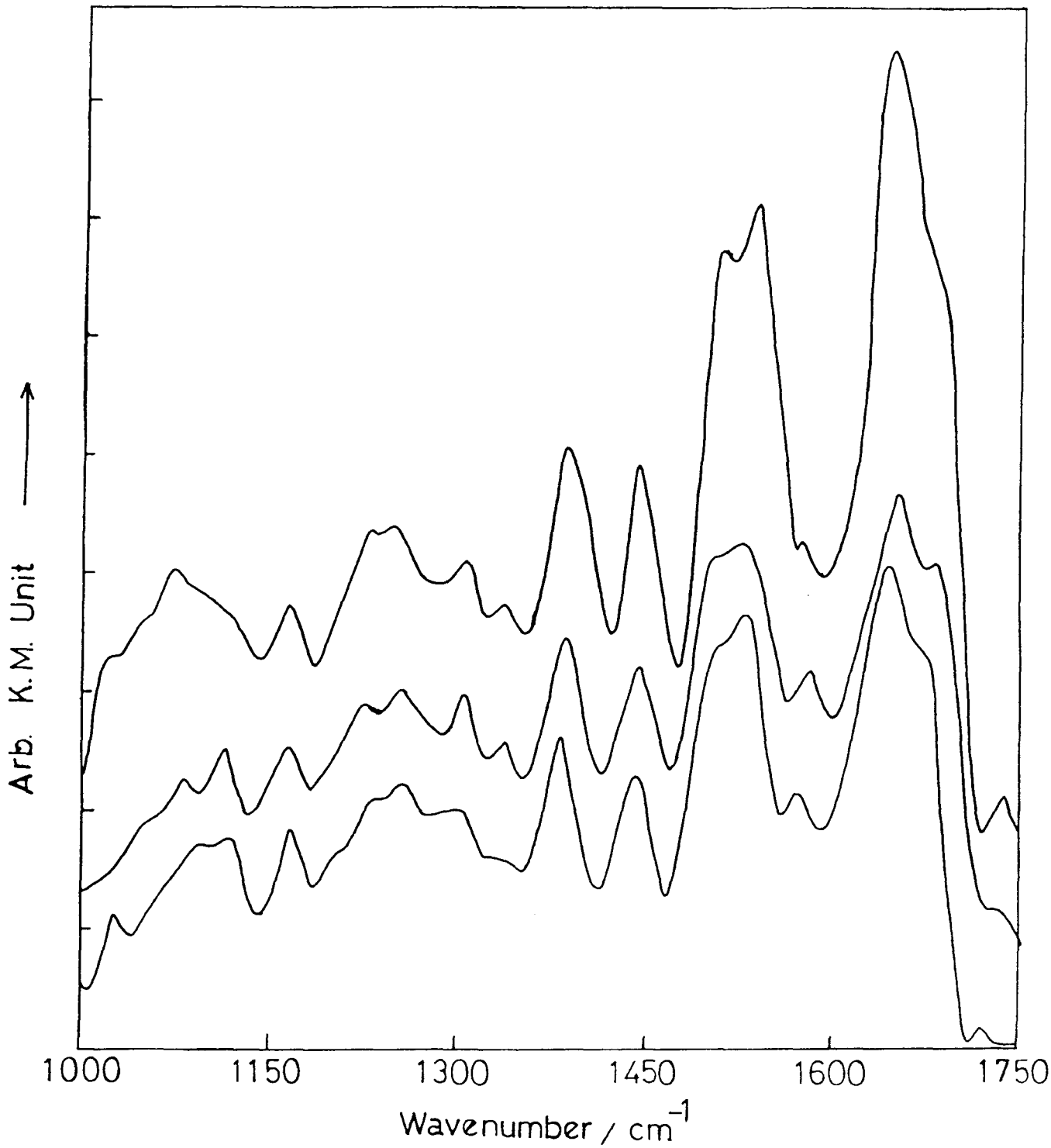

Figure-3.4 Diffused Reflectance Infrared Fourier Transform Spectra of (a)Gelonin, (b)BSA containing fatty acids and (c)BSA fatty acids free.

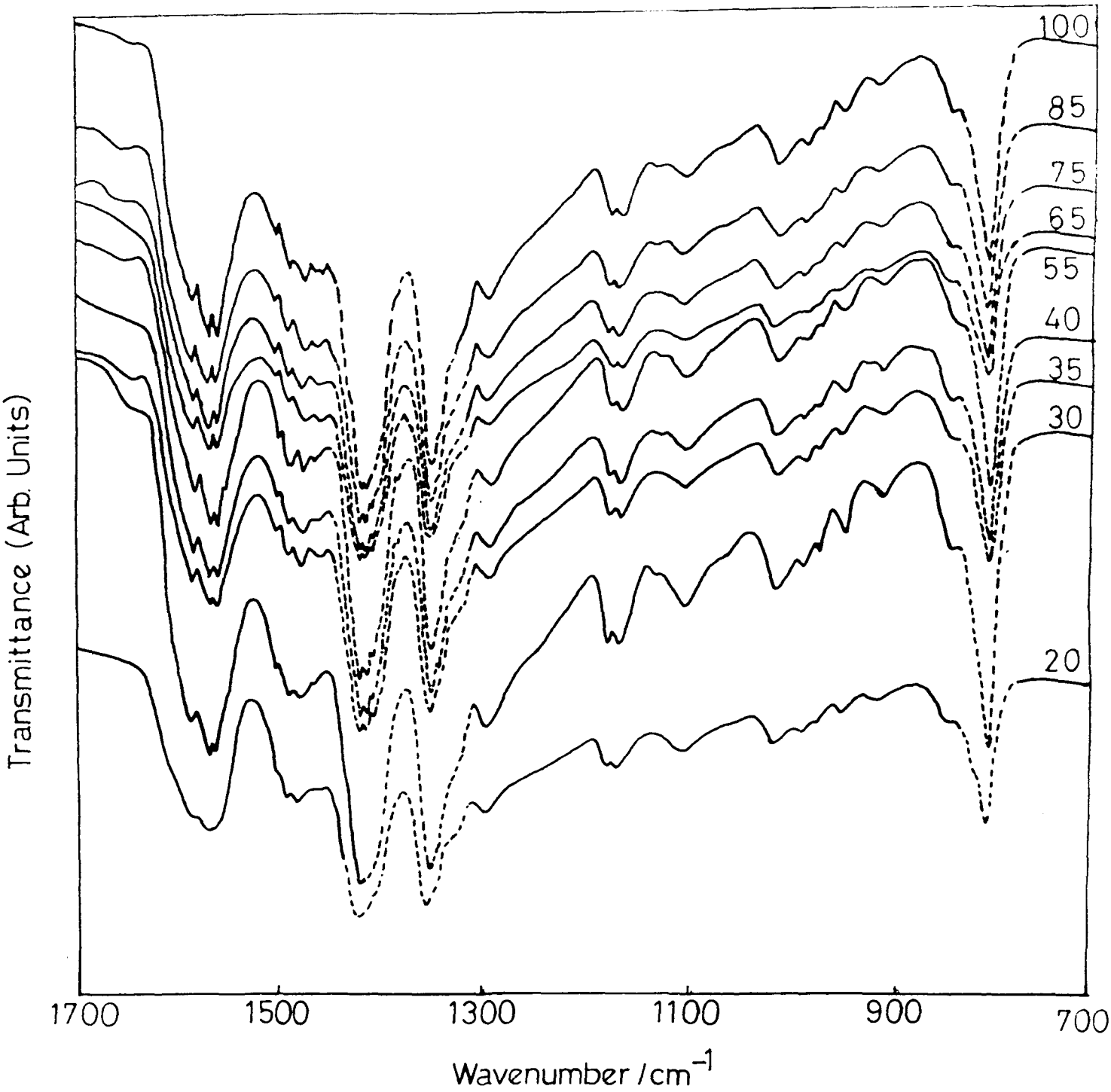

Figure-3.5 Teparature dependent IR spectra of gelonin in 700 - 1700 cm^{-1} region.

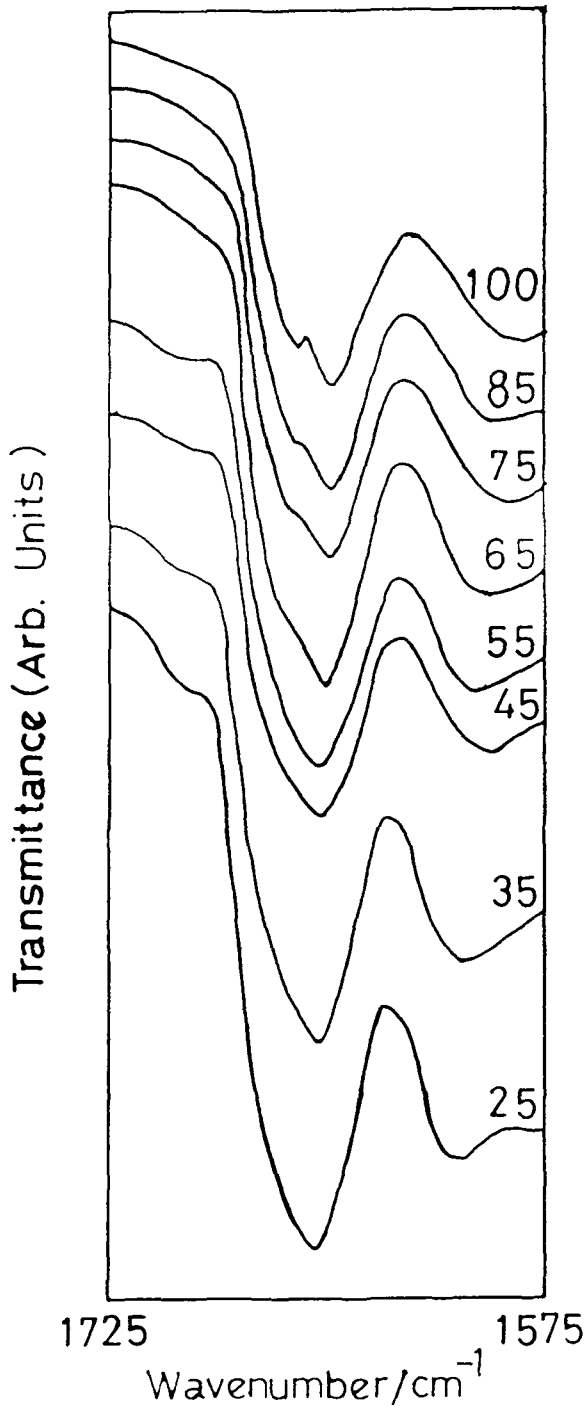

Figure-3.6 Teparature dependent IR spectra of gelonin in 1575-1725 cm^{-1} region.

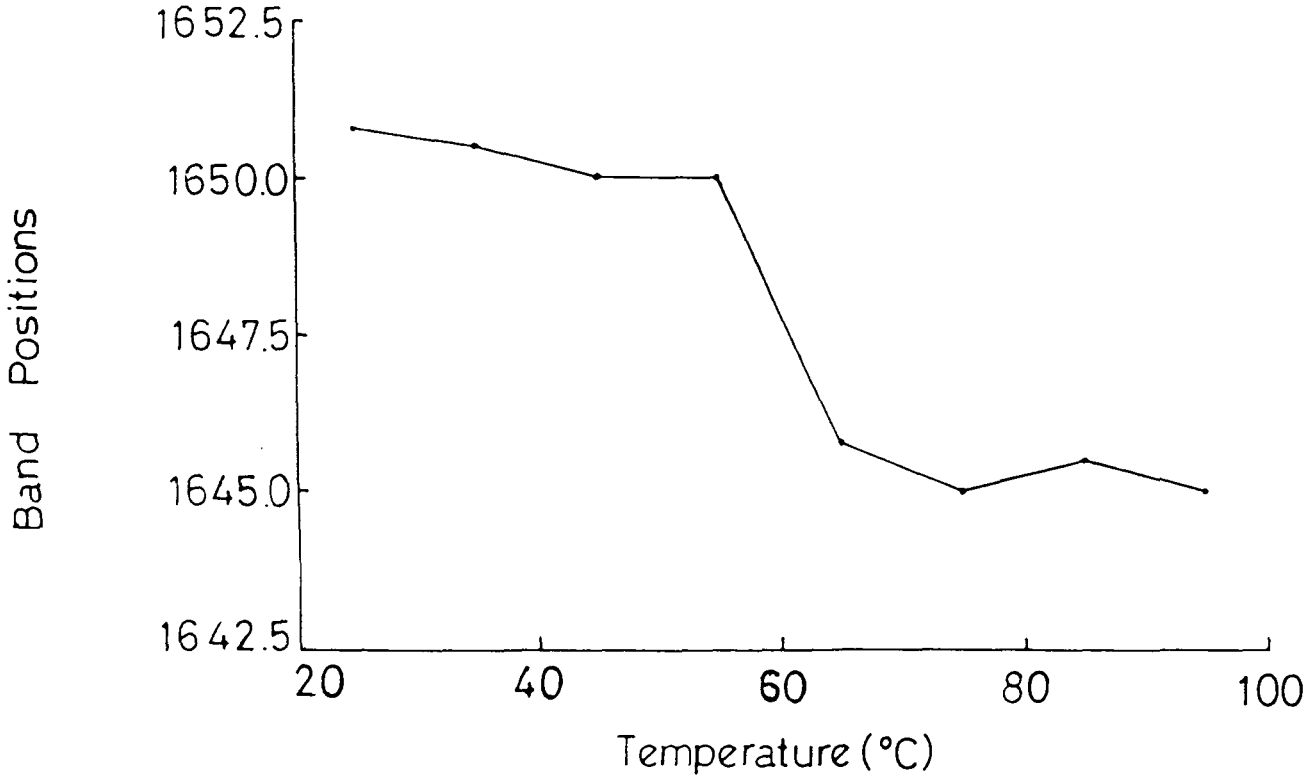

Figure-3.7 Graphical representation of temperature dependent shift in wavenumber in the 1651 cm^{-1} region of Amide-I.

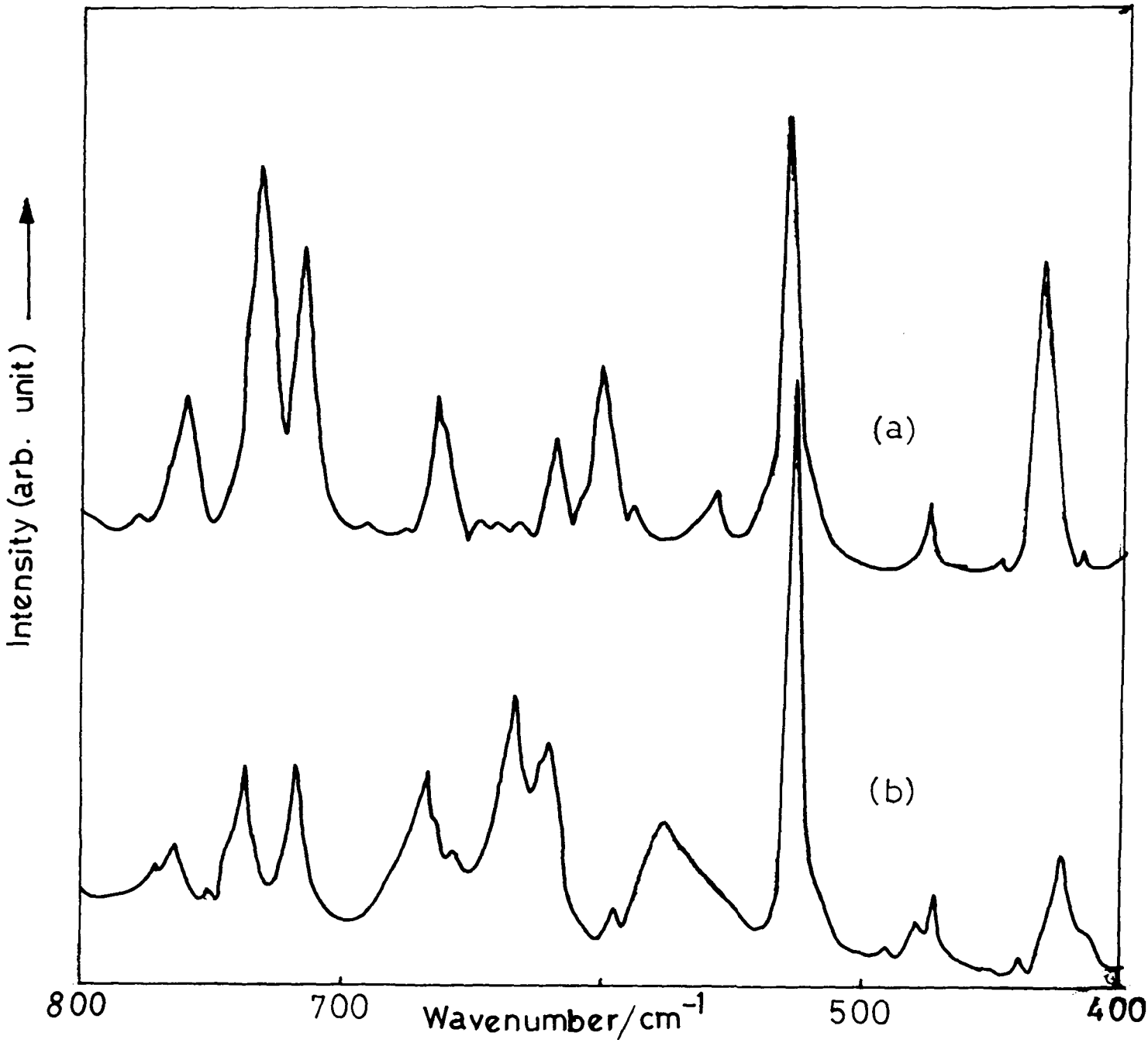

Figure-3.8 Raman spectra of (a)SPDP and (b)LC-SPDP (400-800 cm^{-1}) region.

CHAPTER - IV

SPECTROSCOPIC STUDIES OF SOME HYDROXY AZO DYES : STRUCTURAL MOTIFS AND TAUTOMERIC EQUILIBRIA

We have synthesized a series of azo dyes e.g. (2-hydroxy-5-methylphenylazo)benzene (HMPAB) and (2-hydroxy-naphthylazo)benzene (HNAB) and their derivatives viz. (2-hydroxy-5-methyl-phenylazo)methoxybenzene (HMPAMB), (2-hydroxy-5-methyl-phenylazo)chlorobenzene (HMPACB) (2-hydroxynaphthylazo)methoxy-benzene (HNAMB) (2-hydroxynaphthylazo)chlorobenzene (HNACB) 5-(phenyl)azoquinolin-8-ol (PAQ), 5-(2'-carboxyphenyl)azo-quinolin-8-ol (CPAQ) and 5-(2'-carbomethoxyphenyl)azoquinolin-8-ol (CMPAQ) and copper complexes viz. $(PAQ)_2Cu$ and $(CMPAQ)_2Cu$ and studied their vibrational spectra using Resonance Raman (RR)technique as the main experimental tool, in order to understand the type of structure in solid state, effect of substitution and the structural changes on both sides of acid-base equilibria in solutions. Further, results of the 5-(aryl)azo-8-quinolinols type have been compared with that of copper complexes of the dyes known to exist in azo form. Fourier Transform Infrared analysis on these dyes were also performed to corroborate the Raman data. Moreover, the changes in the RR spectra as a result of pH induced tautomeric equilibrium shifts are correlated with electronic spectral changes.

Based on these studies, following papers have been published :

1. Structure of some arylazophenols and arylazonaphthols in solid state : A Resonance Raman study.
   P.K. Bajpai, Biswajit Pal and T.S. Basu Baul
   J.Raman Spectrosc. 26, 217 (1995).

2. Structural characterization of some quinolin-8-ol-containing azo dyes in solid and solution state as probed by Resonance Raman, FT-IR and Electronic Spectroscopic techniques.
   P.K. Bajpai, Biswajit Pal and T.S. Basu Baul
   J. Raman Spectrosc. 26, 351 (1995).

4.0 INTRODUCTION

Azo dyes form an important group of compounds which have been used as acid base indicators in analytical chemistry [1]. These have also been used as spectrophotometric probes in protein chemistry as the binding of these dyes to proteins or surface active reagents gives rise to anomalous color changes [1]. Structures of these compounds are considerably different; some may exist in azo tautomer while others in hydrazone form or mixture of both tautomers. Different spectroscopic techniques such as UV-Visible, Nuclear Magnetic Resonance, Infrared (IR), Resonance Raman (RR) etc. are being used [1-2] to determine mainly

(i) the tautomeric equilibria

(ii) various resonating forms of protonated and deprotonated species

(iii) the assignment of vibrational modes sensitive to a resonating electronic excited state and,

(iv) the effect of binding with protein molecule/surfactant.

In case of hydroxy azo dyes, if the hydroxyl group is *ortho* to the azo group, it may lead to intra-molecular H-bond interaction. For *o*-hydroxy azo dyes, RR studies are concerned mainly with tautomeric equilibria in solutions [1,3-8]. Reports in solid state are scanty except for one in which the solution state (in CCl_4) results were used for analyzing the solid state

spectra [4]. This may lead to an incorrect assignment of the vibrational modes. Further, the report lacks a complete assignment of the bands and the role of the substituents. On the other hand information regarding the vibrational spectra of 5-(aryl)azo-8-quinolinols are sporadic, which give a little insight about their structural motifs.

It is, therefore, important to deduce the structure of these dyes initially in solid state, to characterize and assign the bands which are sensitive to a particular resonating excited form. Such characteristic modes may be used to propose the structural forms in solutions where the tautomerism is possible. Fourier- Transform Infrared (FT-IR) and RR spectra of these compounds are analyzed from this point of view. In addition, pH dependent changes leading to shift in tautomeric equilibria were also critically analyzed. Further, electronic spectra in solutions are used to correlate the spectral changes with the electronic resonating excited states.

RR spectra of solid state is found to be particularly useful in characterizing the bands indicative of a particular type of structure. Systematic RR study of some *o*-hydroxy azo dyes viz. (2-hydroxy-5-methylphenylazo)benzene and (2-hydroxy-naphthylazo)benzene and their derivatives (Figure-4.1 a,b) have provided the characteristic modes due to azo and hydrazone forms in solid state. However, it is noticed that the characteristic

bands in arylazophenols and arylazonaphthols establishing azo or hydrazone form can not be considered for 5-(aryl)azoquinolinol (Figure-4.1c) derivatives since the $\nu_{C=N}/\nu_{C-N}$ modes of quinolinol ring interfere with the characteristic modes in hydrazone form.

4.1 EXPERIMENTAL

4.1.1 Synthesis of Dyes

The *o*-hydroxy azodyes viz. (2-hydroxy-5-methylphenyl-azo)benzene (HMPAB) and (2-hydroxy-naphthylazo)benzene (HNAB) and their derivatives viz. (2-hydroxy-5-methyl-phenylazo) methoxybenzene (HMPAMB), (2-hydroxy-5-methyl-phenylazo) chlorobenzene (HMPACB) (2-hydroxynaphthylazo)methoxy-benzene (HNAMB) (2-hydroxynaphthylazo)chlorobenzene (HNACB) were synthesized using the usual method [9-10] of diazotization of aniline, 2-methoxy aniline and 2-chloroaniline, respectively, followed by coupling with *p*-cresol for HMPAB, HMPAMB and HMPACB and β-naphthol for the HNAB, HNAMB and HNACB.

The quinolinol dyes viz. 5-(phenyl)azoquinolin-8-ol (PAQ), 5-(2'-carboxyphenyl)azoquinolin-8-ol (CPAQ) and 5-(2'-carbomethoxyphenyl)azoquinolin-8-ol (CMPAQ) were prepared by usual diazotization of aniline, anthranilic acid and methylanthranilate, respectively, followed by coupling with 8-hydroxyquinoline [11]. Copper complexes viz.$(PAQ)_2Cu$ and $(CMPAQ)_2Cu$ were synthesized by adding acidified copper acetate

solution to the hot solution of PAQ and CMPAQ respectively [12]. The various anilines used for synthesizing the dyes were distilled or recrystallized. Triply distilled water was used throughout. Other reagents were of analytical grade. The spectroscopic grade solvents were used for spectral measurements.

Purities of the compounds were established by melting point and elemental analysis. The compounds were identified by Mass spectrometry, NMR and IR techniques. Mass spectrum were recorded with JEOL SX-102 mass spectrometer. NMR data were obtained using EM-390 Varian NMR spectrometer in $CDCl_3$ and the shifts were relative to internal Me_4Si. PE-983 IR spectrophotometer was used for IR spectra. The spectra were recorded in KBr pellet form 4000-600 cm^{-1}. The resolution was $\approx 2cm^{-1}$. The analytical data for the three compounds were consistent with the desired chemical structure of the compounds.

4.1.2 Spectral Details

RR spectra in the range 1000-1700 cm^{-1} were recorded using spinning disc. For RR measurements, excitation lines were selected according to the observed absorption maxima in the UV-Vis spectra of the corresponding compound in benzene solution for solids and at different pH in case of solutions. Since it was not possible to select the exact excitation line, the closest possible excitation with absorption maxima, giving minimum

fluorescence was selected. A plasma filter was used to screen the plasma lines. The power at the laser head was 400 mW for 488.0 100 nm, 180 mW for 476.5 nm and 70 mW for 457.9 nm. The experimental slit width was 5 cm^{-1} for all the experiments.

Solution used for recording the RR spectra at pH $\approx$ 1 was prepared by dissolving the compounds in conc.HCl. For pH dependent study, the compounds were dissolved in water containing sodium hydroxide and the pH of the solution was lowered by successive dilution with HCl. The concentration of the solutions were $\approx 10^{-4}$M.

FT-IR spectra in the solid phase were recorded by using KBr or polyethylene pellet. The resolution with 25 coadded scans was 2 cm^{-1}. Hamming function was used for apodization.

Visible spectra of the compounds were recorded using 10 mm quartz cell in the range 300-600 nm. The pH of the solutions were adjusted using HCl solution in the acidic pH range and NaOH solution in the alkaline pH range. Electronic spectra of each dye were recorded at various pH ranging both side of the color change interval as well as in conc.HCl, in methanol or in hexane.

4.2 RESULTS AND DISCUSSIONS

4.2.1 Solid State

4.2.1.1 Assignments and Structure

Raman spectra of these dyes are shown in Figure-4.2 for HMPAB and its derivatives, Figure-4.3 for HNAB and its derivatives, and Figure-4.4 for PAQ, CPAQ and CMPAQ. Figures- 4.5 - 4.7 represents the FT-IR spectra of these dyes, respectively. Figure-4.4 also includes the solid state spectra of copper complexes of the PAQ and CMPAQ. The observed band positions and their tentative assignments are shown in Table-4.1 for HMPAB and its derivatives; Table-4.2 for HNAB and its derivatives and Table-4.3 for PAQ, Table-4.4 for CPAQ and Table-4.5 for CMPAQ.

Generally a satisfactory assignment of the spectra should be possible by comparing the complementary spectra (e.g Raman and IR spectra). The FT-IR spectra are complicated because of the bands arising from all molecular groups in the complex molecule whereas in the Raman spectra only those bands which are resonantly enhanced are observed. The assignment of the IR spectra is, therefore, preliminary and is done on the basis of IR assignments of compounds having similar types of structural groups, viz. azobenzene, arylazophenols, arylazonaphthols and quinolin-8-ol and its derivatives [2,7,13-17]. One of the reasons for assigning FT-IR spectra was the assignment of vibrational modes originating from substituent groups, which are either

absent or very weak in the RR spectra, and hence difficult to assign. The observed wavenumber difference in the bands in FT-IR and Raman spectra may arise for various reasons, such as the different band resolutions obtained in the two techniques as well as different selection rules. This will be particularly so if the crystalline form has more than one molecule in the unit cell. In the absence of crystal structural data on these compounds, it is not possible to calculate precisely the band splitting due to intra-molecular interactions in the unit cell.

In the solid state, it is general presumption that the dyes will remain dominantly in one tautomeric form; attention has, therefore, been paid to those modes which are observed exclusively in one form or very weak in the other form. However, some reports suggest the presence of tautomaric mixtures even in the solid state [17]. In such a situation, solid state spectra may be interpreted convincingly by assuming that the solid dye is an agglomerate of tautomers (an azo form and a hydrazone form).

In general azo dyes are characterized by bands due to the Ph-N=N-Ph skeleton. The presence of the azo form is characterized by a strong band in 1375-1445 cm^{-1} range due to $\nu_{N=N}$ whereas in some cases the appearance of a doublet is also observed, and is attributed to $\nu_{N=N}$ coupled ring modes. In addition, one would expect $\nu_{Ph-N=}$ and ν_{C-N} (azo) for the compounds which exist in azo form while ν_{Ph-NH}, ν_{N-N} and ν_{C-N}

(hydrazone) should be pronounced in the hydrazone form. Moreover, it is well known that in hydrazone form, when excited, Raman intensities of the ring modes are drastically increased due to pre-resonance effect (Table-4.6 for the absorption maxima of these compounds). In the azo form, out of three characteristic modes $\nu_{N=N}$ (1400-1440 cm^{-1}), $\nu_{Ph-N=}$ (1150 cm^{-1}) and ν_{C-N} (1140 cm^{-1}), mainly $\nu_{N=N}$ is sensitive for ring substitution. Similarly, for hydrazone form $\nu_{C=O}$ (ca.1600 cm^{-1}), $\nu_{C=N}$ and ν_{C-N} (1380 cm^{-1}), ν_{N-N} (1230 cm^{-1}) and ν_{C-N} (1180 cm^{-1}) should be observed. However, in quinolinol compounds, owing to the presence of the quinolinol ring, ν_{C-N} and $\nu_{C=N}$ are expected to appear regardless of the tautomeric form. In the present analysis, the appearance of modes $\approx$1380 cm^{-1} range, therefore, has not been taken as an evidence for the hydrazone from. In some cases, it might be possible to assign separately the $\nu_{C-N}/\nu_{C=N}$ arising due to hydrazone form or quinolinol ring. The observed modes in the solid state for each dye are correlated and assigned, based on the above discussion and also by comparing the spectra of those substituted benzene, azobenzene derivatives and quinolin-8-ol derivatives [1,17-19].

For, HMPAB, a single intense band at 1402 cm^{-1} is observed which is missing in HNAB. In a symmetrical unsubstituted azo system, viz. *trans*-azobenzene, $\nu_{N=N}$ is reported at 1442 cm^{-1} [18], whereas in hydroxy azo dyes this mode is assigned between

1440 and 1400 cm^{-1}. In azo dyes where a resonating quinonoid structure is possible, this mode shifts towards a lower wavenumber, and is observed at 1375 cm^{-1} [1,8,19]. The strong band at 1402 cm^{-1} in HMPAB is, therefore, assigned to $\nu_{N=N}$. Jacques [4] observed this band at 1417 cm^{-1} in 2-hydroxy-5-methylazobenzene. It, therefore, calls for some comments. In hydroxyazodyes, where the hydroxy group is *ortho* to the azo group, a shift of $\nu_{N=N}$ to lower wavenumbers is observed, when it is in the *para* position, there is little effect (Table-4.7). It is, therefore, proposed that the lowering of wavenumber of $\nu_{N=N}$ is due to the interaction of the hydroxy group with the nitrogen atom which is probably intra-molecular. On this basis the possible structure for HMPAB is proposed as shown in Figure-4.8.

To check the validity of this proposal, we have analyzed the IR spectrum of HMPAB in solid state. It is expected that the hydrogen bonded form should give rise to a broad, structureless band due to ν_{OH}, instead of a strong, intense band, in the region 3500-3300 cm^{-1}. The observation of a broad band further supports our conclusion. The appearance of a band at 1315 cm^{-1} in the RR spectra of HMPAB is assigned to ν_{C-O} stretch, which also supports the proposed structure.

In addition, one would expect Ph-N=N-Ph and C-N (azo) stretching modes for the compounds which exist in azo form and ν_{Ph-NH}, ν_{N-N} and ν_{C-N} (hydrazone) stretching modes for the

hydrazone form. A comparison of spectra of HMPAB and HNAB reveals that the bands at 1402, 1315, 1244, 1201 and 1157 cm^{-1} are observed for HMPAB and missing for HNAB. The bands for HNAB at 1555, 1380, 1266, 1230 and 1171 cm^{-1} are not observed for HMPAB. In azobenzene, the $\nu_{Ph-N=}$ stretch is observed [20] at 1155 cm^{-1} and in 3,5-dimethoxy-4-hydroxyazobenzene [4] at 1156 cm^{-1}. Hence the band at 1157 cm^{-1} can safely be assigned to this mode. Similarly, the band at 1143 cm^{-1} could be assigned to C-N (azo) stretching.

In the spectrum of HNAB, the band at 1380 cm^{-1} is attributed to the hydrazone skeleton Ph-NH-. The characteristic N-N stretch is assigned to the band at 1171 cm^{-1} as in other related systems. A weak band observed at 1626 cm^{-1} in HMPAB and at 1555 cm^{-1} in HNAB can be assigned to a di-substituted ring mode, respectively. These assignments were made by comparing the modes of substituted benzene and naphthalene [21-22]. The weak intensities of these bands are due to the selective enhancement of the chromophore group in RR spectra. The bands at around 1600 and 1500 cm^{-1} are generally assigned to the vibration of the benzene ring. In our case, a band at 1593 cm^{-1} is observed in both spectra, although the intensity of the band is found to be much higher for HNAB than HMPAB. It is well known that with appropriate excitation the Raman intensities of the hydrazone tautomer are dramatically increased owing to the pre-resonance

effect. However, there seems no reason why the RR intensity of a benzene ring mode should contribute more in the hydrazone form than in azo form. Hence, the 1593 cm^{-1} band should not be attributed to a benzene ring mode. It can be otherwise explained, if one considers the hydrazone form of HNAB with a quinonoid type of structure (Figure-4.9). In this situation, $\nu_{C=O}$ and $\nu_{C=C}$ of the naphthol ring will contribute strongly. In dyes having a quinonoid structure, a strong band at 1600 cm^{-1} is observed which becomes weak as the equilibrium shifts towards the azoic structure. We, therefore, assign this band to predominantly due to $\nu_{C=O}$(quinonoid) + $\nu_{C=C}$ (naphthol ring) overlapped with weak phenyl ring vibration. The proposed structure of HNAB is supported by the following arguments.

In arylazonaphthol dyes having a quinonoid type of structure, characteristic bands are found at 1632, 1500, 1350, 1260 and 1170 cm^{-1}, with some wavenumber shifts for *ortho* and *para* quinonoid structure differences [23]. In addition, the ring modes in the region 1600-1400 cm^{-1} are enhanced. The appearance of bands at 1593, 1550, 1380, 1266 and 1171 cm^{-1} in HNAB is consistent with the quinonoid type of structure, as proposed. Moreover, the bands at 1500 and 1450 cm^{-1} appear fairly strong bands. It should be noted that the vibrations of the Ph-N=N-Ph group are not much affected by the position of the substituents on the aromatic ring. However, in the assignments of Ph-NH-N=Ph

skeleton modes in systems having *ortho* and *para* - quinonoid structures, some discrepancies are encountered [3,6]. As discussed earlier, in the case of HMPAB, it seems that the substituent at the *ortho* position even in the hydrazone form interacts with the chromophore group.

$(PAQ)_2Cu$ and $(CMPAQ)_2Cu$, which exist in the azo form, exhibit two bands of almost equal intensity at 1425 and 1379 cm^{-1} and at 1416 and 1380 cm^{-1}, respectively. The bands at 1416 and 1425 cm^{-1} are assigned to $\nu_{N=N}$, which matches well with the reported assignment of this mode [4,24-25]. The presence of the strong bands at 1425 and 1416 cm^{-1} clearly indicates the azo form for these systems. The other two bands are assigned to the ν_{C-C} skeletal mode of the quinolinol ring, in accordance with the reported assignment in quinolin-8-ol derivatives [26]. The strong band due to the C-C skeletal mode may be the result of its coupling with $\nu_{N=N}$. The existence of a pure azo structure in the copper complexes is also supported by the appearance of weak bands in the 1450-1600 cm^{-1} region, mainly due to ring modes. Other characteristic modes due to the azo form are assigned later.

Based on this, the azo-hydrazone forms of PAQ, CPAQ and CMAPQ are deduced in the solid state (Figure-4.10). In PAQ, the characteristic modes of the azo form at 1419 cm^{-1}, $\nu_{N=N}$, and 1138 cm^{-1} ν_{C-N} (azo), are strong. However, the modes in the 1450-1600

cm^{-1} region are also enhanced in comparison with its complex and two additional bands at 1392 cm^{-1} assigned to $\nu_{C=N}/\nu_{C-N}$ and that at 1265 cm^{-1} to ν_{C-C} (in plane) in the hydrazone form, indicating that even in the solid state possibly both forms are present. The decrease in wavenumber (1425 → 1419 cm^{-1}) of $\nu_{N=N}$ and its enhanced intensity suggest that this modes decoupled with ring vibration. Further, $\nu_{C=N}$ modes due to the hydrazone form and quinolinol ring seem to be coupled together, appearing at 1392 and 1370 cm^{-1}, respectively at higher and lower wavenumber than expected (at ≈1380 cm^{-1}). In CPAQ also, a similar spectral pattern is observed with a difference that the modes characterizing the hydrazone form are very strong, whereas the modes due to the azo form are comparatively weak, reflecting the hydrazone form as the dominant one. Also, an additional band at 1618 cm^{-1} is observed which is assigned to $\nu_{C=O}$ of substituents in H-bonded form.

In CMPAQ, the spectrum in the solid state resembles that of copper complex fairly closely; the ring modes increasing slightly in intensity along with the emergence of some new bands at 1024, 1090 and 1648 cm^{-1}, clearly revealing that the compound exists in the azo form. The band at 1648 cm^{-1} in the RR spectrum is assigned to $\nu_{C=O}$ of the substituent and and is observed at 1649 cm^{-1} in the FT-IR spectrum. The higher wavenumber of this band in CMPAQ in comparison with CPAQ suggests that the compound

remains in a non-H-bonded form. It should be pointed out that in CMPAQ, H-bonding with substituents is not possible if the compound exists in the azo form, which also supports our assignment and proposed structural form.

It can, therefore, be concluded that PAQ and CPAQ in solid state are mixtures of the two tautomers whereas CMPAQ is in the pure azo form.

The possible difference in the solid-state spectra of three compounds can be understood in terms of intra-molecular H-bonding, which may play an important role in stabilizing the structure in a particular tautomeric form and may also distort the planar configuration of the system. Competing intra-molecular H-bonding between six- and five-membered rings will try to shift the tautomeric form depending on their strength. In addition to intra-molecular H-bonding (discussed earlier), inter-molecular H-bonding between the hydroxyl group of one molecule to a nearby phenyl nitrogen of the arylazo group or carbonyl group of another molecule is also possible in these compounds.

In the light of the above discussion, the dominant hydrazone form in CPAQ can be explained as a result of strong hydrogen bonding between -COOH and Ph-N=N; inter-molecular H-bonding at Ph-N=N cannot be ruled out since the distorted planar configuration resulting from such bonding has been associated with the hydrazone tautomer [27]. The later

interaction does not seem plausible because of a strong band at 1270 cm^{-1} assigned to the ν_{C-C} in-plane mode. In PAQ, no intra-molecular H-bonding is possible with the azo group. Hence, the five-membered ring formed due to H-bonding at quinolinol will try to stabilize the azo structure. Such intra-molecular H-bonding was supported by earlier studies on the basis of IR spectra [11]. Electronic spectra also corroborate this effect.

The spectral bands in the range 1600 - 1450 cm^{-1} could be attributed to ring modes. The bands at 1580 and 1491cm^{-1} are very strong in CPAQ. The corresponding bands at 1589 and 1491 cm^{-1} in CMPAQ and at 1590 and 1485 cm^{-1} in PAQ are weak, except for the band at 1590 cm^{-1} in PAQ which is fairly strong. These observations suggest that the enhancement of the intensity of the bands at 1590 and 1491 cm^{-1} in CPAQ is due to its hydrazone form, where, in addition to the phenyl ring modes the $\nu_{C=O}$ and $\nu_{C=C}$ of the quinolinol ring will contribute strongly, increasing the intensity of these bands. We, therefore, assign the band at 1580 cm^{-1} in CPAQ to $\nu_{C=O}$ and $\nu_{C=C}$ of the quinolinol ring overlapped with a weak phenyl ring vibration. The band at 1545 cm^{-1} is due to benzene ring mode. The strong band at 1231 cm^{-1} is assigned to ν_{N-N} and is absent in the other two systems. The bands at 1270, 1066 and 1028 cm^{-1} can be assigned to various ring modes of the quinolinol ring. The fact that hydrazone form, when excited, ring mode intensities are increased, can be taken as an evidence for

the hydrazone form of CPAQ. Further support for the hydrazone form comes from the absence of the ν_{C-O} band of the quinolinol ring. This band is reported at 1330 cm^{-1}. From the above discussion, it is clear that in the solid state the systems remain dominantly in one form and also there are bands sensitive to specific resonating form. Bands at ca. 1420, 1330, 1187 and 1138 cm^{-1} are strong in the azo form whereas those at ca. 1590, 1500, 1390 and 1230 cm^{-1} are strong in the hydrazone form. Also, both types of characteristic modes are present in PAQ and CPAQ.

4.2.1.2 Effect of Substitution : Arylazophenols and Arylazonaphthols

It has been discussed (in section 4.2.1.1) that HMPAB exists in azo form and HNAB in hydrazone form, exclusively. A comparative study of these compounds should, therefore, reflect the characteristic features of each form. Figures -4.2 and 4.3 represent the RR spectra of HMPAB and HNAB along with their derivatives, respectively.

To understand the role of substituents on the chromophore vibrational modes and to make their assignments more reliable, we studied the spectra of derivatives of HMPAB (e.g. HMPAMB and HMPACB) and of HNAB (e.g. HNAMB and HNACB) by varying the substituents in the *ortho* position of ring A and keeping the hydroxy substitution constant in ring B. The observed bands are

summerised in Table-4.7 and 4.8 together with their assignments. A comparison of the bands of the derivatives of HMPAB and HNAB reveals that the bands observed at 1402, 1157, 1143 cm^{-1} are characteristic of the azo form, whereas those 1600, 1500, 1380, 1260 and 1170 cm^{-1} are associated with the hydrazone form. To analyze the effect of substitution, a correlation table is made in which the shifts in the positions of characteristic modes with substitution in both rings are shown (Table - 4.7 for characteristic bands of azo structure in aryl azo phenols and Table-4.8 for characteristic bands of hydrazone structure in aryl azo naphthols). Since most of the data available in the literature are for the solution phase in various solvents, care was taken in selecting the dyes for comparison.

It is clear from the Tables -4.7 and 4.8 that the substitution of -OH in the *para* position is much less effective than in the *ortho* position for $\nu_{N=N}$. A comparison of $\nu_{N=N}$, observed in those dyes where groups with grater electron-donating character are sustituted at the *para* position, shows that the wavenumber decreases with increasing electron-donating character of the substituents. It seems that for *para* substituents this is due to charge transfer, whereas for *ortho* susbtitution this may be the result of an Hydrogen bonded interaction with N atom of the azo group. It is also clear that the 1315 cm^{-1} band is absent in all derivatives of naphthol dyes (quinonoid structure), except

in HNAMB where a doublet is observed at 1316 and 1293 cm^{-1}. A similar doublet is also observed in HMBAMB. In both, an $-OCH_3$ substituent is present. This doublet may be attributed to ν_{C-O} of the substituent coupled with a $-CH_3$ deformation mode. This supports the assignment of the 1315 cm^{-1} band as due to ν_{C-O} in the azo form. It is also clear that other characteristic modes (C-N and Ph-N= stretches) are not very sensitive to substitution. This may be taken as an indication of the azo structure in such systems.

The effect of substituents on the characteristic modes in the hydrazone form can be seen from Table- 4.8. It is clear that substitution at *para* and *ortho* positions of ring B influences all modes. However, an interesting change is observed in ν_{N-N} and $\nu_{C=O}$ (quinonoid). In *para*-substituted systems, ν_{N-N} is lower than in an *ortho*-substituted system, whereas the reverse is true for $\nu_{C=O}$. It is also noted that for dyes Sl.No. 7 - 9 in Table-4.8 the *ortho* substitution on ring A influences the band position. This may be due to the interaction with the N atom or steric reasons.

From Tables -4.7 and 4.8, it is clear that the characteristic bands assigned for each form match closely in related systems. This can, therefore, be taken as an index for characterizing the structural form in such systems. Moreover the data confirm that the arylazophenol derivatives, studied in the

present work, remain in the azo form with the structure shown in Figure-4.8, whereas those of the aryl azonaphthol derivatives are in the hydrazone form with a quinonoid type of structure as shown in Figure-4.9.

4.2.2 Solution State

4.2.2.1 Electronic Absorption Spectra : pH Dependence and Tautomeric Equilibria

Three dyes, PAQ, CPAQ and CMPAQ were studied in aqueous solution. PAQ is selected as it has the simplest structure with no substitution at phenyl ring which can serve as a model for describing the structural changes involved with the protonation-deprotonation and to investigate tautomeric equilibria in quinolinol containing dyes. Moreover, semi-empirical CNDO/2 calculations, which are reported for this compound [12], can be taken as the basis for analyzing the electronic spectra, considering different substitution at PAQ as perturbation on the molecular orbitals. The other dyes used viz. CPAQ and CMPAQ have substitution at *ortho*-position in the phenyl ring and can form H-bonding with azo group. This enabled us to study the effect of intra-molecular H-bonding on the structure of the dyes.

pH dependent electronic absorption spectra of PAQ, is shown in Figure-4.11. Spectrum at pH $\approx$ 7 shows a band maxima at

413 nm with a weak asymmetry at ≈480 nm. The asymmetry becomes pronounced as the pH of the solution increase and the band maxima shows a subtle bathochromic shift up to pH 9. Above this pH, band maxima shifts to 480 nm and the band at 420 nm appears as a weak shoulder. This has been attributed to the shift in tautomeric equilibria around pH 9. The presence of a isobestic point support the existence of equilibria. The electronic transitions involving hydrazone form in general appears at higher wavelength than those due to azo form [28]. Also, for 5-(aryl)azo-8- quinolinols, at acidic pH, the absorption spectra exhibits intense band in the long wavelength region, which decreases with increasing pH and in the neutral form a maxima ≈400 nm appears which has been associated with azo form [29]. Thus the bands at 413 nm and 480 nm can be assigned to azo and hydrazone form, respectively. Such a bathochromic shift with increasing pH has also been reported for other azo dyes and support the azo-hydrazone equilibria [30].

It may be noted that acid-base transformations in solutions lead to a change in electronic spectra of azoquinolinols and a number of equilibria are investigated and characterized as mono-, di-protonated and deprotonated species [29-30]. The shift in the observed maxima in PAQ from 420 nm to 480 nm at pH 9 indicate that equilibria shifts towards hydrazone form for deprotonated species probably due to dissociation of hydroxy group at 8- quinolinol moiety. Since, the spectra below

pH ≈ 7 could not be recorded in aqueous solution owing to the precipitation, the existence of equilibria for monoprotonated form could not be established. However, we have recorded the spectrum in conc.HCl (pH ≈ 1) by directly dissolving the dye in acid. The spectral pattern drastically changes with bands appearing at 617, 502.5 and 364 nm. The bands at 617 and 502.5 nm are assigned to hydrazone and azo form, respectively. This has been confirmed by RR spectra obtained by exciting 502 nm band exclusively, which support azoic structure associated with this band. The band at 364 nm is observed in conc. HCl for all the compounds investigated. This band shifts towards lower wavelength with increasing pH (Table-4.6) and disappears above pH ≈ 9. This could originate from $\pi \rightarrow \pi^*$ transition involving higher excited state [31].

From the above discussion, it may be inferred that neutral species for PAQ remains dominantly in azo form and deprotonated one in hydrazone form whereas monoprotonated species exist in azo-hydrazone equilibria. Possible tautomeric structures involving various species are shown in Figure-4.12.

Information regarding protonation can be derived from electronic spectra in the light of CNDO/2 results. In CNDO/2 calculations, the transition density (charge migration) of the first $\pi \rightarrow \pi^*$ transition shows that the longest wavelength transition involves mostly a transfer of electron charge from the

quinolinol ring, more particularly from the N-atom and C-8 to the azo group (Figure-4.13), the a-nitrogen getting somewhat greater share. A substitution of H-atom by an electron releasing substituent like -OH should obviously lower the transition energy of the first $\pi \rightarrow \pi^*$ transition, since it involves a transfer of electron from the C8 atom to the azo groups. The reverse is expected in case of binding /protonation at C8 or N position. Thus, the observed higher wavelength of protonated species in comparison to neutral/deprotonated species can be explained if the protonation of the azo group is considered. The invariance of the absorption band maxima in PAQ and $(PAQ)_2Cu$ in acidic pH further supports the protonation of azo group, since the protonation at quinolinol moiety is restricted in the later due to complexation.

The electronic spectra of CPAQ (Figure-4.14) and CMPAQ (Figure-4.15) show almost identical pattern in the whole pH range investigated, however, they differ from PAQ. In conc. HCl, the band at 617 nm in PAQ is missing in both CPAQ and CMPAQ. Also, unlike PAQ where absorption band at 420 nm (pH $\approx$ 7) bathochromically shifts and disappears above pH 9 and a new band at 480 nm emerges, in CPAQ and CMPAQ only a shift in the maxima is observed with the appearance of a shoulder at $\approx$ 420 nm above pH $\approx$ 9, which is maintained up to pH 12 in acidic pH. The band at 515 nm is attributed to azo form in both CPAQ and CMPAQ,

suggesting that the monoprotonated species are in azo form. Accordingly, the observed band at 485 nm in aqueous solution is assigned to azo form. The bathochromic shift in aqueous solution with increasing pH is associated with the different species of the same tautomer.

The reason for difference in spectral pattern in CPAQ and CMPAQ with respect to PAQ may lie in different types of intra-molecular H-bonding in them, which is known to influence the azo-hydrazone tautomeric equilibria in the azo dyes of 8-quinolinols [32]. In PAQ, H-bonding is possible only at quinolinol moiety forming a five membered ring, whereas in the later two, there will be competition between six membered H-bonding at azo group and five membered H-bonding at quinolinol moiety. The observed blue shift of 416 nm band to 397 nm from aqueous solution to methanol is attributed to this intra-molecular H- bonding. This is supported by the fact that in $(PAQ)_2Cu$, where H-bonding is not possible,the absorption band maxima in methanol appears at much higher wavelength (437 nm). In CPAQ and CMPAQ, the H-bonding involving azo N-atom may stabilize one kind of structure which is reflected in the single absorption band. The higher observed value of λ_{max} in acidic solution compared to aqueous solution in both compounds is due to weakening of H- bonding as a result of protonation at the N-atom of the azo group. The invariance of absorption bands in

$(CMPAQ)_2Cu$ and CMPAQ in acidic pH supports protonation of azo N-atom as in case of PAQ. Further, the shift towards higher wavelength in aqueous solution as compared to methanol is due to the stronger H-bonding with solvent (methanol) which inhibits electron transfer from -OH to azo group, thus increasing the extent of transition. Copper complex of CMPAQ, which is known to exist in azo form, display a band at 437 nm in methanol instead of two bands in its parent compound CMPAQ. Hence, the appearance of a single band and a higher wavelength shift in the copper complex may be attributed to H- bonding effect. In view of this, the various structural form for CPAQ and CMPAQ are shown in Figures - 4.16 and 4.17, respectively.

It may be argued that electronic spectra at various pH gives artifact due to protonation and mesomeric effect, hence the conclusion regarding the structural forms and protonation should not be taken as reliable measures until these are confirmed by some independent technique such as RR technique. We have, therefore, opted for RR studies of these compounds in solution.

4.2.2.2 Resonance Raman Study : Assignments and Structure

The pH dependent RR spectra of PAQ at pH $\approx$ 1 and pH $\approx$ 9 in the range 1000-1700 cm^{-1} are shown in Figure-4.18. The observed wavenumbers and the assignments are given in the

Table-4.3. Two spectra resembles closely; the characteristic bands identified for azo form in solid state at 1415, 1327, 1189 and 1130 cm^{-1} are quite strong, while the hydrazone modes are very weak suggesting azoic structure as the dominant one. It may be noted that from the electronic spectra, the protonated form appears to exist in the tautomeric equilibria, while RR spectra gives azoic form. This should not be surprising since the excitation line is far away from the absorption band due to hydrzone form. From the RR result, the structural form in solution state are corroborated as proposed by electronic absorption spectra.

pH dependent RR spectra of CPAQ is shown in Figure-4.19. Form the figure it is clear that in acidic pH, CPAQ shows strong bands in 1450-1600 cm^{-1} range. Bands at 1456, 1501, 1515, 1564 and 1593 cm^{-1} are arising due to various ring modes . Moreover, the modes at 1130, 1190 and 1330 cm^{-1} are either absent or weak while the bands at 1261 and 1151 cm^{-1} are quite strong (Table-4.4).

These observations clearly indicate that the structure is dominantly hydrazone. This corroborates with the observed single band at $\approx$ 515 nm associated with hydrazone form in electronic spectra. In aqueous solution at pH 9 and pH 12 the spectra differ completely from that of solid state as well as in acidic pH. At these pH, the absorption band maximum lies at $\approx$480

nm. The excited RR spectra using 488 nm line will be very close to resonance. Observed spectra clearly show the presence of azoic structure as the dominant one. It may be mentioned that the band at 485 nm in electronic spectra is due to azo form as RR spectra clearly reflect the azoic structure. This confirms the conclusion drawn on the basis of electronic spectral results.

The RR spectra of CMPAQ is shown in Figure- 4.20. Similar analysis for CMPAQ is made (Table-4.5). It reveals that in acidic solution (pH 1), it remains in hydrazone form, while in aqueous solution the azo form is the dominant one (at pH 12.0). In view of this, the various resonating forms for CPAQ and CMPAQ are shown in Figures - 4.15 and 4.16, respectively.

The change in H-bonding in solution with respect to solid state is also observed in Raman spectra. In CPAQ a strong band at 1618 cm^{-1} is observed in solid state which shifts to 1611 cm^{-1} in acidic pH. The appearance of this mode at lower wavenumber than observed for free C=O suggest the strong H-bonding. This mode does not appear in the aqueous state. The fact that hydrazone form is stabilized when H-bonding is strong at azo group, further corroborates our conclusion of proposed structure. In case of CMPAQ, however, the solid state RR spectra gives a weak band at 1648 cm^{-1} which shifts to 1614 cm^{-1} in acidic solution and disappeared in the aqueous phase, clearly indicating that the H-bonding is absent.

The spectroscopic studies on these hydroxy azo dyes, used as ligands, have successfully been able to deduce various structural forms in solid state and solutions and we were able to demonstrate that electronic and vibrational spectra, especially in these compounds, when used judiciously, can follow the shift in tautomeric equilibria induced due to change in environment around dye molecules such as change in pH.

References

1. K. Machida, *Vibr. Spectra Struct.* 17A, 421 (1989).

2. P.K.Bajpai, B.Pal and T.S.Basu Baul, *J. Raman Spectrosc.* 26, 217 (1995).

3. Y.Saito, B.K.Kim, K.Machida and T.Uno, *Bull. Chem. Soc. Jpn.* 47, 2111 (1974).

4. P. Jaques, *J. Raman Spectrosc.* 12, 102 (1982).

5. A.J.Barnes, M.A.Majid, M.A.Stukey, P.Gregory, and C.V.Stead, *Spectrochim. Acta* 41A, 629 (1985).

6. J.Keleman, S.Moss, H.Santer and T.Winkler, *Dye Pigments* 3, 27 (1982).

7. H.Haker, *Spectrochim. Acta* 21, 1989 (1965).

8. P.J.Trotler, Appl. Spectrosc. 31, 30 (1977).

9. A.I.Vogel *Text Book of Practical Organic Chemistry.* Longman, London (1978).

10. T.S.Basu Baul, *Bull. Soc. Chim. Fr.* 128, 454 (1991).

11. T.S.Basu Baul, T.K.Chattopadhyay and B.Majee, *Polyhedron*, 2, 635 (1983).

12. T.S.Basu Baul, T.K.Chattopadhyay and B.Majee, *Indian J. Chem.* 23A, 470 (1984).

13. G.M.Badger and R.G.Buttery, *J. Chem. Soc.* 614 (1956).

14. R.J.W. LeFevre, M.F.O'Dwyer and R.L.Werner, *Aust. J. Chem.* 6, 341 (1953).

15. B.Marchon, L.Bokobza, and G.Cote, *Spectrochim. Acta*, 42A, 537 (1986).

16. C.V.L.Narshima Rao, M.Rangacharyulu and D.Premaswarup, *Indian J. Pure Appl. Phys.* 19, 373 (1981).

17. A.H.Jubert, A.Gonzalez Baro, R.Pis Dies and E.J.Baran, *J. Raman Spectrsc.* 23, 273 (1992).

18. Y.Matsunaga, *Bull. Chem. Soc. Jpn.* 44, 878 (1971).

19. L.J.Bellamy, *The Infrared Spectra of Complex Molecules.* Chapman and Hall, London (1975).

20. J.L.Houben, G.Masetti, E.Campani and G.Gorini, *J. Raman Spectrosc.* 13, 15 (1982).

21. F.R.Dollish, W.G.Fatoley and F.F.Bentley, *Characteristic Raman Frequencies of Organic Compounds*, Wiley, New York (1974).

22. E.P.Krainov, *Opt. Spektrosk.* 16, 763 (1964).

23. K.Kawai, H.Masago, K.Kanamori,, T.Kanaseka, I.Kasahara and K.Goto, *J. Raman Spectrosc.* 18, 205 (1987).

24. K.Machida, H.Lee and A.Kuwae, *J. Raman Spectrosc.* 9, 198 (1980).

25. F.Ni and T.M.Cotton, *J. Ramam Spectrosc.* 19, 429 (1988).

26. B.Marchon, L.Bokobza and G.Cote, *Spectrochim. Acta*, 42A, 537 (1986).

27. K.Machida, B.K.Kim, Y.Saito, K.Igarashi and T.Uno, *Bull. Chem. Soc. Jpn.* 47, 78 (1974).

28. J.Griffiths, *Colour and Constitution of Organic Molecules.* Academic Press, New York (1976).

29. V.M.Ivanov and T.F.Rudometkina, *Zh. Anal. Khim.* 33, 2426 (1978).

30. I.S.Mustafin and O.S.Sivanova, *Tr. Kom. Anal. Khim., Akad. Nauk SSSR* 17, 133 (1969).

31. A.Binacalana, E.Campani, G.D.Domenico and G.Gorini, *J. Raman Spectrosc.* 24, 43 (1993).

32. E.Sawicki, *J.Org.Chem.*, 22, 365 (1957).

Table 4.1 : Wavenumbers (cm^{-1}) of Observed Vibrational Bands and Their Assignments in Arylazophenols in Solid form.

HMPAB		HMPAMB		HMPACB		Assignments
Raman	FT-IR	Raman	FT-IR	Raman	FT-IR	
1626	1623	1636	1633	1633		Distributed ring stretch
			1619		1622	
1593	1596		1598			Ring stretch +($\nu_{C=C}$+$\nu_{C=O}$)
	1588	1588	1587	1582	1588	Ring stretch +($\nu_{C=C}$+$\nu_{C=O}$)
	1576		1573		1577	
1500	1499		1499		1498	Benzene ring stretch
	1481		1487			
	1473		1467		1467	
	1457	1442	1456	1453	1449	
			1439		1433	
	1422					
1402	1407	1411	1409	1410	1404	$\nu_{N=N}$
	1382		1384		1379	ν_{C-C}
1358	1357	1364	1359	1356	1350	ν_{C-N} + Ring Vibration
1315	1314	1316	1312	1310	1308	ν_{C-O}
		1306				OCH_3 deformation
	1281		1288		1284	
	1274					
1255	1251		1253		1259	
1244	1244	1240	1246	1235	1231	$\nu_{C-N=N-C}$
		1224				ν_{N-N} (H)
	1216		1213	1215		
1201	1199		1199		1199	
	1191		1179			
1157	1156	1164	1162		1156	$\nu_{Pn-N=}$
1145	1144	1144	1145	1145	1141	ν_{C-N} (azo)
1129	1130		1134			
		1110	1111	1115		
	1170		1176			
	1042		1042		1054	Ring modes
	1020		1025			
	1007		1005			

Table 4.2 : Wavenumbers (cm^{-1}) of Observed Vibrational Bands and Their Assignments in Arylazonaphthols in Solid Form

HNAB		HNAMB		HNACNB		Assignments[a]
Raman	FT-IR	Raman	FT-IR	Raman	FT-IR	
	1619		1616		1621	Distributed ring stretch
1593	1597	1593	1592	1598	1602	Ring stretch +($\nu_{C=C}$+$\nu_{C=O}$)
	1562		1557		1562	
1555	1550	1548	1545	1551	1551	Naphthol ring stretch
1500	1502	1500	1500	1480	1505	Benzene ring stretch
			1483			
	1456		1468			
1450	1448	1460	1449	1450	1448	Benzene ring stretch
	1400		1399		1402	$\nu_{N=N}$
1380	1390	1384	1386	1384	1386	$\nu_{C=N/C-C}$
1340	1338	1340	1341	1335	1338	ν_{C-N}
	1322	1323	1330		1326	ν_{C-O}
	1296		1318			
		1293	1295			OCH_3 deformation
					1284	
1266	1266	1252	1253	1253	1256	Naphthol C-H bend
	1256		1246		1246	$\nu_{C-N=N-C}$
1230	1230	1224	1224	1224	1227	ν_{N-N} (H)
	1210		1207		1207	
1171	1176	1210	1207	1179	1180	ν_{C-N} (H)
	1164		1161		1159	$\nu_{Ph-N=}$
	1151					
1141	1143	1155	1150	1153	1153	ν_{C-N} (azo)
	1131		1130		1136	
					1125	
			1107		1108	
1090	1093	1089	1091	1093	1097	Naphthol ring deformation
	1071		1079		1070	
				1049	1050	
			1041		1040	
	1033				1033	
	1023					

[a] H stands for Hydrazone form

Table 4.3: Wavenumbers (cm^{-1}) Observed of Vibrational bands and their assignments in PAQ and its copper complex [$(PAQ)_2Cu$]

Resonance Raman				FT-IR	
Solid State (in KBr)		Solution State pH 1.0	State pH 9.0	Polyethylene Pellet	
PAQ	$(PAQ)_2Cu$	PAQ	PAQ	PAQ	Assignment[a]
(488.0nm) (A⇌H)	(476.5nm) (A)	(476.5nm) (A⇌H)	(A⇌H)		
1590	1593	1592	1595	1578	$\nu_{Ph-r} + \nu_{C=C}$ (Q-r)
1539	1566	1544	1558	1524	$\nu_{Ph-ring}$
1485	1500	1502	1503	1477	$\nu_{Ph-ring}$
1458	1462	1461	1465	1463	$\nu_{Ph-ring}$
1419	1425	1415		1409	$\nu_{N=N}$
1392		1402	1406		$\nu_{C=N}/\nu_{C-N}$ Coupled
1370	1379	1381	1379	1379	ν_{C-C} (Q-r)
1309	1324	1327	1331	1284	ν_{C-O}
1265		1305		1268	ν_{C-C} in plane(H)
			1240	1242	ν_{N-N} (H)
1187	1190	1189	1198	1193	
		1167	1167		$\nu_{Ph-N=}$
1138	1134	1130	1130	1149	ν_{C-N} (azo)
				1119	
			1097		
1052	1052	1055	1055	1068	Ring modes.
1022		1022	1022	1018	

[a] Q-r stands for Quinolinol ring and H stands for Hydrazone form

Table 4.4: Wavenumbers (cm^{-1}) Observed of Vibrational bands (cm^{-1}) and their assignments in CPAQ

Resonance Raman Solid State (in KBr) (488.0nm) (H⟷A)	Resonance Raman Solution State pH 1.0 (H⟷A)	Resonance Raman Solution State pH 9.0 (488.0nm) (A⟷H)	Resonance Raman Solution State pH 12.0 (A⟷H)	FT-IR Polyethylene Pellet	Assignment
	1652			1643	
1618	1611	1600	1600		$\nu_{C=O}$(H-bonded)
1580	1593			1589	ν_{Ph-r} + $\nu_{C=C}$(Q-r)
1546	1564	1565	1563		$\nu_{Ph-ring}$
	1515			1520	$\nu_{Ph-ring}$
1491	1501			1470	$\nu_{Ph-ring}$
1452	1456			1433	$\nu_{Ph-ring}$
1420	1424	1418	1420	1413	$\nu_{N=N}$
				1408	$\nu_{C=N}$
1369	1376	1385	1379	1362	$\nu_{C=N}/\nu_{C-C}$(Q-ring)
1350	1346	1341	1330		ν_{C-N}
	1290				
1270	1261	1271	1258	1264	ν_{C-C} in plane (H)
1231	1210			1217	ν_{N-N}
1188		1190	1192	1172	$\nu_{Ph-N=}$
		1172	1169		ν_{C-N} (azo)
1149	1151	1140	1143		
	1092	1090	1095		
1066	1050	1060	1054	1062	Ring modes
1028	1040	1020	1015	1019	

Table 4.5 : Wavenumbers (cm^{-1}) Observed of Vibrational bands (cm^{-1}) and their assignments in CMPAQ and its copper complex [$(CMPAQ)_2Cu$]

Resonance Raman				FT-IR	
Solid State (in KBr)		Solution State		Polyethylene Pellet	Assignment
CMPAQ	$(CMPAQ)_2Cu$	pH 1.0 CMPAQ	pH 12.0	CMPAQ	
(476.5nm)		(457.9nm)			
(A)	(A)	($H \rightleftharpoons A$)	($H \rightleftharpoons A$)		
				1676	
1648		1614		1649	$\nu_{C=O}$(non-H-bonded)
				1605	
1589	1593	1588	1592	1589	$\nu_{Ph-r} + \nu_{C=C}$(Q-r)
		1566	1558		
1491	1500	1510	1503	1521	$\nu_{Ph-ring}$
				1469	
1454	1450	1452	1456	1453	$\nu_{Ph-ring}$
			1448	1440	$\nu_{Ph-ring}$
1419	1416		1426		$\nu_{N=N}$
		1403	1406	1410	$\nu_{C=N}$
1376	1380	1372	1387		ν_{C-C} (Q-ring)
			1346	1352	
1328	1330	1328	1327	1328	ν_{C-O}
				1308	
		1286		1295	
1250		1253		1257	ν_{C-C} in plane (H)
	1238			1241	
				1214	
				1193	
1186	1180	1179	1175	1175	$\nu_{Ph-N=}$
1139	1134	1149	1145		ν_{C-N} (azo)
				1129	
				1122	
1090		1089	1097	1085	
		1063	1061	1062	
1024		1034	1020		Ring modes
				1013	

Table 4.6: Electronic Absorption Maxima (λ_{max} in nm) of some ligands in Different Solvents

Solvent	pH	Ligand					
		PAQ	CPAQ	CMPAQ	$(PAQ)_2Cu$	$(CMPAQ)_2Cu$	
		617			616.5		
Conc.HCl	-	502.5	515.5	515.5	507	516	
		364	369	365	369.5	370.5	
	5	-	485	484			
			338	344.5			
	6	-	485.5	484			
			344.5	344.5			
	7	480	483	483			
		416	344.5	344.5			
	8	480	482	481.5			
		413	344.5	344.5			
Aqueous							
	9	480	481.5	479.5			
		412.5	344.5				
	10	480	475.5	476.5			
		420	420	420			
	11	481	474.5	475			
		420	420	420			
	12	481	474.5	475			
		420	420	420			
Methanol	-	360	462.5	455.5	437	437	
		383.5	400	397.5	321	-	
		HMPAB	HMPAMB	HMPACB	HNAB	HNAMB	HNCCB
		398.5	406	413	462.5	512	-
Hexane	-	323.5	359.5	331	433	486.5	471.5
		-	318.5	-	304	312.5	304

Table 4.7 : Effect of Substitution on the Characteristic Vibrational Modes (cm^{-1}) of Azo Form in Arylazophenols

Sl. No.[a]	Substituents of ring A	Substituents of ring B	$\nu_{N=N}$	$\nu_{Ph-N=}$	ν_{C-N} (azo)	References
1	H	H	1444	1155	1143	4
2	4-SO_3Na	4 - OH	1445	b	1150	3
3	H	4 - OH	1440	b	1145	1
4	4 - SO_2NH_2	4 - OH	1440	b	b	1
5	H	4 - OH, 3,5-OCH_3	1424	1156	1122	4
6	2 - OCH_3	2 - OH, 5 - CH_3	1411	1164	1144	2 / This Work
7	2 - Cl	2 - OH, 5 - CH_3	1410	1157	1144	2 / This Work
8	H	2 - OH, 5 - CH_3	1402	1157	1145	2 / This Work
9	4 - SO_3Na	4 - NHC_6H_5	1437	b	1150	27
10	H	4 - NH_2	1420	b	1147	27
11	H	4 - $N(CH_3)_2$	1415	b	1150	27

a Compounds Sl.No. 1-5 and 9-11 have been incorporated here for comparison.

b Corresponding bands are not assigned.

Table 4.8 : Effect of Substitution on the Characteristic Vibrational Modes (cm^{-1}) of Hydrazone Form in Azonaphthols.

Sl. No.[a]	Substituents on ring A	Substituents on ring B	$\nu_{C=O}$ + $\nu_{C=O}$ (quinonoid form)	$\nu_{C=N}$ + ν_{C-C} Stretch	ν_{N-N}	ν_{C-N} (hydrazone form)	References
1	4 - SO_3H	2 - OH	1600	1389	1230	1185	5
2	4 - NO_2	2 - OH	1598	1392	1227	1185	5
3	2 - SO_3Na	2 - OH	1595	1399	1229	a	3
4	H	2 - OH	1608	1396	1236	a	3
5	4 - SO_3H	4 - OH	1629	a	1208	a	3
6	2 - SO_3Na	4-OH,3-CO_2H	1595	1398	1213	1185	1
7	H	2 - OH	1601	1390	1230	1171	2 / This Work
8	2 - Cl	2 - OH	1585	1384	1224	1179	2 This Work
9	2 - OCH_3	2 - OH	1593	1384	1224	1210	2 This Work

a Compounds Sl.No. 1-6 have been incorporated here for comparison.
b Corresponding bands are not assigned.

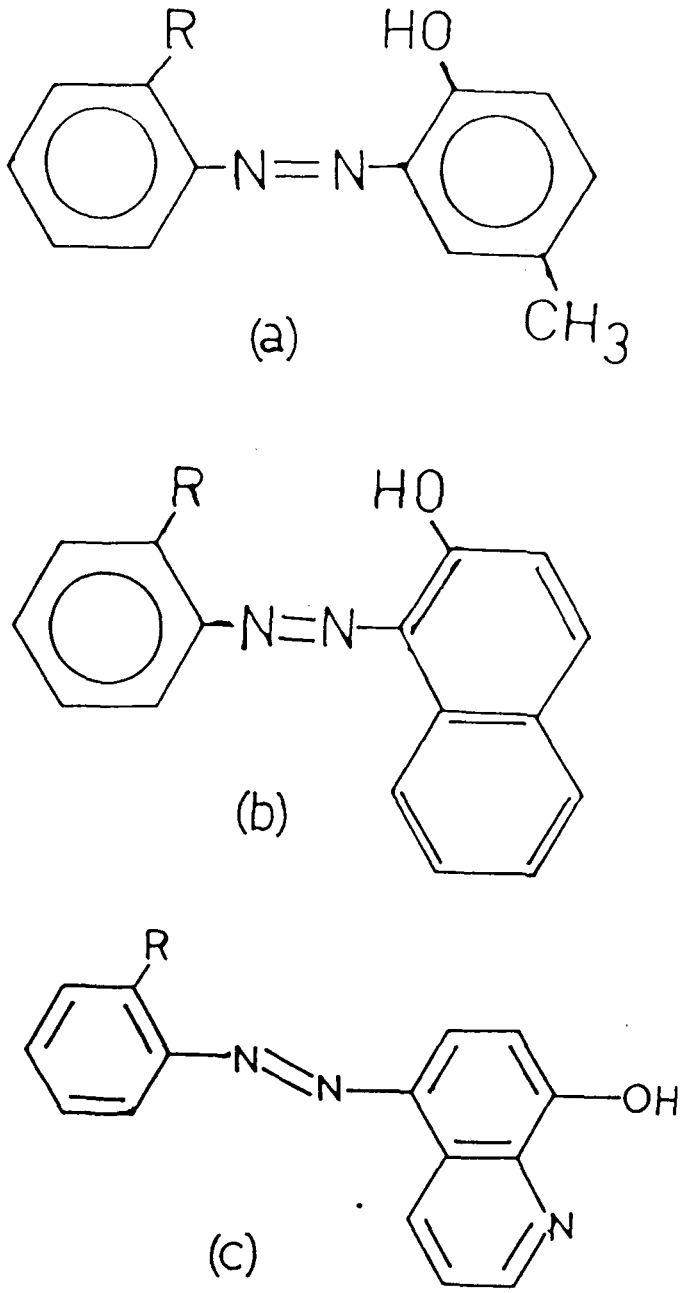

Figure 4.1 Structure of azo dyes (a) *o*-hydroxyphenyl-azobenzene (HMPAB for R = H, HMPAMB for R = $COOCH_3$, HMPACB for R = Cl), (b) *o*-hydroxynaphthyl-azobenzene (HNAB for R = H, HNAMB for R = $COOCH_3$, HNACB for R = Cl) and (c) azoquinolin-8-ol (PAQ for R = H, CPAQ for R = COOH, CMPAQ for R = $COOCH_3$)

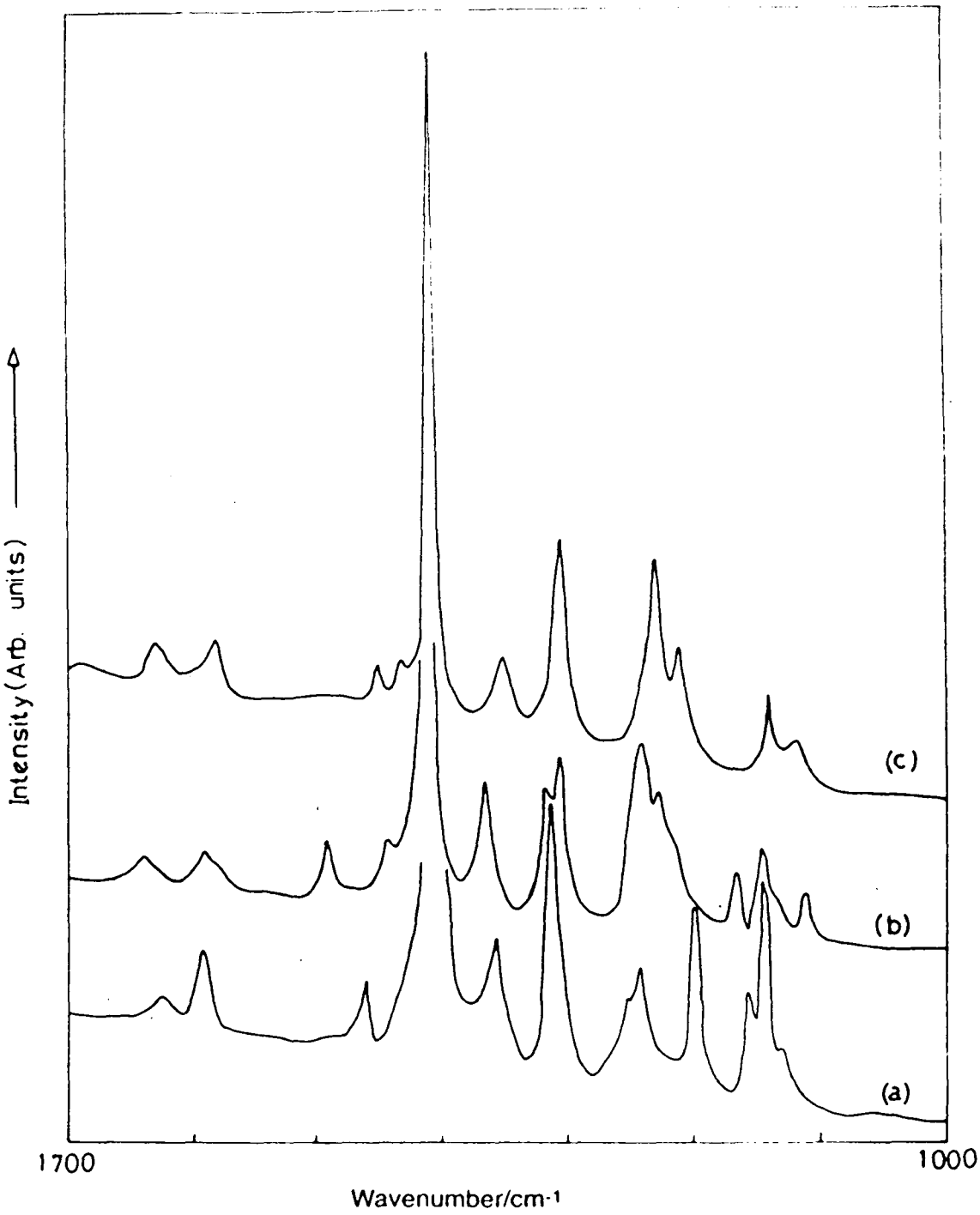

Figure 4.2 Resonance Raman spectra (in the range 1700 - 1000 cm^{-1}) of (a) HMPAB, (b) HMPAMB, and (c) HMPACB in the solid state. All the spectra were recorded by exciting with 488.0 nm line of the Ar^{+} laser.

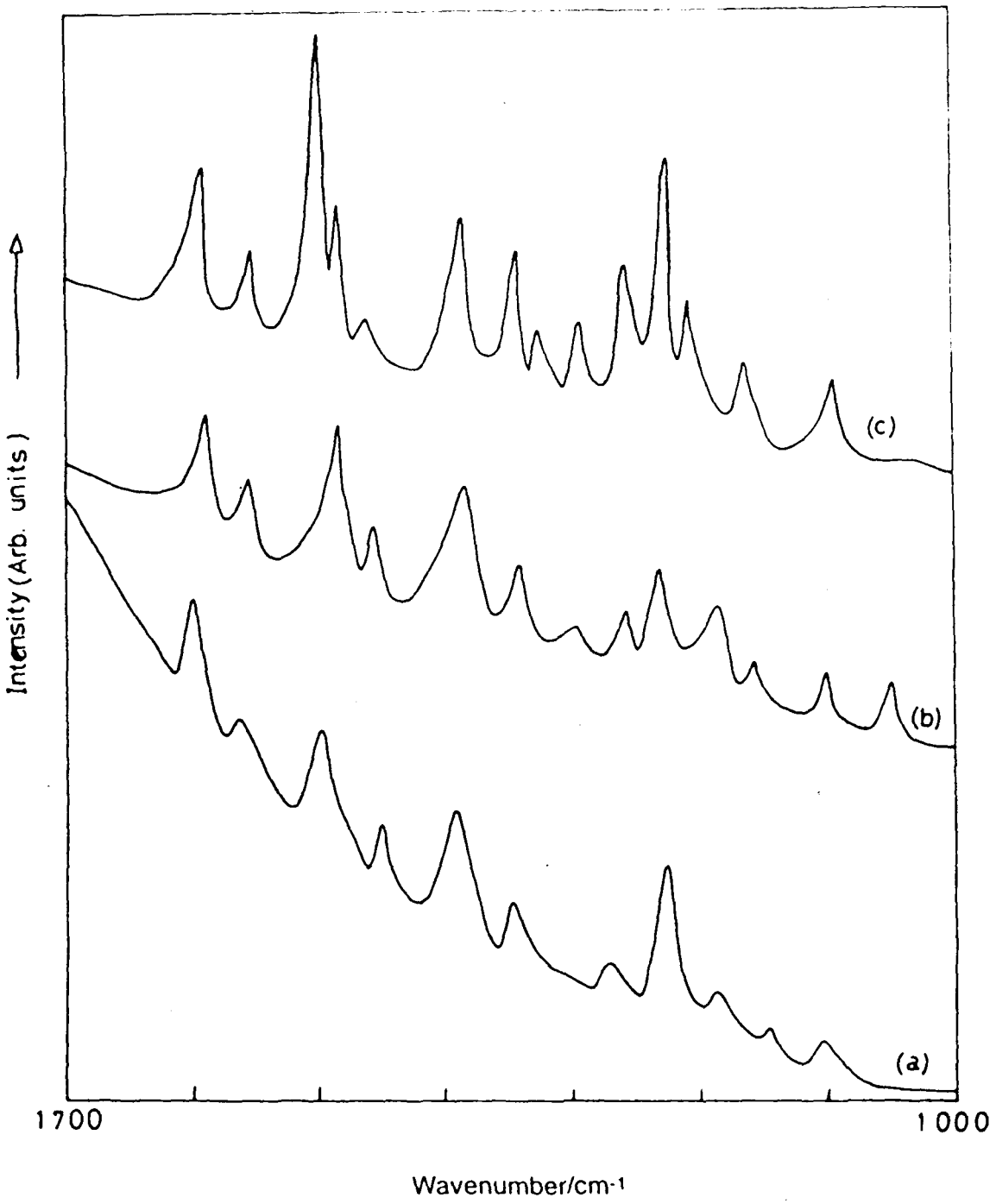

Figure 4.3 Resonance Raman spectra (in the range 1700 - 1000 cm^{-1}) of (a) HNAB, (b) HNACB, and (c) HNAMB in the solid state. All the spectra were recorded by exciting with 476.5 nm line of Ar^{+} laser.

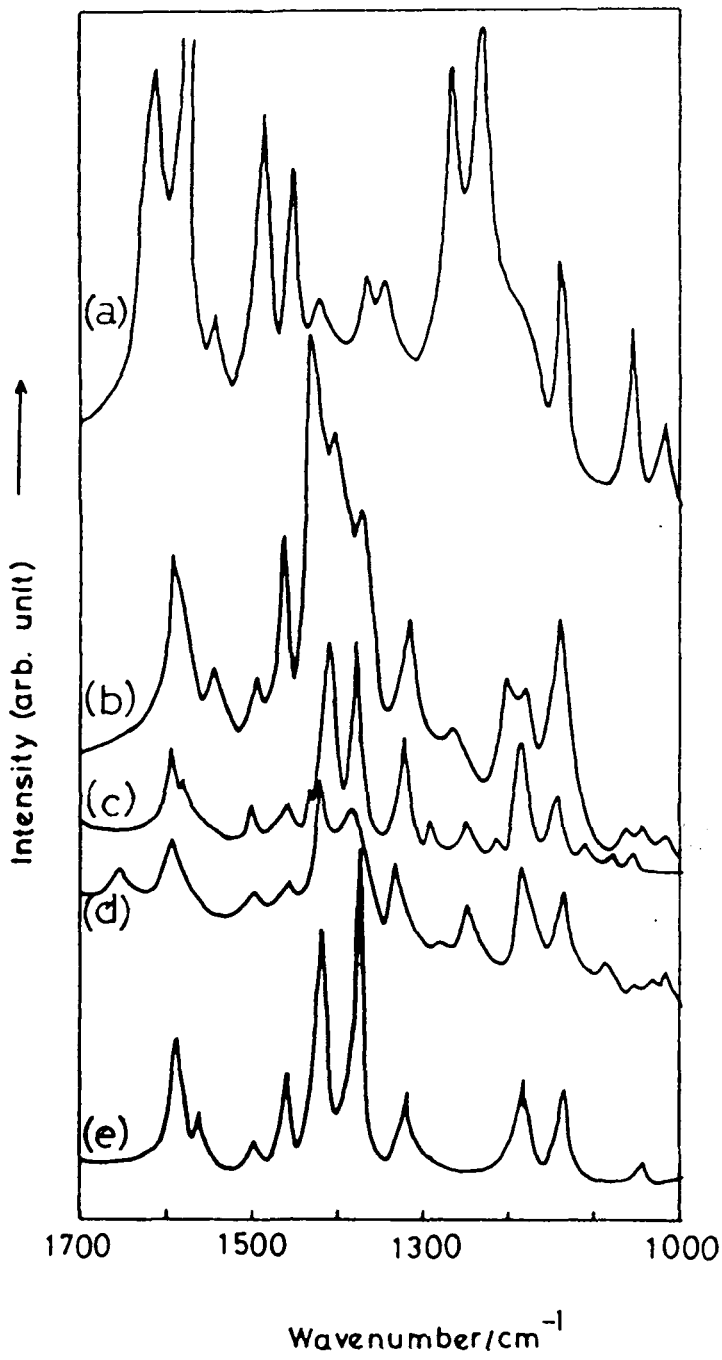

Figure 4.4 Resonance Raman Spectra of (a)PAQ, (b)CPAQ, (c)$(CMPAQ)_2Cu$, (d)CMPAQ, and (e)$(PAQ)_2Cu$ in the solid state. Laser excitation wavelength used: (a)-(b) 488.0 nm; (c)-(e) 476.5 nm of Ar^+ laser.

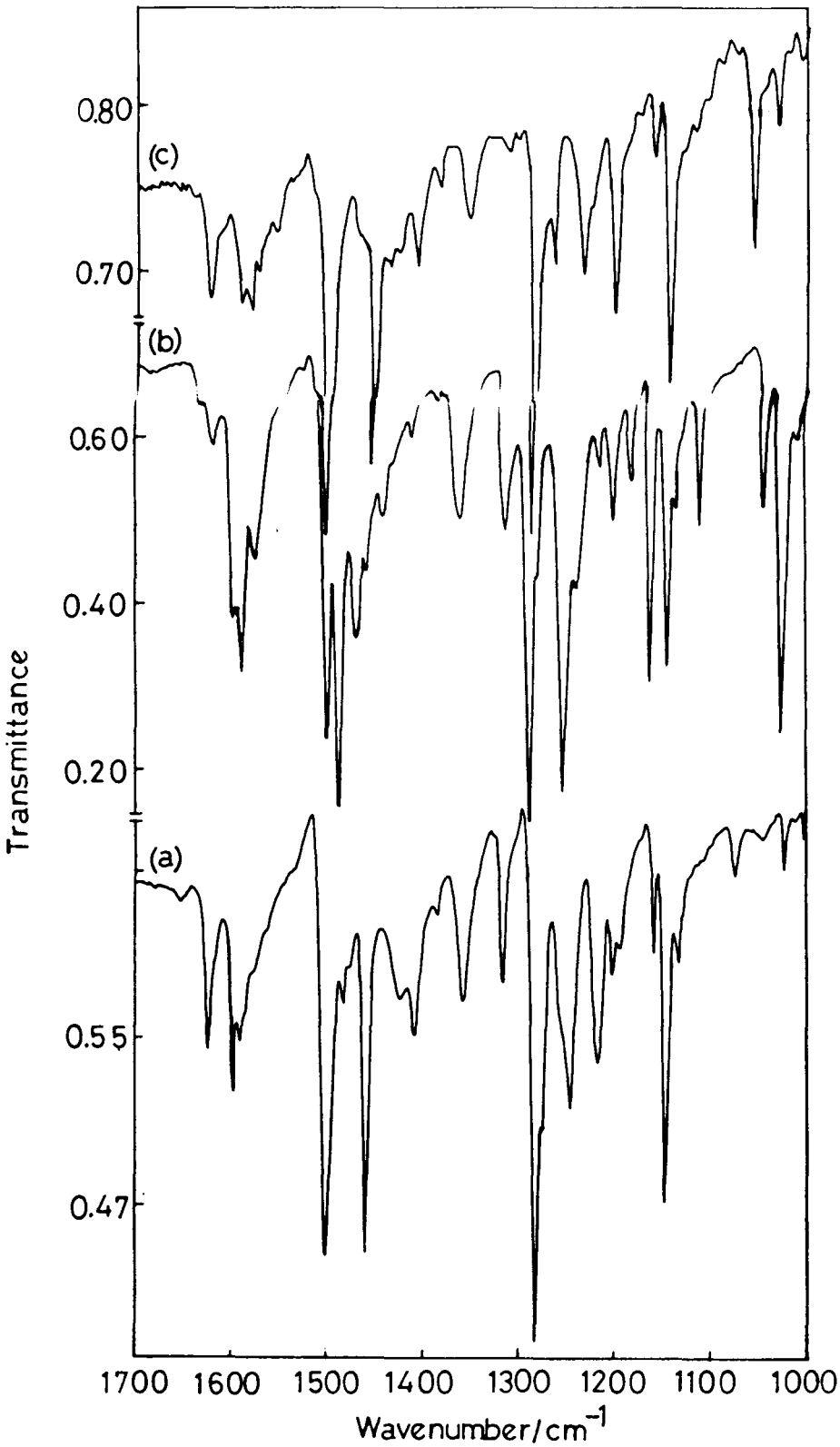

Figure 4.5 FT-IR spectra (in the range 1700 - 1000 cm^{-1}) of (a) HMPAB, (b) HMPAMB, and (c) HMPACB in the solid state.

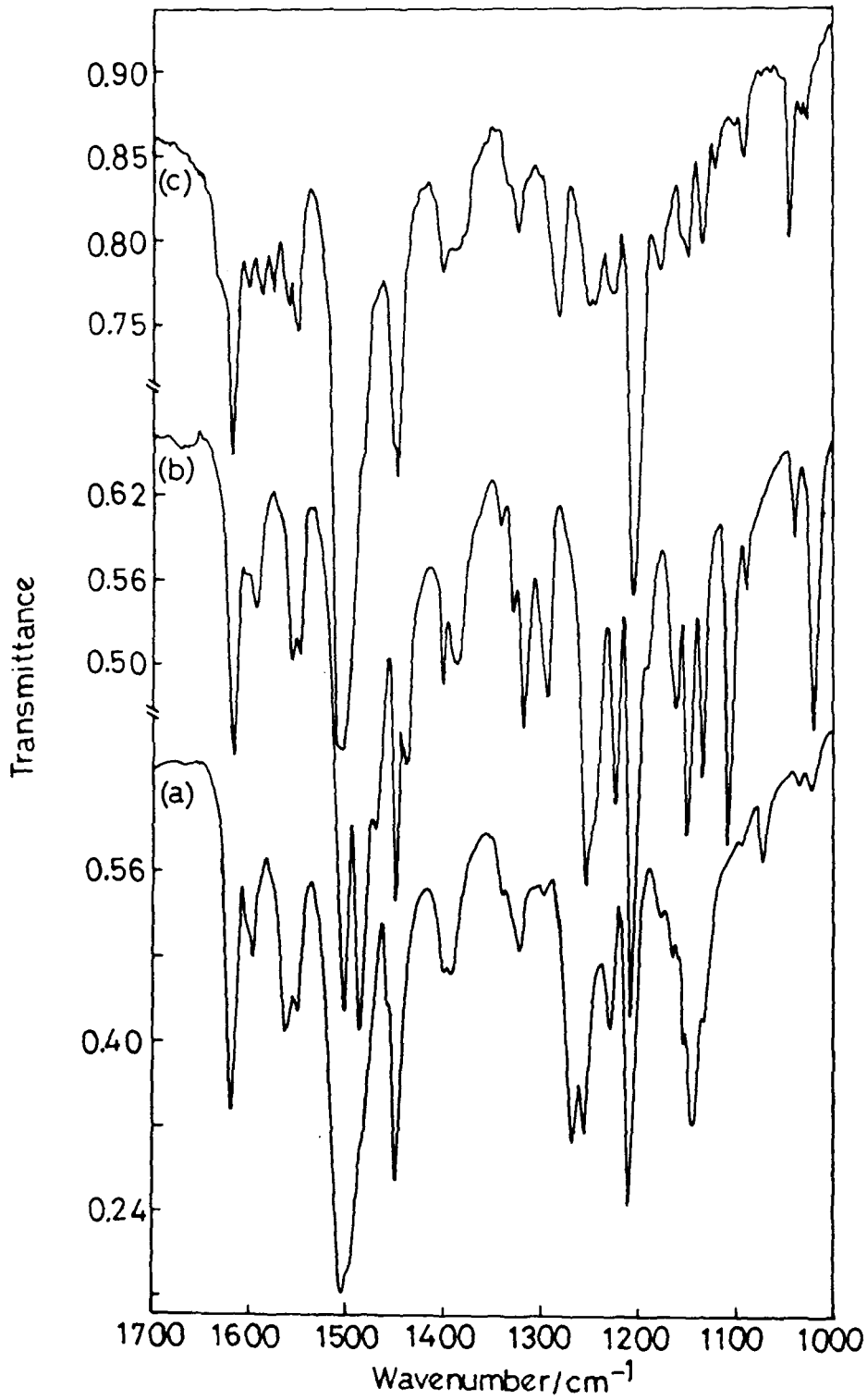

Figure 4.6 FT-IR spectra (in the range 1700 - 1000 cm^{-1}) of (a) HNAB, (b) HNAMB, and (c) HNACB in the solid state.

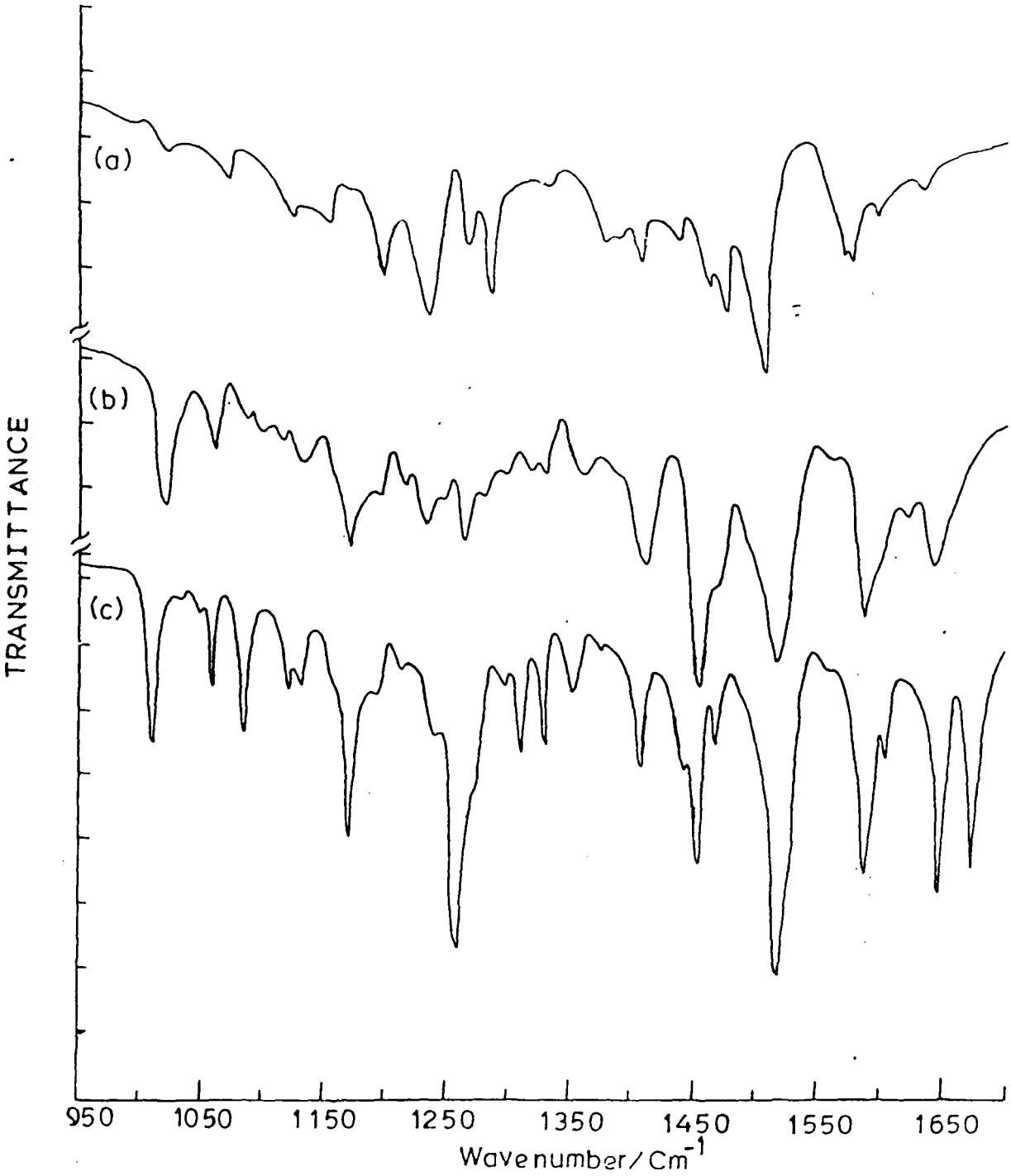

Figure 4.7 FT-IR spectra (in the range 1700 - 1000 cm^{-1}) of (a) PAQ, (b) CPAQ, and (c) CMPAQ in the solid state.

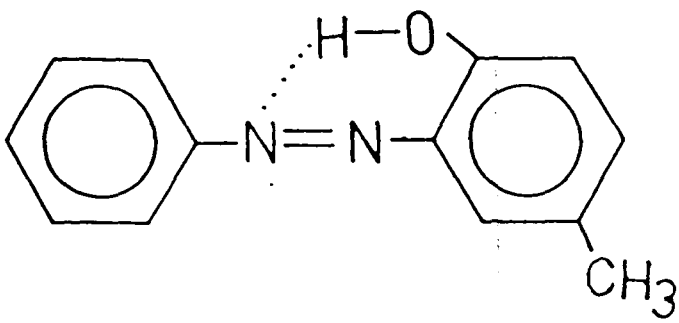

Figure 4.8 Proposed solid state structure of HMPAB in hydrogen bonded form.

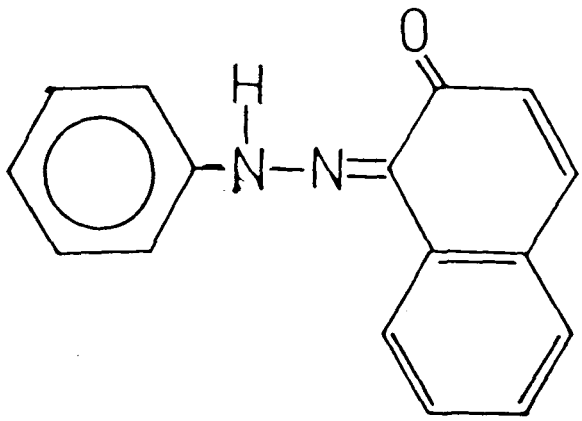

Figure 4.9 Proposed quinonoid type structure of HNAB in solid state.

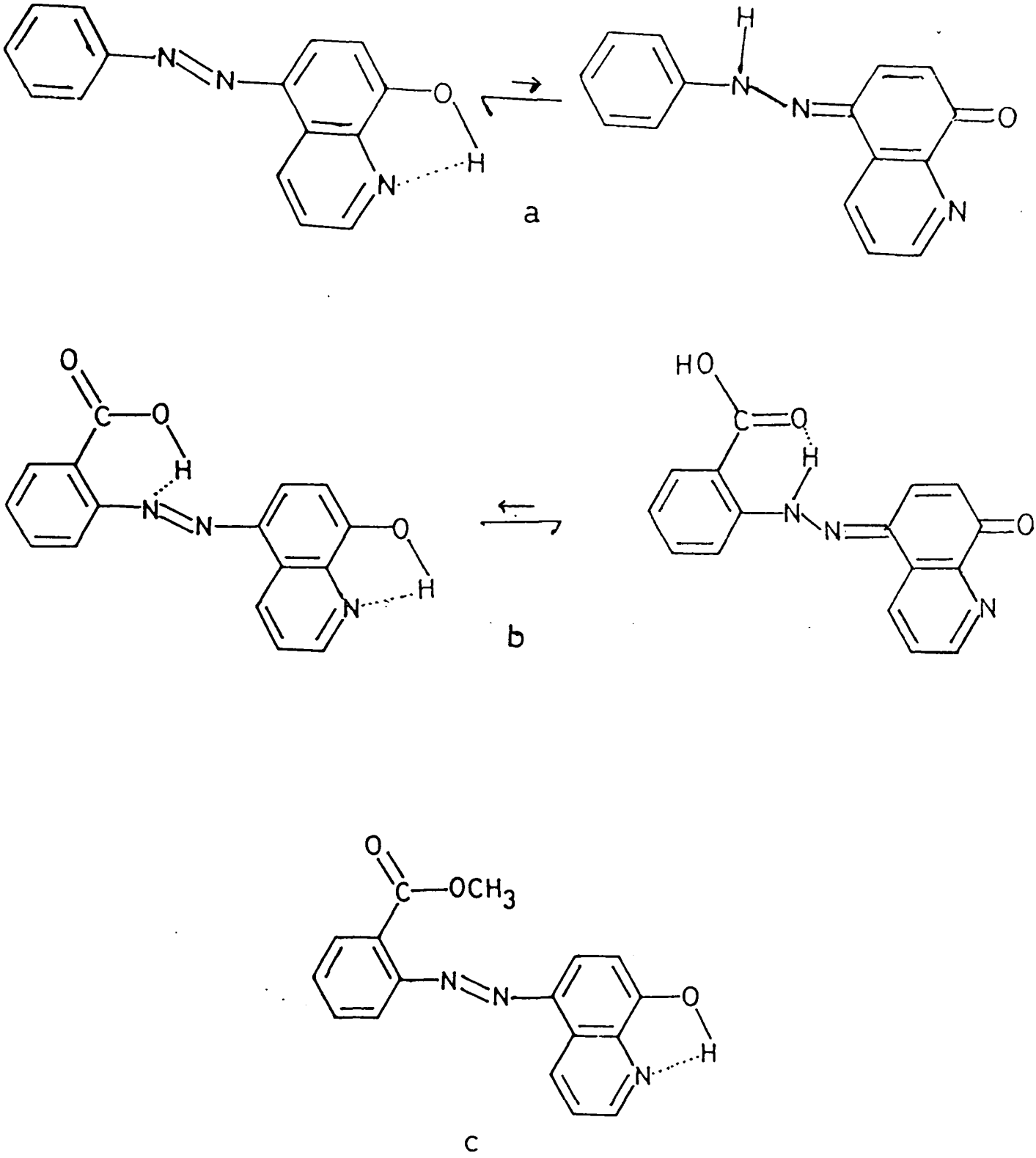

Figure 4.10 Proposed solid state structure of (a)PAQ, (b)CPAQ and (c)CMAPQ.

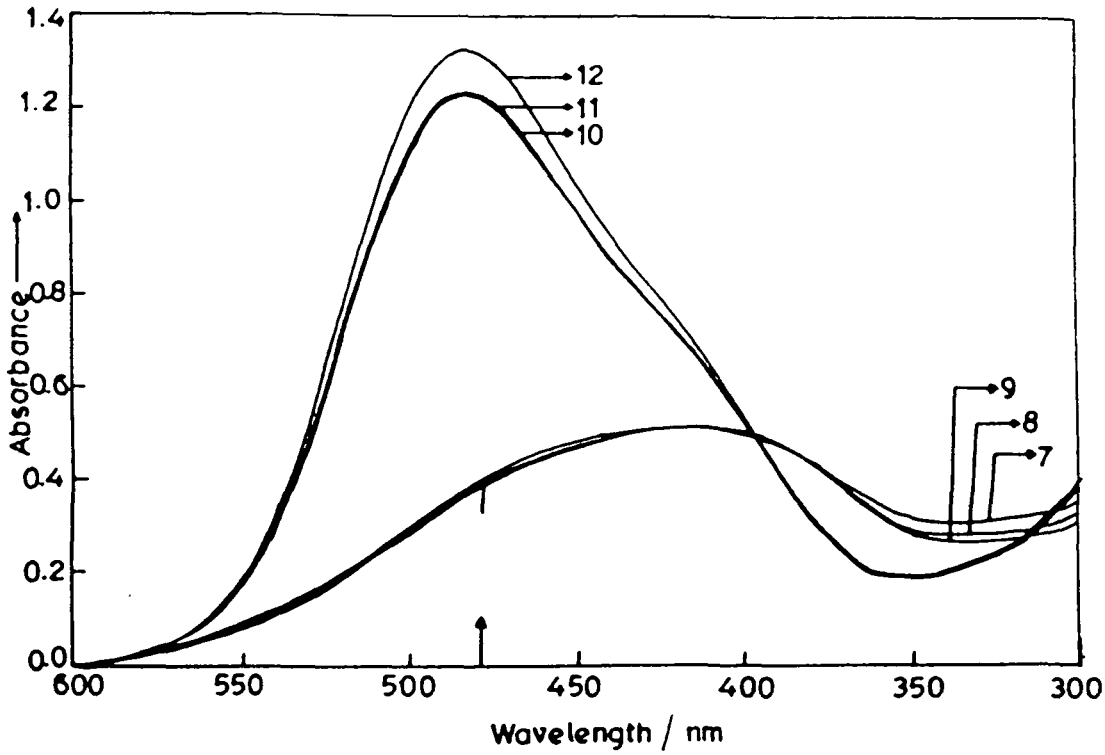

Figure 4.11 pH dependent electronic absorption spectra of PAQ. Numbers on each spectrum denote the corresponding pH. The arrow at the bottom indicates the excitation wave length used for the RR spectra.

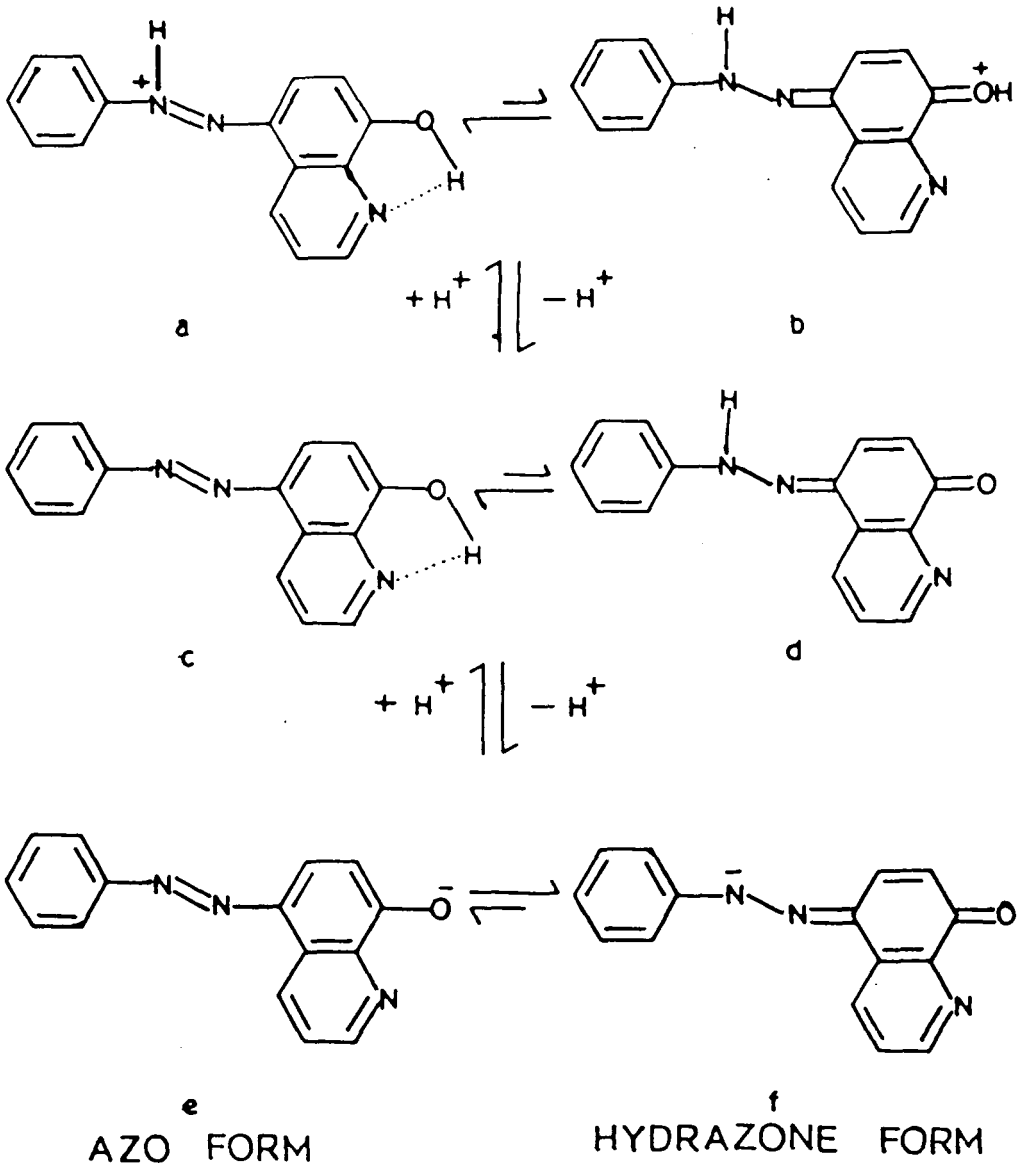

Figure 4.12 Proposed resonating structural forms of PAQ in protonated species (a,b), neutral species (c,d) and deprotonated species (e,f).

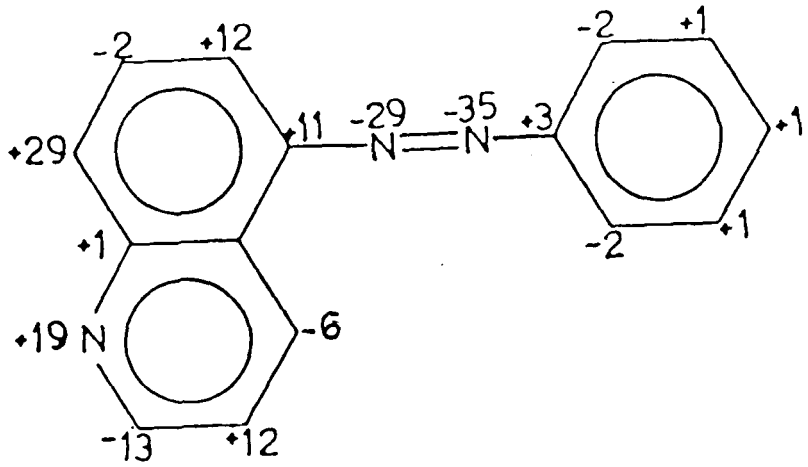

Figure 4.13 Charge migration in the lowest energy $\pi \rightarrow \pi^*$ transition in PAQ (in units of 10^{-3}eV; positive sign indicates decrease in electron density on excitation and vice versa). Dta taken from Ref.12.

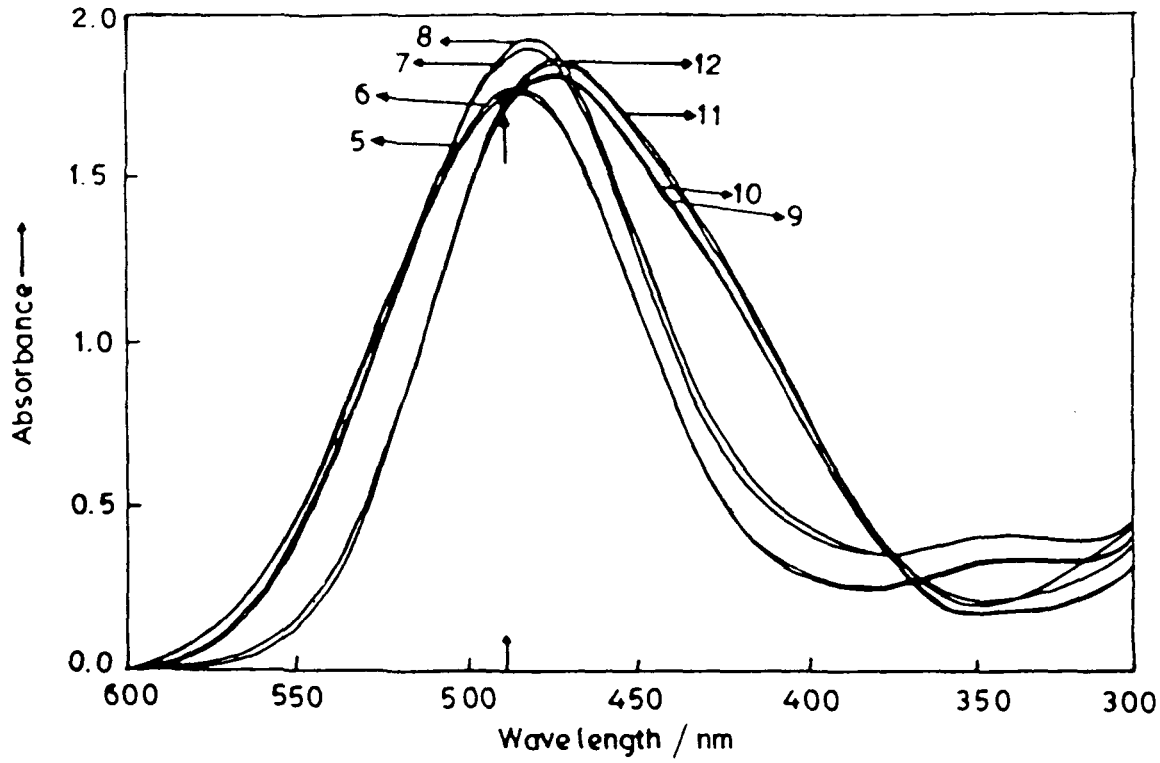

Figure 4.14 pH dependent electronic absorption spectra of CPAQ. Numbers on each spectrum denote the corresponding pH. The arrow at the bottom indicates the excitation wave length used for the RR spectra.

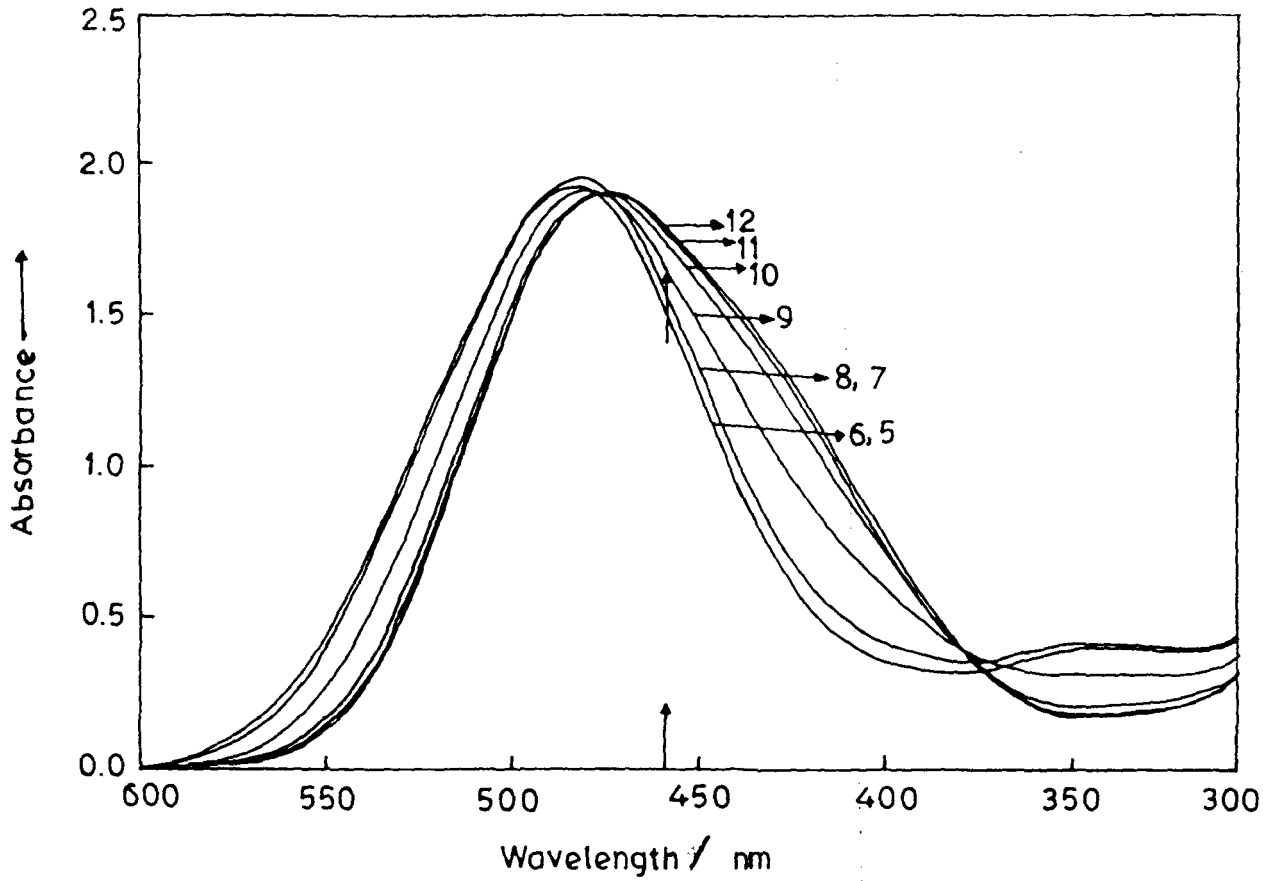

Figure 4.15 pH dependent electronic absorption spectra of CMPAQ. Numbers on each spectrum denote the corresponding pH. The arrow at the bottom indicates the excitation wave length used for the RR spectra.

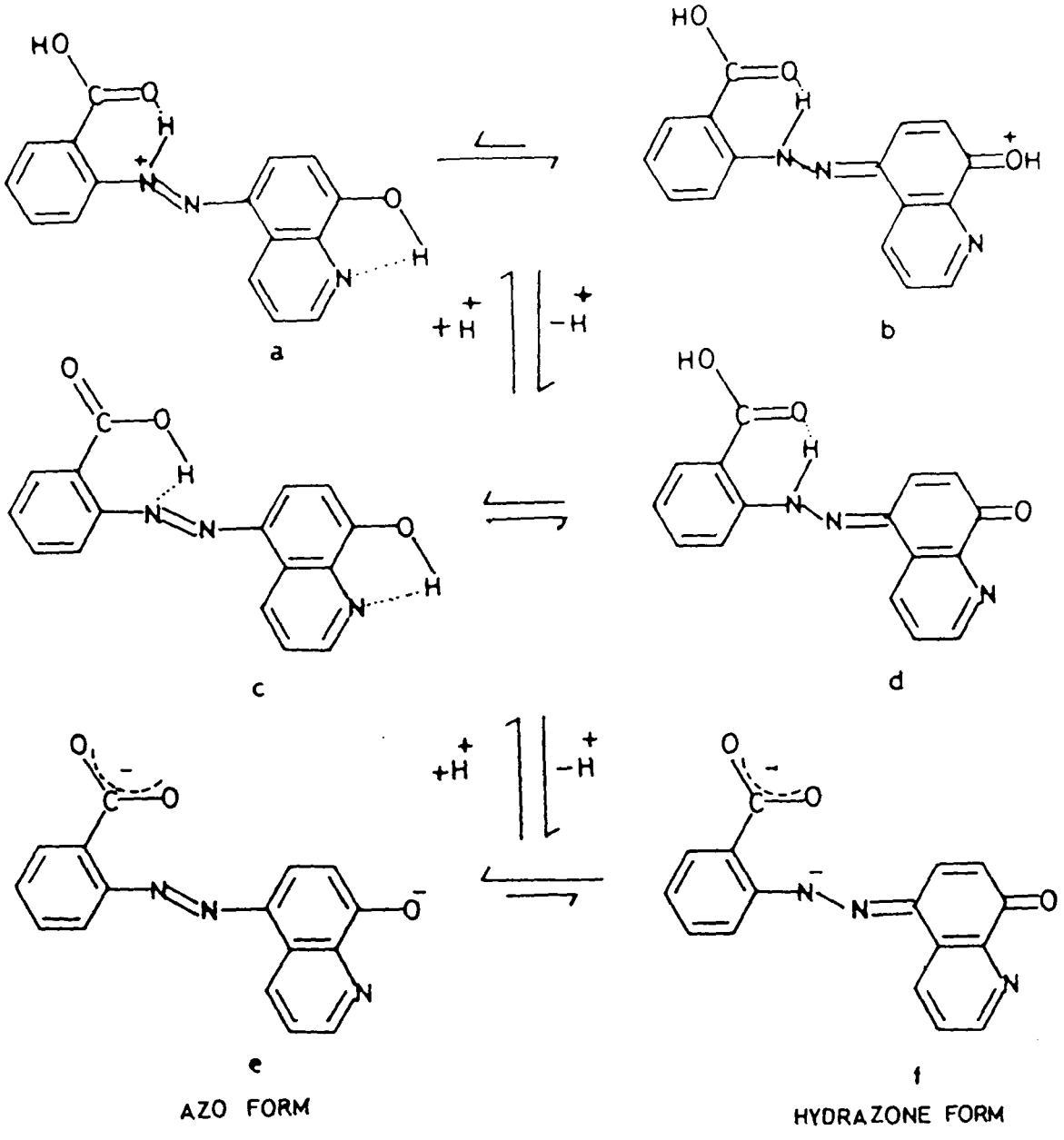

Figure 4.16 Proposed resonating structural forms of CPAQ in protonated species (a,b), neutral species (c,d) and deprotonated species (e,f).

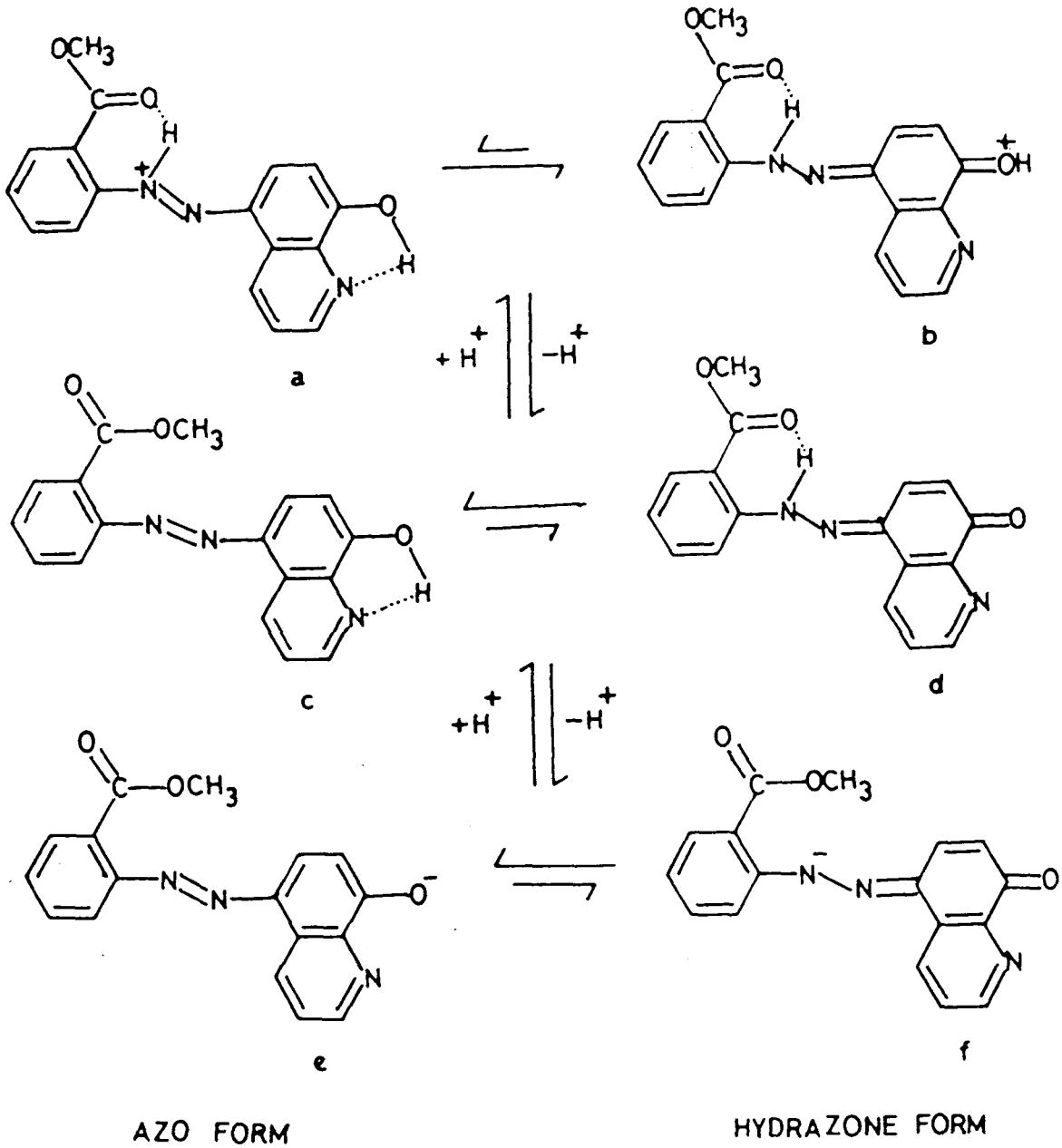

Figure 4.17 Proposed resonating structural forms of CMPAQ in protonated species (a,b), neutral species (c,d) and deprotonated species (e,f).

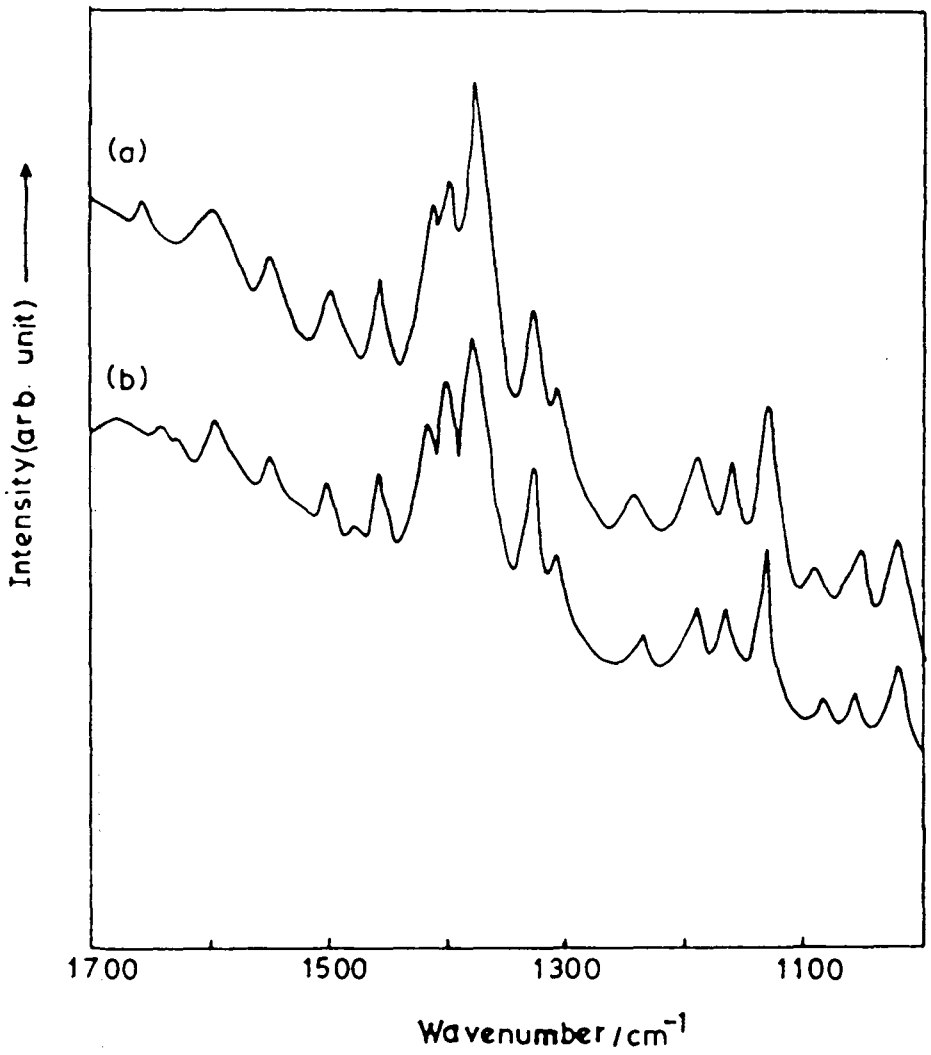

Figure 4.18 Resonance Raman spectra of PAQ at (a) pH 1 and (b) pH 9. Laser excitation wavelength used was 476.5 nm of Ar^{+} laser.

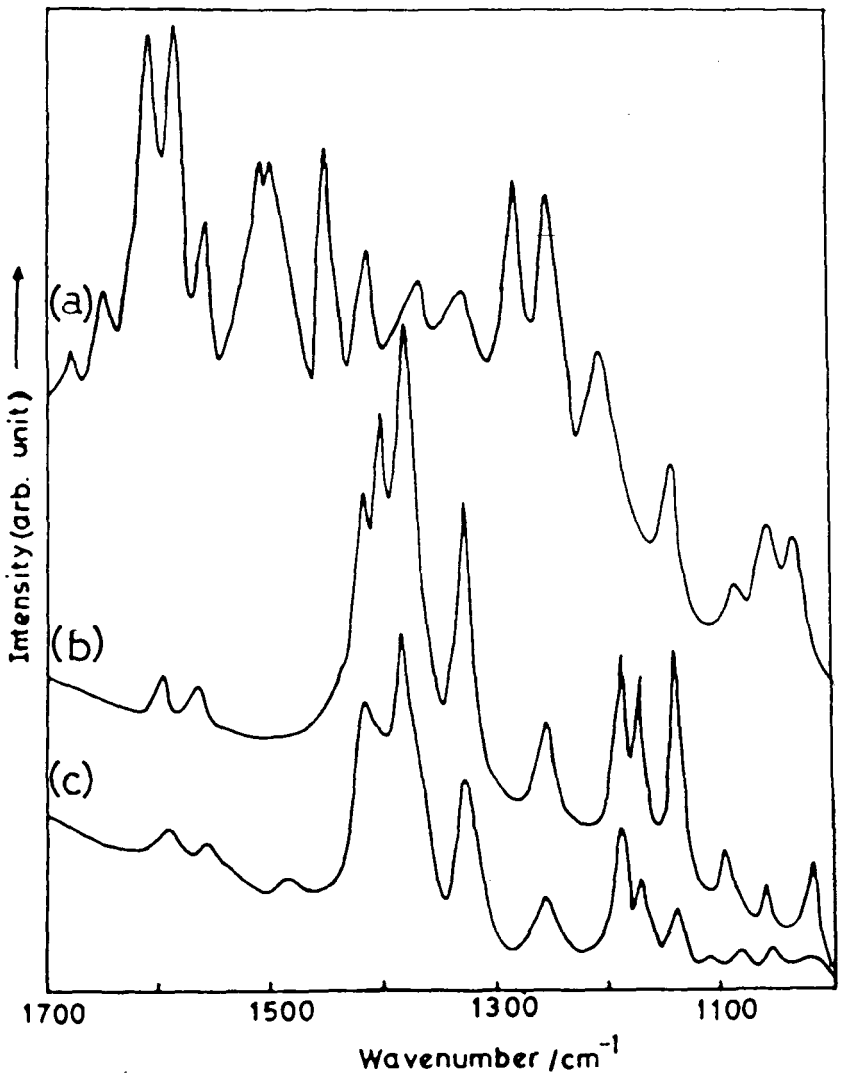

Figure 4.19 Resonance Raman spectra of CPAQ at (a) pH 9, (b) pH 1 and (c) pH 12. Laser excitation wavelength used was 488.0 nm of Ar^+ laser.

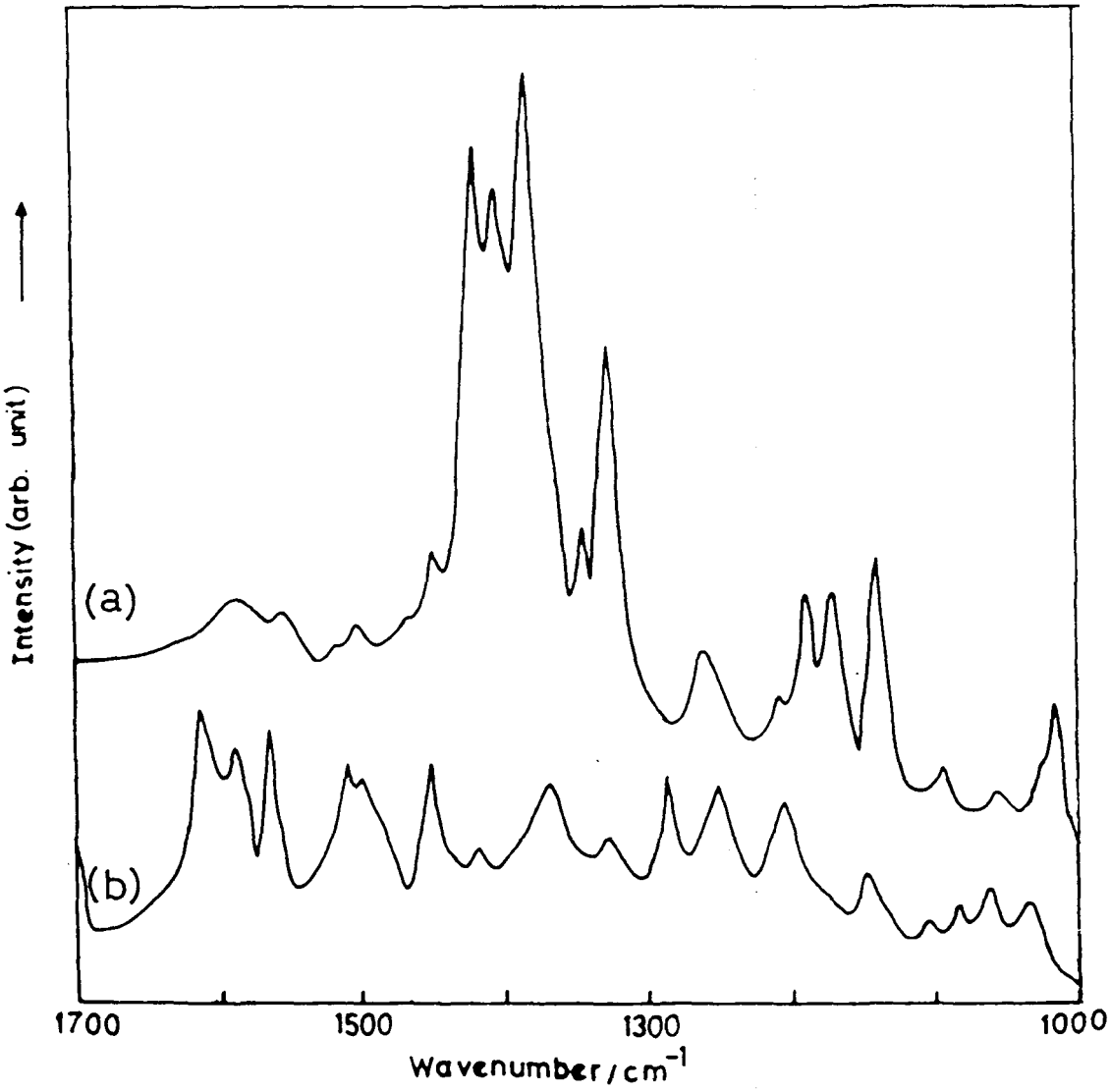

Figure 4.20 Resonance Raman spectra of CMPAQ at (a) pH 12 and (b) pH 1. Laser excitation wavelength used was 457.9 nm of Ar^+ laser.

CHAPTER - V

SPECTROSCOPIC INVESTIGATION OF SOME DYE-PROTEIN INTERACTIONS

In this Chapter, spectroscopic study of dye-protein interactions are presented. It has been shown that Bovine Serum Albumin (BSA) has 6 independent binding sites for 5-(2'-carboxyphenyl)-azoquinolin- 8-ol (CPAQ), binding constant being 6.2×10^3 at physiological pH. Gelonin does not form complex with CPAQ, though it binds Rose Bengal (RB). Gelonin has two types of binding sites for RB; high affinity site and low affinity site. There are about 12 low affinity sites per Gelonin molecule having binding constant of 8.9×10^4 and only 2 high affinity binding sites per Gelonin molecule with binding constant 2.99×10^6. Vibrational assignment of BSA bound CPAQ is also presented. It is found that bound CPAQ exits exclusively in hydrazone form. Azo group nitrogen, adjacent to the phenyl ring probably participates in the formation of the CPAQ-BSA complex.

5.0 INTRODUCTION

Most of the important biochemical interactions are related with highly specialized active site. Elucidation of these ligand - active site interactions is extremely necessary to explain the mechanism of specific biological activity. The functional behavior of a protein is primarily governed by its active site conformation i.e. the chemical properties of the site, where the enzymatic action takes place or the ligand binding occurs. To study the biological activity of a protein, it is extremely important to know the number and/or nature of binding sites of a particular protein molecule.

Albumin has been used as a model protein for a number of diverse physico-chemical studies [1-3]. Most important property of this protein is its ability to bind hydrophobic ligands such as fatty acids, lysolechithin, bilirubin, tryptophan, steroids, thyroxine, drugs, dyes, etc. Binding of drugs to plasma proteins also reduces the toxic effect of the ligand, since it is the concentration of the unbound ligand that is related to its pharmacological effect [4].

A high helix content, indicates that α-helices are the major structural components of albumin [5]. Serum Albumin is a single chain of about 580 residues and is crosslinked by 17 disulfide bridges into a series of nine loops, six large and three small. Sequencing of albumin shows a repeating pattern

[6-7]. It has also been proposed [7] that the domain of albumin is a cylindrical structure formed by six anti parallel helical segments. A hole through this cylinder parallel to the axes of the helices is proposed as the binding site for fatty acids. The pattern of three repeated homologous units suggested that these similar sequences may be folded similarly into distinct structural units or domains. When Bovine Serum Albumin (BSA) was cleaved by limited pepsin digestion between residues 306 and 307 near the middle of the molecule, each half retained ligand binding properties and two halves reassociate to form a tight complex with increased binding compared to the separated halves [8]. Each subdomain shares a number of common features with the others, such as the hydrophobic face, the clusters of basic residues, and the Pro residues at the tips of the long loop. However, each subdomain is also unique and exhibits a degree of specificity in binding. The grooves in domain structure contain plus- charged amino acids and act as binding sites for anions having relatively large size.

Albumin has conformational adaptability and thus binds to a great variety of compounds with high affinity, which is a special feature of albumin and is different from the binding of ligands exhibited by other proteins such as enzymes or antibodies [9].

In a general way, binding studies of fatty acids, drugs

and other ligands indicate that albumin contains multiple binding sites. The repeated structural features of albumin are also consistent with multiple binding sites. For a number of ligands association constant and number of binding sites with BSA were calculated. The results for such equilibrium studies are summarized in Table-5.1.

The proposed three domain structure in BSA is further divided into two sub-domains for each domain, viz. 1-AB, 1-C; 2-AB, 2-C; 3-AB and 3-C, with binding sites on each subdomain, giving a total of six binding sites [14]. Binding studies indicate that these sites are not equivalent and they vary in specificity and binding affinity. The difference in specificity is evident by the numerous studies that indicate that the primary binding sites for long chain fatty acids are different from the primary binding sites for bilirubin and many drugs. Among the six sub-domains, 1-AB contains the single sulfhydryl group, but there is no direct evidence of ligand binding. 1-C binds long chain fatty acids, dansylaziridine, and is probably the secondary indole binding site. 2-AB binds bilirubin, short chain fatty acids, dyes and drugs whereas 2-C binds steroids and long chain fatty acids. 3-AB binds drugs and is the primary site for short chain fatty acids and probably for indole. On the other hand, 3-C is probably the primary long chain fatty acid binding site.

Binding behavior of Gelonin with ligand molecule is yet

to be explored extensively. Recently, active site for this protein has been proposed based on X-ray crystallographic data [15]. Residues identified by sequence and alignments are Tyr74, Arg169, Gly111, Glu166, Tyr113 and Trp198. These residues are located at the cleft between the two domains. There are a number of hydrogen bonding interactions between the residues in the active site. It is also reported that there are three water molecule inside the active cavity.

Organic ions interact with proteins on both side of their isoelectric point [1]. The extent of binding has been analyzed, in terms of statistical and electrostatic interactions, which influence binding. Formation of aggregates of dye molecules adds complication in investigating anion-protein equilibria, which in general reflects in deviation from Beer's law. The two major effects (statistical and electrostatic) influencing binding are dominant in different proportion in various ligand. For example, in methyl orange-BSA binding, the statistical effect is found to be dominant, whereas in azosulphathiazole-BSA, electrostatic effect is more pronounced. In later system, the anions are more strongly bound to protein, initially, due to additional van der Waals interaction which decreases as more ligand reaches the protein molecule, due to electrostatic repulsion exerted by the already existing anions. The electrostatic free energy change has been calculated as :

$$\Delta F_{elect} = \frac{-Nz^2e^2}{D}\left(\frac{1}{b} - \frac{k}{1+ka}\right) \qquad (5.1)$$

where, N is the Avogadro number, z is the number of charges on anion, e is electronic charge, D is dielectric constant of the medium, b, the radius of protein molecule, a, the closest distance of protein to charged ion and k is expressed as

$$k = \left(\frac{4\pi Ne^2}{1000DkT}\right)^{1/2}\Gamma^{1/2} \qquad (5.2)$$

where, T the absolute temperature, Γ, twice the ionic strength of the medium and k is the Boltzman constant.

Similarly, the free energy change due to complex formation is given by

$$-\Delta F^{o} = RT\ln\left[\frac{n-(i-2)}{n-(i-1)}\,\frac{i}{i-1}\right] - \Delta F_{elec} \qquad (5.3)$$

where, n is the number of binding sites and i represent for the ith reaction. The first term is due to statistical effect and is generally calculated using

$$k_i = \frac{n-(i-1)}{i}\,\frac{1}{K} \qquad (5.4)$$

where, K is a constant which depends upon the nature of anions as well as character of the protein and is determined experimentally using

$$\frac{1}{r} = \frac{K}{n}\,\frac{1}{[L]} + \frac{1}{n} \qquad (5.5)$$

where, [L] represents the concentration of the ligand molecule and K could be represented as $1/K_a$ (K_a being binding constant). As discussed in Chapter I, this equation was first determined by I.M. Klotz [1]. In the present work we shall use the term Klotz

equation (or Klotz Plot) for it. Thus, the analysis based on Klotz equation (eqn. no. 5.5) essentially reflects the statistical effect on binding and electrostatic as well as cooperativity in binding is not included in this equation. However, it may be noted that the free energy change due to statistical effect is order of magnitude higher in comparison to electrostatic interaction energy.

As summarized earlier [Chapter I], various techniques used for binding studies are conceptually the measurement of change in physical or chemical properties of ligand molecule. Experimentally, spectroscopic methods are divided into two groups (i) equilibrium dialysis and (ii) titration. This could also be followed by monitoring the change in property of the receptor viz. protein. Different types of ligand molecules are used to study the dye-protein interactions. Among these, the colored ligands have some advantages as in these ligands, chromophores act as probe to study these interactions spectroscopically. Ligand containing azo groups (especially azo dyes) are very much useful for these purposes. These dyes are used as labels in Resonance Raman (RR) spectroscopy. Besides, the changes in RR spectra as a result of pH induced tautomeric equilibria are also reported for a number of azo dyes [16]. Thus, spectroscopic studies combined with RR spectroscopy can reveal dye-protein binding and structure of the bound complex simultaneously. To

study of the effect of binding of these azo dyes with protein, we have selected 5-(2'-carboxyphenyl)azo- quinolin-8-ol (CPAQ) out of three dyes studied in the present work. This is due to the fact that 5-(2'-carbomethoxyphenyl)azo- quinolin-8-ol (CMPAQ) does not bind (or binds very feebly) with BSA and 5-(2'-phenyl)azoquinolin-8-ol (PAQ) though binds, in the bound form the pattern of the absorption band changes drastically, making it difficult to study the equilibrium binding. It is also observed that Gelonin does not bind (or the binding is very weak) with the azo dyes.

Therefore, besides these azo dyes, we have also investigated the binding properties of an additional dye, Rose Bengal (RB), with Gelonin, which is known to bind with BSA. This dye has recently found application as a model organic anion for liver plasma membrane [17]. Moreover, its structure is well characterized [18] and its binding properties with other proteins are widely reported [10-11]. Structure of RB is given in Figure-5.1. This dye has two stable structural forms; acidic quinoid and lactone [18].

The structure and tautomeric equilibria of CPAQ is discussed in detail in Chapter -IV. At pH < 8 and even in solid state it exists mainly in hydrazone form, whereas at higher pH, tautomeric equilibria shifts towards azo form [19]. From absorption studies it is found that CPAQ binds with BSA at

physiological pH. On the other hand, at pH < 5 the dye becomes insoluble and its binding could not be investigated. On the contrary RB binds with BSA irrespective of the pH of the solution [10]. In case of Gelonin, however, it binds only at pH ≈ 7 apparently.

5.1 EXPERIMENTAL

5.1.1 Preparation of Solution of Azo Dyes

Azo dyes, PAQ, CPAQ and CMPAQ are sparingly soluble in water; the sodium salt of these dyes are, however, soluble. To prepare the solution, dyes were taken in volumetric flask and little excess of 1:1 molar of NaOH (1M) was added along with little water. The mixture was kept at 50^{o}C for ≈2 hours (till the solid particles of dyes disappear). Thereafter, the solution was cooled at room temperature and volume was made up to the mark. In this way a 10^{-3}M solution was prepared. Measured amount of this solution was taken and the pH of the solution was adjusted to 7.0 with dilute HCl (initially with 0.1M and then with 0.01M) from a burette and volume correction was made to get the actual concentration of the solution. This solution was kept in dark and used as stock solution.

Rose Bengal is highly soluble in water. RB recrystallized from ethanol-water mixture was directly dissolved in corresponding buffer to prepare 10^{-3}M solution. The solution

was kept in dark and used as stock solution.

Phosphate buffer was used for pH 7.2, whereas Glycine-HCl buffer and Glycine-NaOH buffers were chosen for pH around 4 and 12, respectively. Various buffers were prepared using standard protocol.

5.1.2 Dye-Protein Interactions

Dye-protein interactions were studied using titration method. Two sets of experiments were performed in each case; one without protein, which served as the control experiment and another containing protein. A fixed concentration of dye solution was titrated by an increment of 100μL of protein solution. The experiments were repeated and found to be reproducible within experimental errors. All the absorption spectra were recorded at room temperature.

Concentration of the protein solutions as well as the dye solutions were checked spectroscopically. The extinction coefficient (ε) of the protein as well as dyes were determined. Extinction coefficients so determined are used for determining the concentration of dye in solutions. Extinction coefficient of the bound dyes were determined by mixing protein and dye at 100:1 ratio and then incubating at 37^{o}C for 2 hours in an incubator before scanning the absorption spectra. Further, the method of Westphal et. al [20] was also used. With regard to the presence of dimerization / aggregation, our studies reveal its absence for

both the proteins as well as for dyes in the concentration range studied.

To determine the fraction of bound ligand, a series of experiments along with the control sets were carried out keeping the dye concentration constant (10^{-4}M) and titrating it with increasing concentration of protein from 10^{-6}M to 10^{-4}M and incubating at 37°C for two hours each time, before absorption spectra is recorded.

Association constant K_a could be found directly from the equation of Klotz [1,21] :

$$\frac{1}{r} = \frac{1}{nK_a(1-\alpha)[L]_T} + \frac{1}{n} \qquad \text{(eqn. 1.13 of Chapter I)}$$

and concentration of the bound dye, $[L]_B$ was expressed as

$$[L]_B = \frac{A_{Cal} - A_{Obs}}{\varepsilon_{free} - \varepsilon_{Bound}}, \qquad \text{(eqn. 1.15 of Chapter I)}$$

where, A_{Cal} and A_{Obs} are the absorption for free and bound dye at at the λ_{max} of free form and ε_{free} and ε_{Bound} are the molar extinction coefficient of free and bound dye at λ_{max} of free dye as determined earlier. ε_{Bound} could be calculated by the literature method [20] plotting ε_{Obs} [or A_{Obs}(absorption)] vs. $[L]_T/C_P$. r is calculated using the calculated value of $[L]_B$.

10^{-4}M dye solution in buffer and 10^{-4}M protein solution in buffer were mixed at 1:1 ratio and incubated at 37°C for 2 hours. The solution is then mounted in a rotating quartz cell for Raman study. Laser line used was 488 nm. Laser power was 400 mW at the laser head and slit width was 5 cm^{-1}.

5.2 RESULTS AND DISCUSSIONS

5.2.1 Binding Studies using Electronic Absorption Spectra:

In an attempt to investigate the binding of azo dyes and RB with two proteins under consideration, we have observed their absorption spectra for free dye and dye-protein mixture, with an excess amount of protein (100:1, for protein:dye). Presuming that binding is taking place the two spectra in each case were compared. The preliminary screening is done on this basis. In those cases where some perceptible change in the ligand absorption spectra is observed are considered as positive, i.e. binding may be taking place. Others are simply not persuaded any further. Corresponding spectra are depicted in Figure-5.2 and the results are summarized in Table-5.2.

From the Table, it is clear that PAQ binds with BSA at pH 7.2 and 12.3, whereas CPAQ binds only at pH 7.2. Binding at low pH (around 4) could not be investigated owing to the precipitation of these dyes in this range. PAQ and CPAQ do not bind with Gelonin at either pH. RB binds with Gelonin at pH 7.2 and with BSA at both pH. In case of PAQ, absorption peak is broad and featureless, making it difficult to follow the changes during binding, therefore, further binding studies on this ligand is not carried out.

Results of titration in terms of change in absorbance against protein concentration are shown in Figures 5.3-5.5 for

BSA-CPAQ, BSA-RB and Gelonin-RB, respectively, at pH 7.2. From these Figures it is clear that binding increases up to a certain concentration of protein against a fixed concentration of dye. In the following, each case is analyzed in detail.

5.2.1.1 BSA-CPAQ

Figure- 5.6 shows the absorption spectra of fixed concentration CPAQ titrated against variable concentration of BSA. Peak positions (λ_{max}), absorbances at λ_{max} (A_{Obs}) and absorbance at 482.5 nm are shown in Table- 5.3 along with the concentration of the protein C_p and dye $[L]_T$. We have used the Klotz equation to calculate the binding sites and binding constants. For this purpose identical and independent binding sites have been assumed, initially.

Calculated values of extinction coefficients (ε) are shown in Table-5.4. Extinction coefficients for bound dye (ε_b) was determined by literature method [20](Figure-5.7). Table- also represents the number of binding sites (n) and binding constant (K_a) as determined from the Klotz plot (Figure-5.8).

From Table-5.4 it is clear that BSA has six independent binding sites and its association constant is 6.19×10^3. This result matches satisfactorily with an earlier report of binding of human serum albumin (HSA) with a ligand 2-(4'-hydroxybenzeneazo)benzoic acid (HABA) [2] similar to CPAQ

(Table- 5.1). It also suggests that the number of binding sites and the value of binding constants differs considerably depending on the concentration of the protein as well as that of the ligand.

5.2.1.2 BSA - Rose Bengal

A comparison of absorption spectra (Figure-5.2) of free and bound form of RB show that in case of totally bound form, λ_{max} shifts towards the higher wavelength side (red shift or bathochromic shift) associated with increase in absorbance. A series of careful experiments (Figure- 5.9 and Table- 5.5), however, show that this change is apparent. At very low concentration of BSA, λ_{max} shows a red shift but the absorbance decreases instead of increasing up to a certain concentration of the protein. As C_p further increases, the absorbance increases along with the red shift in λ_{max} giving rise to a sharp isobestic point. This result matches with other reported result where this aspect of binding was overlooked [10]. Presence of a sharp isobestic point shows the different structural forms of ligand in bound state. This complicates the scenario and calculations of binding parameters in the normal way becomes misleading. We have, therefore, not attempted it. However, number of probable binding sites could still be obtained if one consider the situation in a different way. Once $[L]_T:C_p$ ratio reaches 3:1, shift in λ_{max} and

also the change in absorbance becomes minimal. This indicates that the number of binding sites may be taken as 3 for this concentration range. Reported result [10] does not deal with this aspect of binding. They have estimated K_a from the Lineweaver-Burk method [22], plotting $1/\Delta A$ vs $1/[L]_T$. However, number and nature of binding sites are not reported.

Extinction coefficient of BSA bound RB is determined as is done in case of CPAQ (Figure-5.10), however, in this case, it gives totally different curve. We extrapolate the observed curve and got two different extinction coefficients (Table- 5.6). This might be due to the presence of two different structural forms of ligands. However, it is argued that the ε_{bound}, determined by this method is at times overestimated for lower concentration and underestimated at higher concentration of protein. In our work, however, ε_{bound} determined for higher concentration range by extrapolation result matches with the experimental result, which has been calculated at 548 nm of bound dye. It seems that at the lower protein concentration, the binding is non-specific and some short of ionic interactions are present up to the dye protein ratio of nearly 3. Then the total structural change of dye occurs and the binding becomes specific.

5.2.1.3 Gelonin - RB

In case of Gelonin, unlike BSA, the shift of peak

position is not accompanied by a sharp difference in absorbance (Figure-5.11, Table-5.7). Even, in totally bound form of RB, the change in absorbance is almost negligible. In this case also ε_{Bound} is calculated by the same way (Figure-5.12). Klotz plot of these results are presented in Figure-5.13. In this case, instead of a straight line we get a curve which could be resolved into two components giving rise to two different type of binding sites along with two different binding constants (Table- 5.8). At low concentration range of protein (C_p), number of binding sites are higher (12) than at high C_p range where they are calculated as only 2. Assumption of independent sites may not be valid in this case as the results obtained show prominent non-linearity.

5.2.2 Resonance Raman Study of BSA - CPAQ Interactions

In order to understand the site environment of the ligand precisely, we have also attempted RR study for CPAQ. For, RR spectroscopy may enable enables us to understand the structure of the complex in bound form. The absorption band of bound CPAQ is spread from 400 nm to 600 nm and is peaking around 517 nm. We have therefore selected 488.0 nm line of Ar^+ laser to excite CPAQ at pre-resonance state. Attempt to excite near the peak of the band was not successful as 514.5 nm line of Ar^+ laser when used resulted into high fluorescence.

λ_{max} of CPAQ is 482.5 nm at pH 7.2 and it shift to 515

nm due to binding. As already discussed CPAQ exists mainly in hydrazone form at pH < 8 and at higher pH, tautomeric equilibria shifts towards azo form giving λ_{max} at lower wavelength. Therefore, shifting of 482.5 nm band to 515 nm due to binding shows that in bound form it exists in monoprotonated hydrazone form [19].

To further clarify the structure of the bound CPAQ we have analyzed different Raman modes (Figure-5.14) and the results are compared with Raman spectra of the ligand obtained at different pH (Table-5.9). It is found that the spectrum of the bound dye matches well with the spectrum of the dye at pH ≈1, where mainly hydrazone tautomer exists. It is also noted that the bound dye spectrum matches very well with the solid state spectrum of CPAQ, which exists in hydrazone form. The $\nu_{N=N}$, which appears as a strong band between 1440-1375 cm^{-1} in Raman Spectrum in azo form is not there in bound CPAQ. Instead, a band appears at around 1232 cm^{-1}, which is assigned to ν_{N-N}. Other characteristic bands of hydrazone form are also prominent in bound CPAQ. The band at 1617 cm^{-1} is assigned to $\nu_{C=O}$ (hydrogen bonded). Therefore, it could be argued that CPAQ is in hydrazone form in the complex.

5.2.3 Structure of Bound CPAQ : Binding Site

Bathochromic shift in the wavelength upon complex

formation may suggest that: (1) the electronic state in the dye-protein complex has been extended over an additional electron delocalization center or (2) the aromatic chromophore was placed in a hydrophobic environment [11]. It is argued that the binding of RB occurs through the $-COO^-$ group [11] by delocalization of electrons of carboxylic group over one of the $-NH_3^+$ groups on the protein surface. In case of RB-protein complex, hyrdophobic interactions are also involved.

In case of azo dyes binding may not be through $-COO^-$ group as PAQ lacks carboxylic group and it binds with BSA. On the other hand CMPAQ does not bind with BSA discarding the possibility of hydrophobic interactions (Figure-4.1,Chapter IV).

PAQ, below pH 9 exists in azo form and equilibria shifts towards hydrazone form above pH 9. On the other hand, below pH 8 and even in solid state, CPAQ exists mainly in hydrazone form, whereas, at higher pH, tautomeric equilibria shifts towards azo form [19]. It is also found that the absorption maxima shifts towards higher wavelength (Red shift) by more than 32 nm due to binding, which indicates that the structure of the dye is shifted towards hydrazone form and the species is monoprotonated. In case of PAQ, λ_{max} shifts at around 502 nm which is azo form. Therefore, it could be argued that PAQ in bound form exist in azo form whereas CPAQ exist in hydrazone form. Form the RR study it is found that bound CPAQ shows a

strong band at 1617 cm^{-1} which is assigned to $\nu_{C=O}$ (H-bonded). Thus the possibility of involvement of carboxyl group may further be excluded. CNDO/2 calculations of PAQ (Figure-4.13, Chapter IV) suggest that the electron delocalization may occur from one of the nitrogen atoms of azo group to a positively charged $-NH_3^+$ group of amino acid. However, the nitrogen atom adjacent to the quinolinol ring is double bonded to the ring. Therefore, the electron delocalization form the other nitrogen atom is more plausible, which may contribute to the binding. In CMPAQ, phenyl ring is substituted by carbomethoxy, unlike carboxy in CPAQ. This carbomethoxy group may cause steric hindrance and thus prevents binding of azo nitrogen to the protein.

As the binding site of CPAQ seems to be situated on the azo skeleton of the dye molecule and on both the sides of the azo group aromatic rings are there, receptor (protein) molecule should be flexible to accommodate CPAQ for binding. Thus, BSA being flexible, binds with CPAQ. On the other hand binding site of RB is carboxyl group, which is a substituent on aromatic ring. In this case dye molecule arranges itself to fit for binding. This may be the probable explanation for CPAQ not bind to Gelonin, whereas RB binds with it.

References

1. I.M.Klotz, F.M.Walker and R.G.Bivan, *J.Am.Chem.Soc.USA* 68, 1486 (1946).

2. C.J.Bowmer and W.E.Lindup, *Biochim.Biophys.Acta* 624, 260 (1980).

3. H.Vorum, K.Fisker and R.Brodersen, *Biochim. Biophys. Acta* 1205, 178 (1994).

4. W.F. van der Giesen and J. Wilting, *Meth. Find. Exptl. Clin. Pharmacol.* 4, 417 (1982).

5. R.G.Reed, R.C.Feldhoff, O.L.Clute and T.Peters, *Biochemistry* 15, 5394 (1977).

6. A.D. McLachlan and J.E.Walker, *J.Mol.Biol* 112, 543 (1977).

7. J.R. Brown, in *Albumin :Structure, Function and Uses* Edited by V.M.Rosenoer, M.Oratz and A. Rothschild, Pergamon Press, New York, (1977).

8. T.P.King, *Arch. Biochem.Biophys.* 156, 509 (1973).

9. F.Karush, *J.Am.Chem.Soc.* 72, 2705 (1950).

10. S Kishore and M Maruthamuthu, *Proc. Indian Acad. Sci. (Chem. Sci.)* 105 279 (1993).

11. A Galat, *Spectrochim. Acta* 42A, 199 (1986).

12. K.Murakami, T.Sano and T.Yasunaga, *Bull.Chem.Soc.Jpn.* 54, 862 (1981).

13. K.Murakami, *Bull.Chem.Soc.Jpn.* 61, 1323 (1988).

14. J.R.Brown and P. Shockley in *Lipid Protein Interactions,* Vol.1, Edited by P.C.Jost and O.H.Griffith, John Wiley and Sons, Inc. New York (1980).

15. M.V.Hosur, Bindu Nair, P.Satyamurthy, S.Misquith, A.Surolia, and K.K.Kannan *J.Mol.Biol.* 250,368 (1995).

16. K. Machida, *Vibr. Spectra Struct.* 17A, 421 (1989).

17. K.Yachi, Y. Sugiyama, Y.Sawada, T. Iga, Y. Ikeda, G. Toda and M. Hanano, *Biochim. Biophys. Acta* 978, 1 (1989).

18. J.J.M.Lamberts and D.C.Neekers, *J. Am. Chem. Soc.* 105, 7465 (1983).

19. P.K.Bajpai, B.Pal and T.S,Basu Baul, *J. Raman Spectrosc.* 26, 217 (1995).

20. U. Westphal, B.B.Ashley and G.L.Shelden, *J. Am. Chem. Soc.* 80, 5735 (1958).

21. S.T.Christian and R.Janetzko, *Arch.Biochem.Biophys.* 145, 169 (1971).

22. K.J.Laidler, *Physical Chemistry with Biological Applications*, Benjamin Cummings, London (1978).

Table.5.1 : Reported Ligand - Protein Interactions (on systems related to the present studies)

Ligand	Protein	No. of sites n_1	n_2	K_a (M^{-1}) K_1	K_2	Reference
Azosulpha-thiazole	BSA	22	-	1.25×10^5	-	1
Methyl Orange	BSA	22	-	4.9×10^4	-	1
	HSA	2	12	1.44×10^5	2.8×10^3	2
HABA	HSA	1	5	2.07×10^4	1.38×10^3	2
Bromocresol Green	HSA	1.6	4.4	1.0×10^6	2.1×10^4	2
Warfarin	HSA	2	4	9.0×10^4	1.4×10^3	3
Phenprocumon	HSA	2	4	1.2×10^5	3.4×10^3	3
Rose Bengal	BSA	-	-	$1.0 - 6.7 \times 10^4$		10
Rose Bengal	CHT	3	1	1.7×10^5	$.37 \times 10^5$	11
	CHTGA	3	1	3.8×10^5	1.0×10^5	11
Bromophenol Blue	BSA	1	3	1.4×10^7	9.5×10^4	12
Orange I	BSA	16	-	9.7×10^3	-	13

Table 5.2 : Interactions of BSA and Gelonin with PAQ, CPAQ, CMPAQ and RB

Dye	Protein			
	BSA		Gelonin	
	pH			
	7.2	12.3	7.2	12.3
PAQ	+	+	-	-
CPAQ	+	-	-	-
CMPAQ	-	-	-	-
RB	+	+	+	-

+ ⇒ Binding - ⇒ Either no binding or very feeble binding

Table 5.3 : Titration of BSA Against CPAQ Representing λ_{max} and Absorbances

Conc. of Dye ($Mx10^5$)	Conc.of Protein ($Mx10^6$)	λ_{max} (in nm)	A at λ_{max} (Arb.Unit)	A at 482.5 (Arb.Unit)
0.7	0	482.5	0.181	0.181
0.7	700	517.0	0.156	0.102
	0	482.5	1.783	1.783
	2.429	482.5	1.626	1.614
	4.740	483.5	1.550	1.548
	6.951	484.5	1.475	1.469
	9.052	485.0	1.423	1.406
6.998	11.063	486.0	1.379	1.359
	12.986	486.0	1.345	1.327
	14.828	487.0	1.328	1.295
	16.600	488.0	1.309	1.264
	18.293	488.0	1.291	1.240
	19.916	488.9	1.276	1.216

Table 5.4 : Deteremination of Extinction Co-efficient and Calculation of Number of Binding Sites and Binding Constant for BSA-CPAQ system

ε_{free}	ε_{bound}	C_p ($Mx10^6$)	$[L]_B$ ($Mx10^5$)	n	K_a (M^{-1})
25800	14470	2.43-19.9	7.0	6.25	$6.193x10^3$

Table 5.5 : Titration of BSA Against RB Representing λ_{max} and Absorbances

Conc. of Dye ($Mx10^5$)	Conc.of Protein ($Mx10^6$)	λ_{max} (in nm)	A at λ_{max} (Arb.Unit)	A at 548.5 (Arb.Unit)	$[L]_T/C_P$
0.3	0	548.5	.117	.117	0
0.3	186.8	563.0	.154	.069	.016
	0	548.5	.740	.740	0
	.2278	549.0	.633	.641	42.827
.9756	.4448	551.0	.586	.605	21.412
	.6516	552.5	.542	.562	14.276
	.8491	555.0	.514	.525	10.707
	1.0378	557.0	.501	.488	8.565
	1.1602	556.5	.561	.497	8.565
	2.3062	561.5	.623	.552	4.283
	3.4380	563.0	.661	.444	2.855
	4.5561	563.0	.668	.452	2.141
	5.6606	563.0	.668	.461	1.713
.9938	6.7518	563.0	.677	.480	1.428
	7.8299	563.0	.674	.488	1.224
	8.8299	563.0	.672	.499	1.078
	9.9479	563.0	.673	.513	0.952
	10.988	563.0	.665	.517	0.857
	12.016	563.0	.671	.538	0.779
	13.033	563.5	.664	.542	0.714
	16.982	563.0	.657	.549	0.535
	20.755	563	.670	.588	0.428

Table 5.6 : Deteremination of Extinction Co-efficients and Number of Binding Sites for BSA-RB system

ε_{free}	ε_{bound}	C_p ($Mx10^7$)	$[L]_B$ ($Mx10^6$)	n	K_a
87000	30000	2.28-23.06	9.76	3	----
87000	65000	34.38-207.5	9.82		

Table 5.7 : Titration of Gelonin Against RB Representing λ_{max} and Absorbances

Conc. of Dye ($Mx10^5$)	Conc.of Protein ($Mx10^6$)	λ_{max} (in nm)	A at λ_{max} (Arb.Unit)	A at 548.5 (Arb.Unit)
.1244	0	548.5	.107	.107
.1244	101.3	563	.106	.062
	0	548.5	.770	.770
	.812	550	a	.556
	1.586	552.5	a	.493
	2.323	555.5	a	.458
	3.027	557.5	a	.418
.9756	3.70	559.5	a	.406
	4.344	559.5	a	.396
	4.960	560	a	.375
	5.555	560.5	a	.368
	6.163	560.5	a	.376
	6.660	561	a	.362
	7.182	561	a	.349
	7.685	561	a	.342

a These values are found to be .770±.0.002

Table 5.8 : Deteremination of Extinction Co-efficient and Calculation of Number of Binding Sites and Binding Constant for Gelonin-RB system

ε_{free}	ε_{bound}	C_p ($Mx10^{7}$)	$[L]_B$ ($Mx10^{6}$)	n	K_a (M^{-1})
87000	25000	8.12-76.85	9.76	12	$8.93x10^{4}$
				2	$2.99x10^{6}$

Table 5.9: Observed Wavenumbers of Vibrational bands (cm^{-1}) and their assignments in BSA bound CPAQ

Solution			Solid	Assignments
Bound	pH1.0	pH12	(in KBr)	
1684				
1635	1652			
1617	1611	1600	1618	$\nu_{C=O}$ (H-bonded)
1586	1593		1580	$\nu_{Ph-ring}+\nu_{C=C}$(Q-ring)
1563	1564	1563		$\nu_{Ph-ring}$
1543			1546	$\nu_{Ph-ring}$
1494	1501		1491	$\nu_{Ph-ring}$
1457	1456		1452	$\nu_{Ph-ring}$
	1424	1420	1420	$\nu_{N=N}$
		1408		$\nu_{C=N}$
1364	1376	1379	1369	$\nu_{C=N}/\nu_{C-C}$(Q-ring)
	1346	1330	1350	ν_{C-N}
	1290			
1265	1261	1258	1270	ν_{C-C} in plane (H)
1232	1210		1231	ν_{N-N}
1185		1192	1188	$\nu_{Ph-N=}$
		1169		ν_{C-N} (azo)
1149	1151	1143	1149	
1113				
1088	1092	1095		
1062	1050	1054	1066	Ring Modes
1040	1040		1028	
1014		1015		

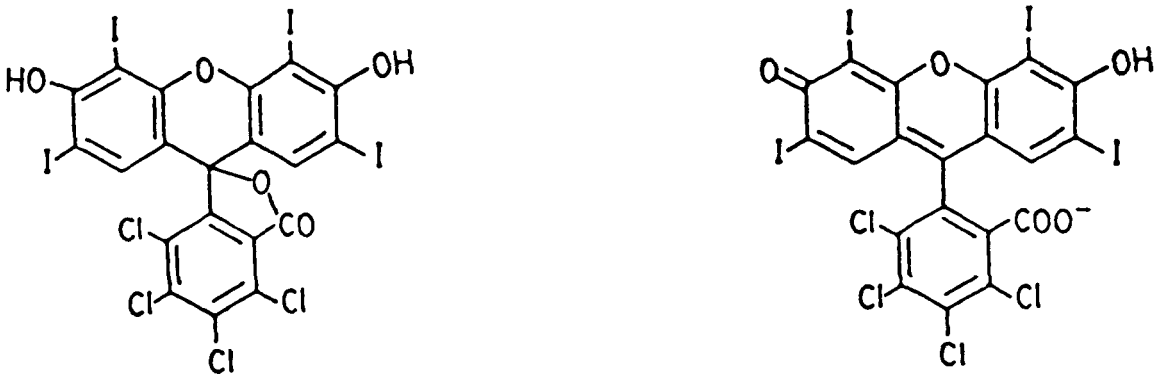

Rose Bengal (RB)

Figure 5.1 Structure of Rose Bengal (a) Lactone Form and (b) Quinoid Form .

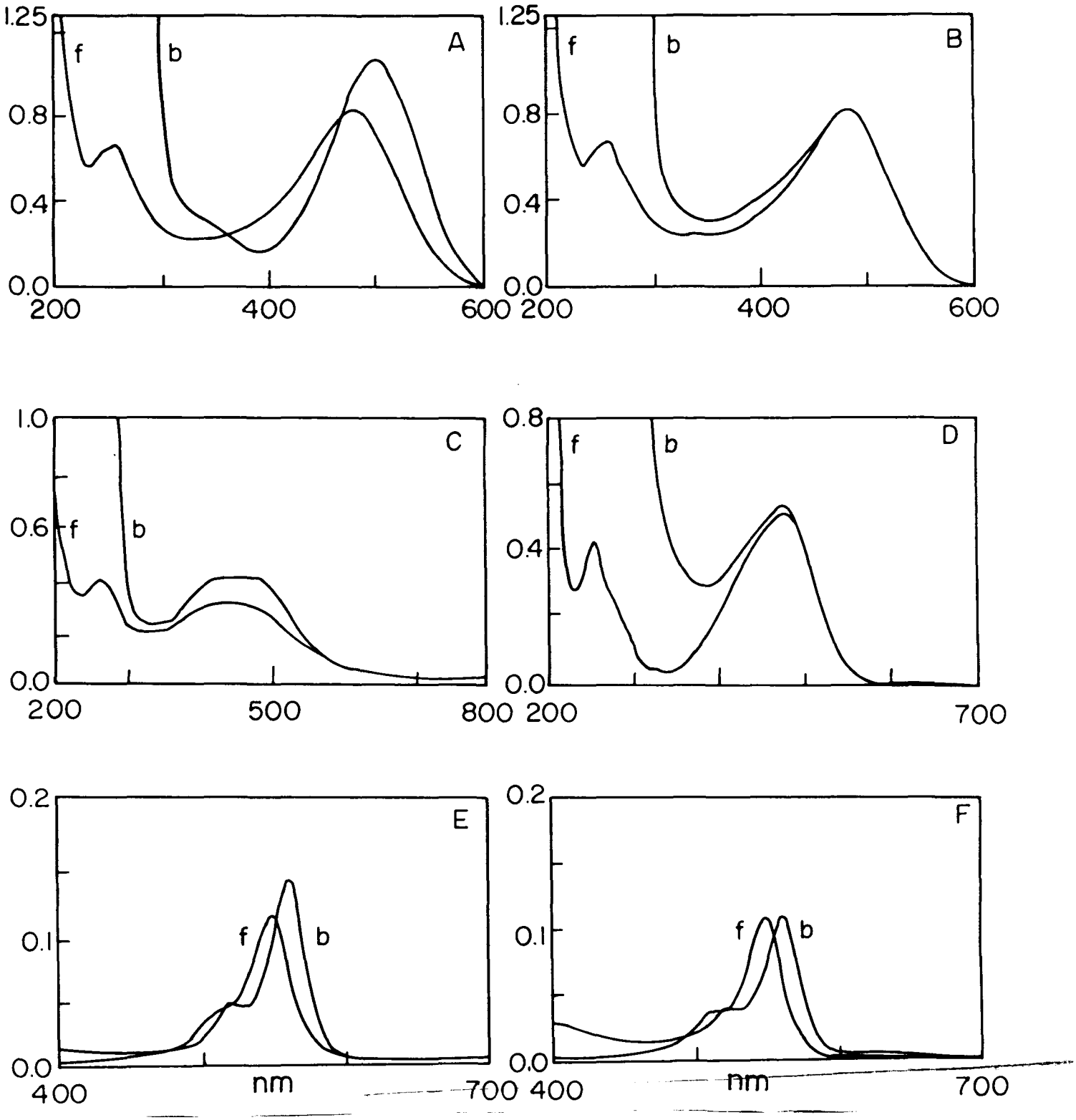

Figure 5.2 Electronic Absorption Spectra of Dye (f) and Dye Protein Mixtures (b). (A) BSA-CPAQ, (B) BSA-PAQ, (C) BSA-CMPAQ, (D) Gelonin-CPAQ, (E) BSA-RB, (F) Gelonin-RB. Concentration of Protein:Concentration of Dye is 100:1. Gelonin-PAQ and Gelonin-CMPAQ Show Similar Pattern as BSA-PAQ and BSA-CMPAQ, respectively.

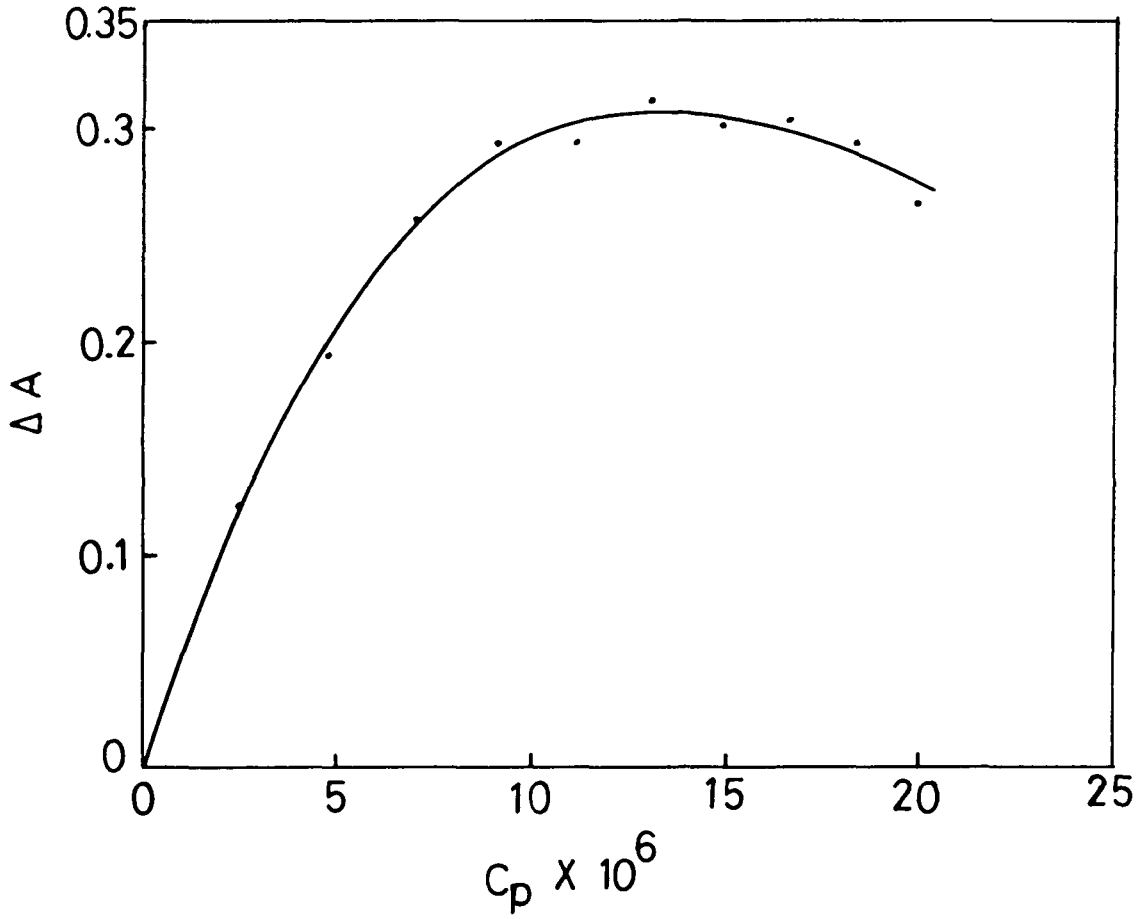

Figure 5.3 Change of Absorbance (Δ A) vs BSA concetration (C_p) (0-19.9 x 10^{-6}M) in BSA-CPAQ Interactions.

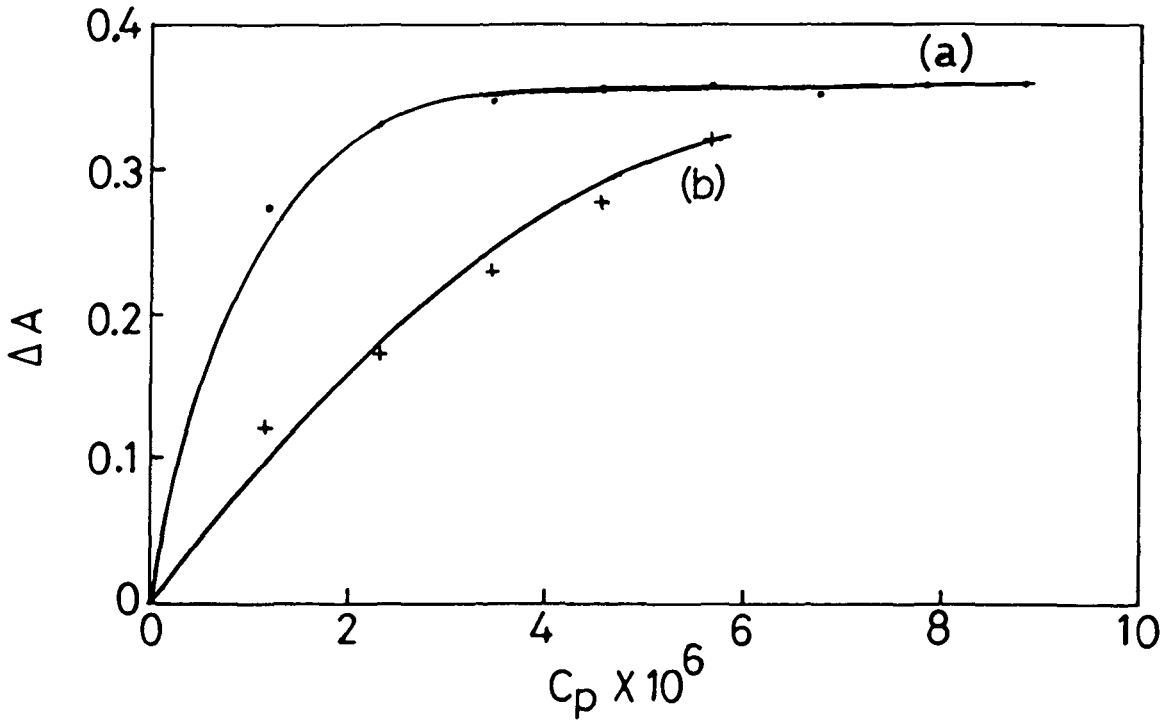

Figure 5.4 Change of Absorbance (Δ A) vs BSA concetration (C_p) in BSA-RB Interactions. (a) BSA concetration 0-1.04 x 10^{-6}M and (b) BSA Concetration 0-8.83 x 10^{-6}M.

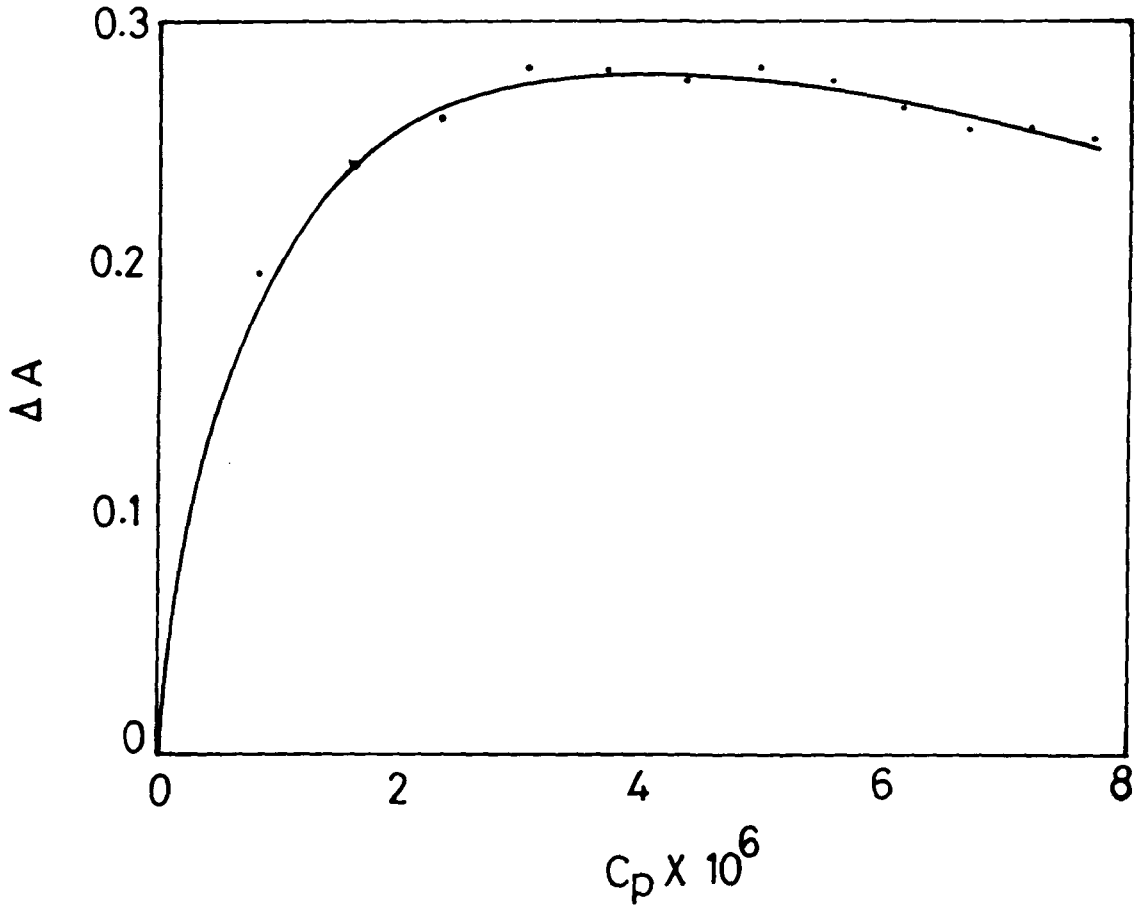

Figure 5.5 Change of Absorbance (Δ A) vs Gelonin concetration (C_p) (0-7.68 x 10^{-6}M) in Gelonin-RB Interactions.

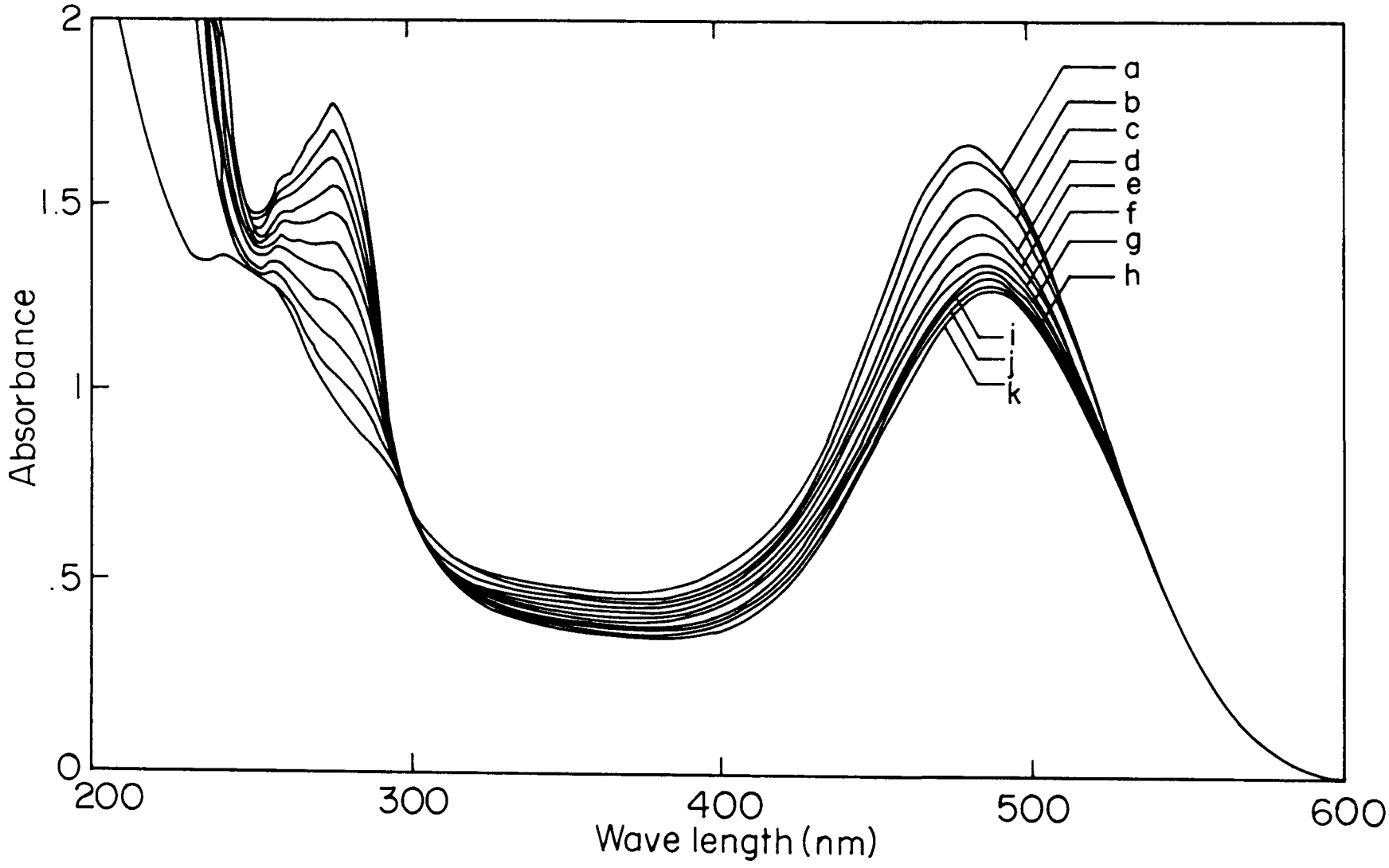

Figure 5.6 Electronic Absorption Sepctra of CPAQ (Concentration 6.99 x 10^{-5}M) Tirated with BSA. Concetration of BSA is (a) Dye only. (b) 2.43 x 10^{-6}M, (c) 4.74 x 10^{-6}M, (d) 6.95 x10^{-6}M, (e) 9.05 x 10^{-6}M, (f) 11.06 x 10^{-6}M, (g) 12.99 x 10^{-6}M, (h) 14.83 x 10^{-6}M, (i) 16.6 x10^{-6}M, (j) 18.29 x 10^{-6}M and (k) 19.9 x 10^{-6}M.

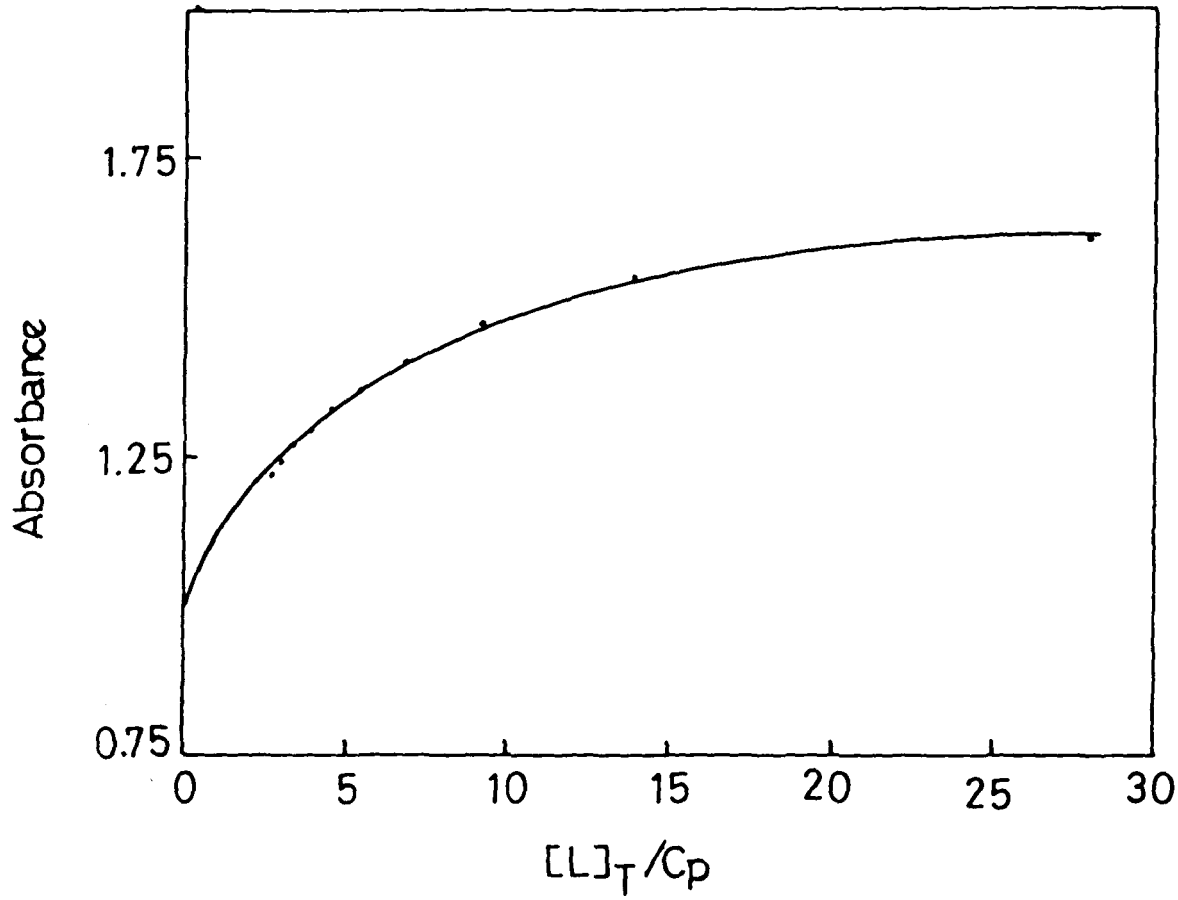

Figure 5.7 Calculation of ε_{bound} of BSA-bound CPAQ. Absorbance vs $[L]_T/C_P$ are Plotted. The Curve is Extrapolated to find the Value of Absorbance at $[L]_T/C_P = 0$), i.e. $C_P = \alpha$. From this value of Aborbance, ε_{bound} is Calculated.

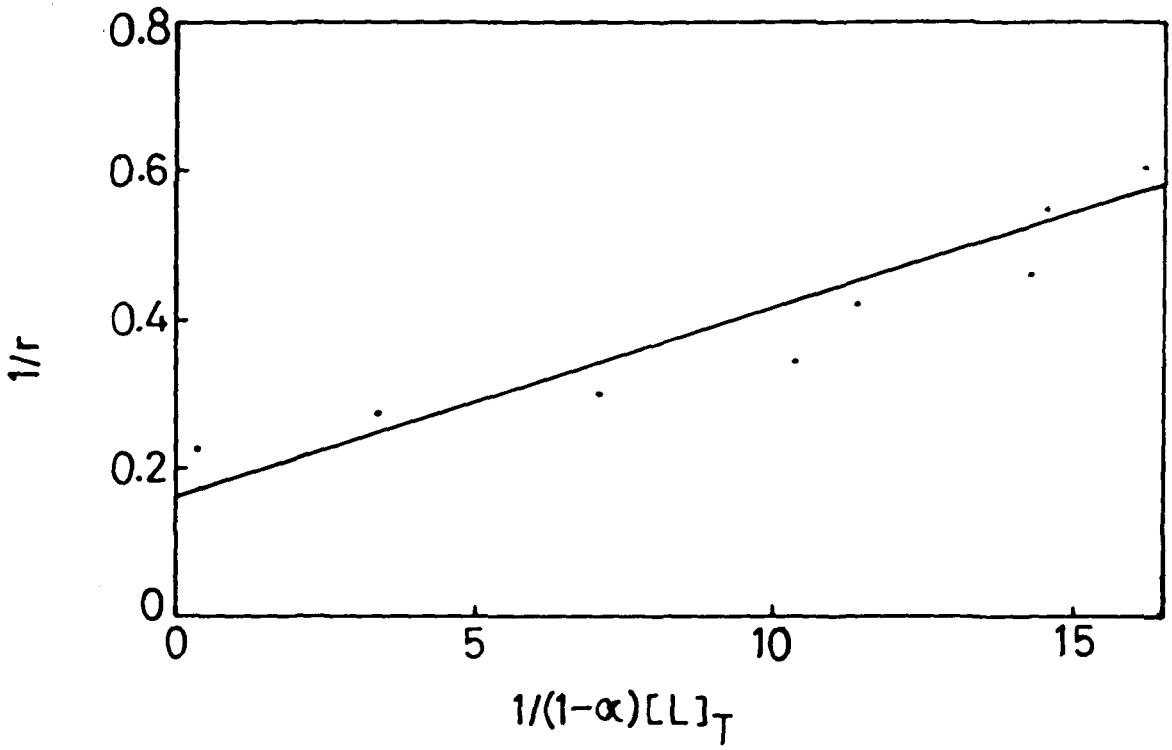

Figure 5.8 Klotz Plot of BSA-CPAQ Interactions. Normalized Values of $1/(1-\alpha)\,[L]_T$ are Plotted. K_a could be Estimated from the Slope and n from the Intercept.

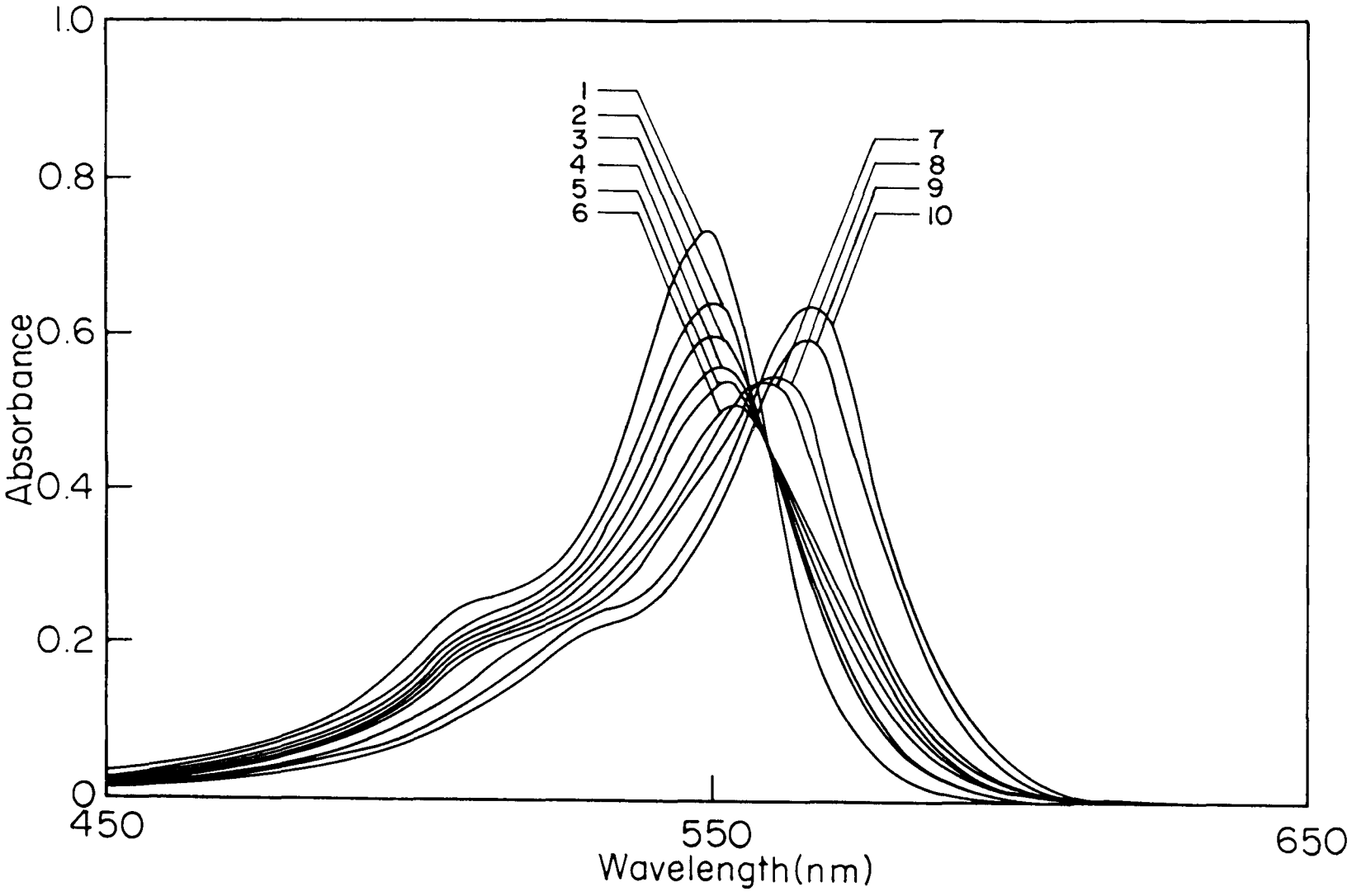

Figure 5.9 Electronic Absorption Sepctra of RB Tirated with BSA. Concetration of RB is 9.76×10^{-6}M for 1-6 and 9.94×10^{-6}M for 7-10. Concetration of BSA is (1) Dye only, (2) 2.28×10^{-7} M, (3) 4.45×10^{-7} M, (4) 6.52×10^{-7} M, (5) 8.49×10^{-7} M, (6) 10.38×10^{-7} M, (7) 11.60×10^{-7} M, (8) 23.06×10^{-7} M, (9) 34.38×10^{-7} M, (10) 45.56×10^{-7} M.

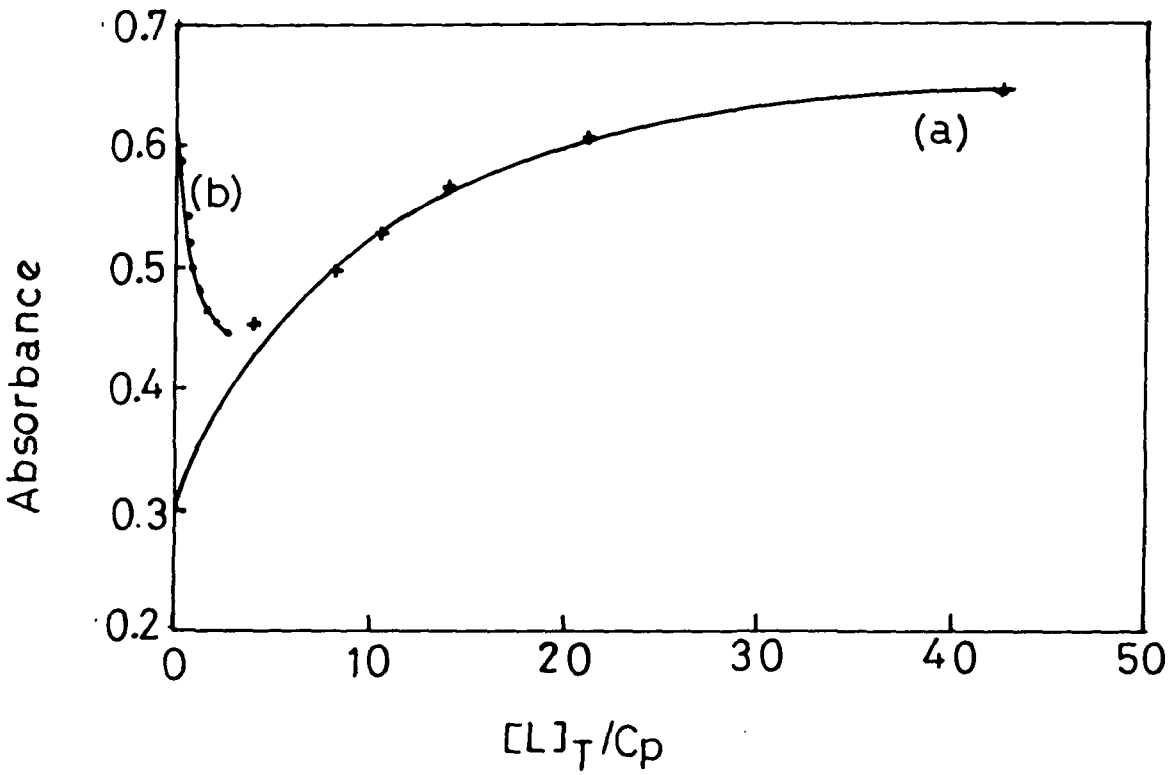

Figure 5.10 Calculation of ε_{bound} of BSA-bound RB. Absorbance vs $[L]_T/C_P$ are Plotted. The Curve is Extrapolated to find the Value of Absorbance at $[L]_T/C_P = 0$), i.e. $C_P = \alpha$. From this value of Aborbance, ε_{bound} is Calculated.

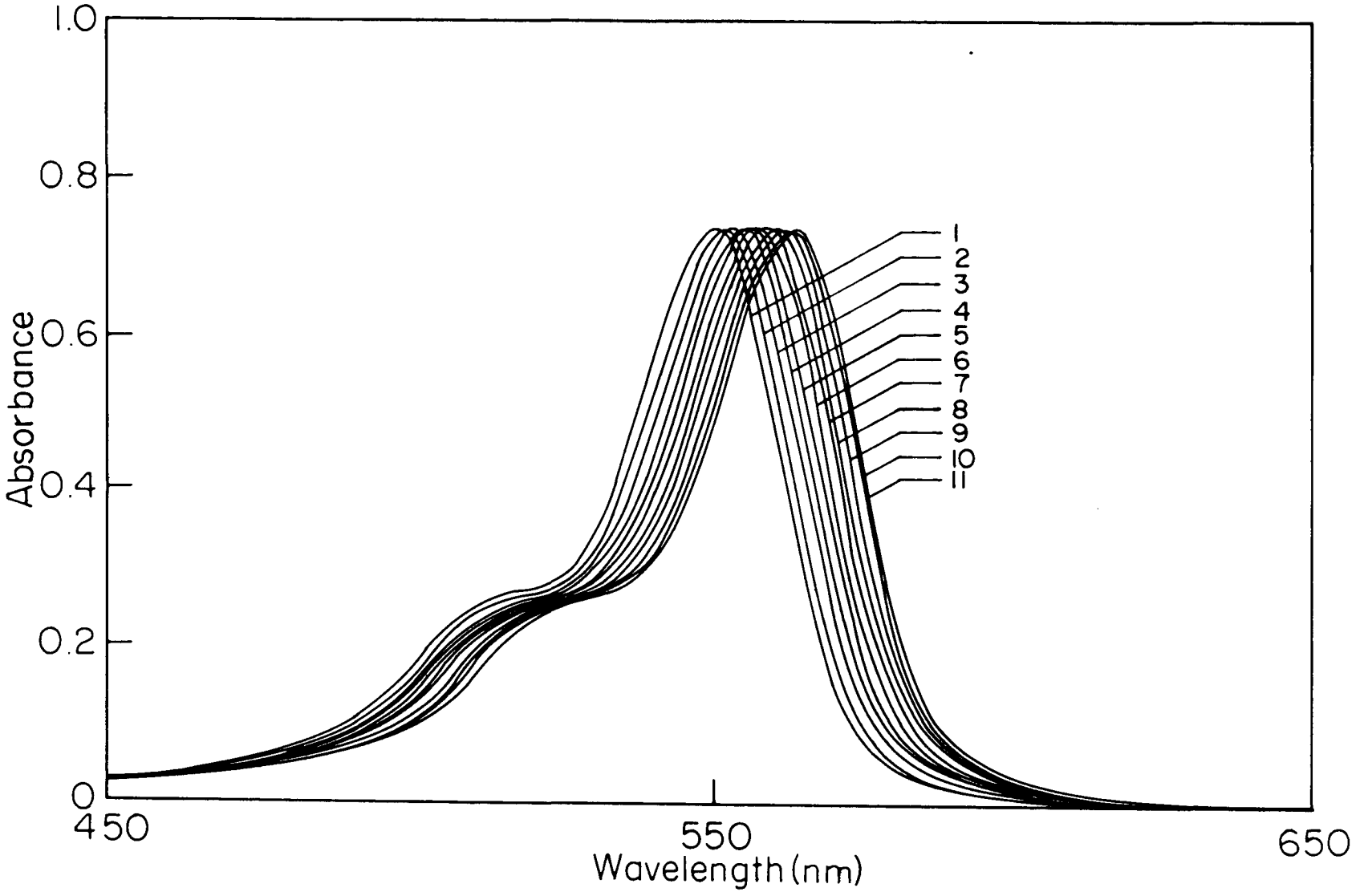

Figure 5.11 Electronic Absorption Spectra of RB (Concentration 9.76 x 10^{-5}M) Titrated with Gelonin. Concetration of Gelonin is (1) Dye only, (2) 0.80 x 10^{-6}M, (3) 1.59 x 10^{-6}M, (4) 2.32 x 10^{-6}M, (5) 3.03 x 10^{-6}M, (6) 3.70 x 10^{-6}M, (7) 4.34 x 10^{-6}M, (8) 4.96 x 10^{-6}M, (9) 5.55 x 10^{-6}M, (10) 6.16 x 10^{-6}M, (11) 6.66 x 10^{-6}M.

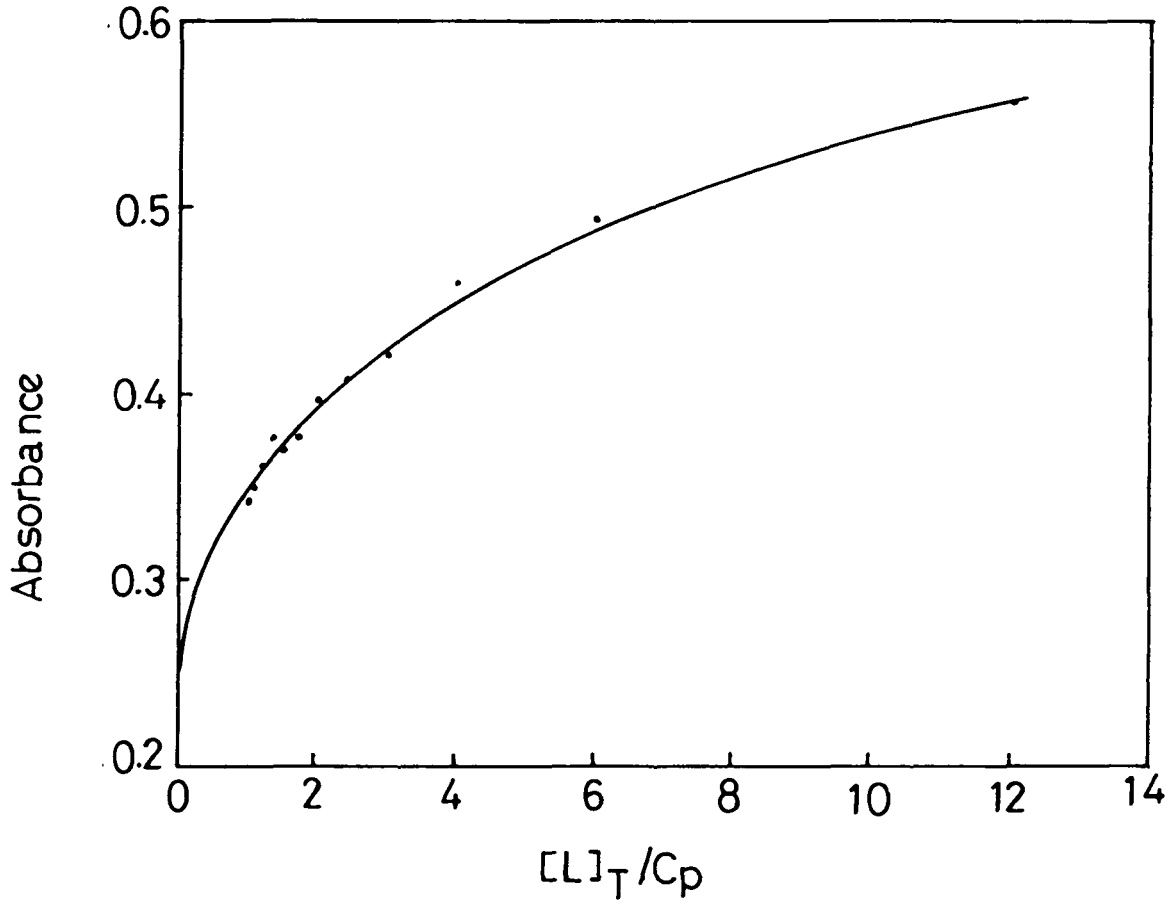

Figure 5.12 Calculation of ε_{bound} of Gelonin - bound RB. Absorbance vs $[L]_T/C_P$ are Plotted. The Curve is Extrapolated to find the Value of Absorbance at $[L]_T/C_P$ = 0), i.e. $C_P = \alpha$. From this value of Aborbance, ε_{bound} is Calculated.

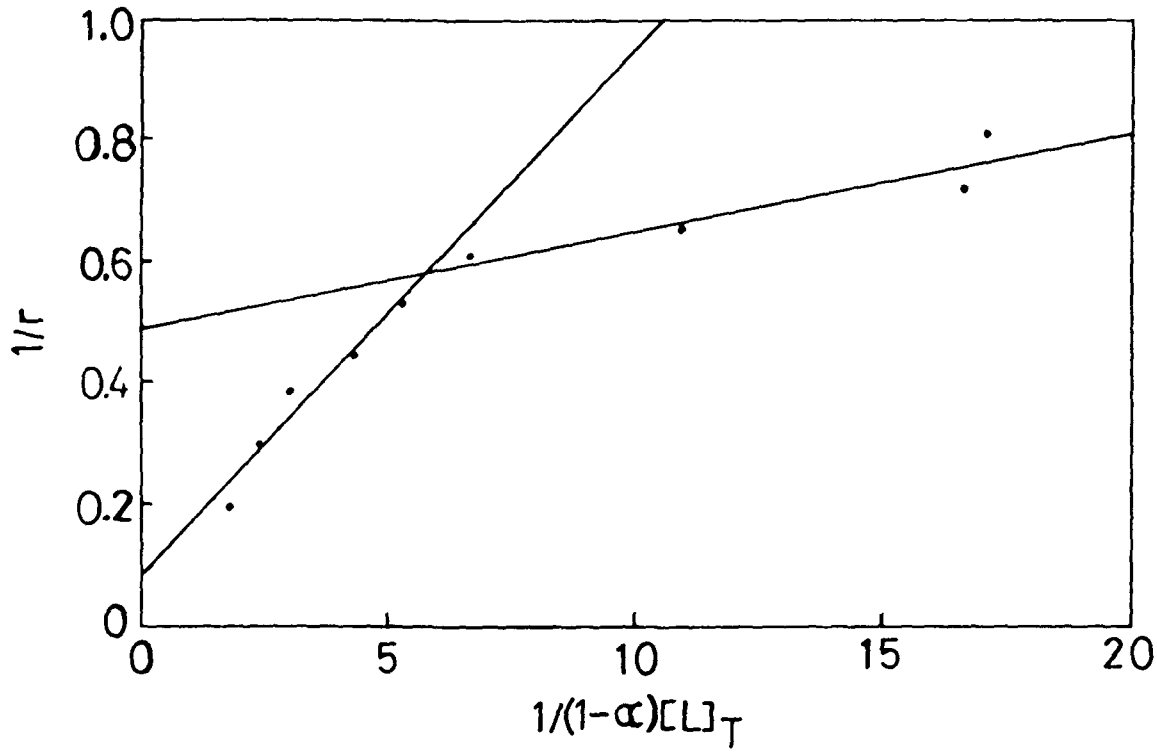

Figure 5.13 Klotz Plot of Gelonin - RB Interactions. Normalized Values of $1/(1-\alpha)\,[L]_T$ are Plotted.Plot Gives Distinct Non - linear Nature and is Well Fitted into Two Components. It give Two Types of Binding Sites as well as Binding Constants (Table 5.8).

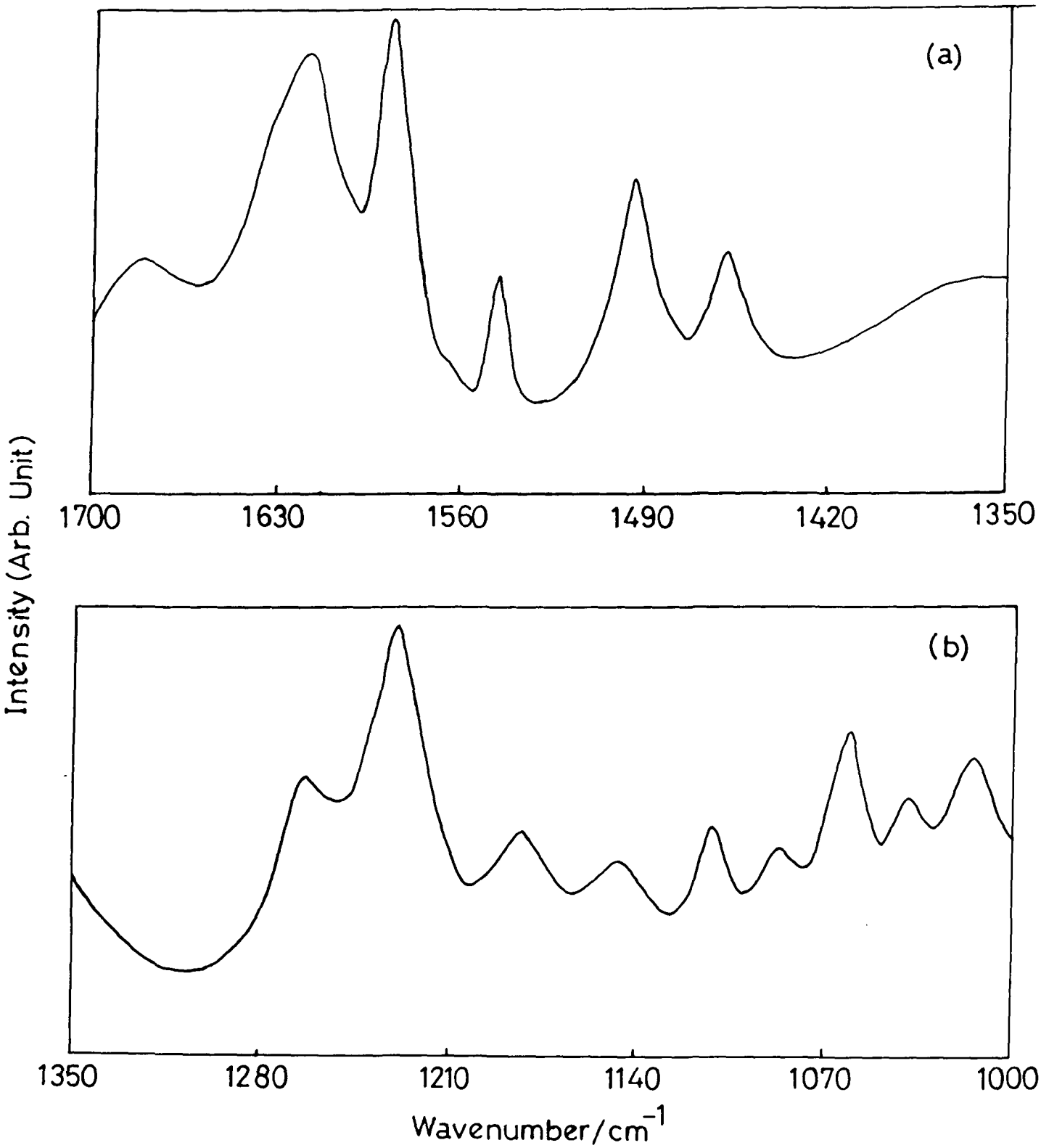

Figure 5.14 Resonance Raman Spectra of BSA Bound CPAQ. (a) 1700 -1350cm^{-1} Region, (b) 1350-1000 cm^{-1} Region.

CHAPTER - VI

SALIENT FEATURES OF THE PRESENT STUDY AND MAJOR CONCLUSIONS

Present work was planned to undertake a systematic study of the determination of secondary structure of a Ribosome Inactivating Protein, Gelonin and Bovine Serum Albumin (BSA) using vibrational spectroscopy as well as to study their binding properties with certain ligands e.g. azo dyes. Various investigators have used vibrational methods to study protein structure quantitatively. However, when these methods are extended to unknown structures, many problems are encountered. We have tried to overcome these difficulties using multiple determination processes. Further, some effects which had been either overlooked in earlier reports or not considered fully have been incorporated. The ligands used are also designed specifically so as to understand the effect of various factors on their structures which are deduced at varied conditions. This is also accomplished with some important aspects of their interactions with proteins. Resonance Raman, FT-IR and electronic spectroscopic results are critically analyzed and structural motifs are confirmed with respect to spectral data to get reliable structural details.

In short in the proposed plan of work, we aimed at achieving the following goals :

(i) to deduce the structural forms and tautomeric equilibria of several specially designed azo dyes (viz. arylazophenols, arylazonaphthols, arylazoquinolinols etc.) under different

conditions (e.g. in solid form, in solutions at various pH etc.) using spectroscopic techniques,

(ii) isolation and spectroscopic characterization of ribosome inactivating protein - Gelonin and estimation of its secondary structure along with BSA as well as study changes occurring under different conditions,

(iii) the nature of protein-azo dye binding of the azo dyes, mainly with Gelonin and BSA.

We have not only been able to achieve these major goals, but also extended our investigation to study the binding of Rose Bengal (RB) with these proteins and deduce the spectral behavior of two crosslinkers SPDP and LC-SPDP.

Thus, the scope of this thesis is not only limited to elucidate the structural aspects of Gelonin and BSA but also extended to their binding properties with various ligands as well as the structure of the ligands using vibrational spectroscopy. BSA has been incorporated for comparison as it is very well studied by various techniques. For the elucidation of binding properties, azo dyes were considered as binding of these systems with proteins and model compounds are widely reported. However, in the course of investigation we found that these dyes do not bind with Gelonin, though they bind with BSA. Thus, another dye RB has also been studied and we could demonstrate that this dye binds with Gelonin as well as with BSA. Further, two crosslinking

agents, which are used for Gelonin conjugate preparation are also studied.

MAJOR CONCLUSIONS OF THE PRESENT STUDY

- Near complete vibrational assignment of the observed bands of BSA and Gelonin are presented.
- Raman, IR and DRIFT study of Gelonin suggest that Gelonin is helix rich proteins with β-sheet and turn structure. It also contains little disorder structure.
- Quantitative methods using Raman and FT-IR spectral data for the secondary structure determination of proteins are presented and used for the proteins studied.
  - Result of the first method (linear regression) matches well with the reported results of BSA. It also matches for Gelonin.
  - Results of the second method (curvefitting) for BSA as well as for Gelonin matches very well with the reported results for BSA and with recently published X-ray crystallographic results for Gelonin (published during the course of this work). BSA contains nearly 50% α-helix and the remaining turn and/or random structure. Gelonin is having nearly 32% α-helix, 20% β-sheet, 26% turn and 22% random structure.

- Gelonin is quite stable at room temperature. Its denaturation temperature is around 60^{o}C.
- Vibrational spectra of crosslinkers SPDP and LC-SPDP are assigned.
- Geometry around the disulfide bond of the crosslinkers are deduced using vibrational correlation tables and confirmed with MNDO calculations. It is found that LC-SPDP experiences less torsion around C-S-S-C skeleton in comparison to SPDP. Difference in bioefficacy of conjugates formed with SPDP and LC-SPDP is correlated with this difference along with spacer arm length difference, reported earlier.
- Solid and solution state vibrational spectra of some hydroxy azo dyes are analyzed.
- It has been shown that in solid state HMPAB, HMPAMB, and HMPACB exist in azo form whereas HNAB, HNAMB and HNACB exist in hydrazone form. It is also concluded that in the solid state the hydroxy group of *o*-hydroxyphenylazo dyes form an intra-molecular hydrogen bond with the distant nitrogen of the azo group to form a stable six membered ring whereas HNAB, HNAMB, HNACB. do not form hydrogen band. Instead, they dominate in hydrazone form giving rise to a quinonoid type of structure at solid state.
- In solid state PAQ and CPAQ exist as a mixture of both the forms with one of the tautomeric form dominating whereas

CMPAQ exist in azo form. PAQ is dominantly in azo form whereas CPAQ is dominantly in hydrazone form.

- Copper complexes of PAQ amd CMPAQ are also studied in solid state which are known to exist in azo form. Spectral data of these compounds are compared with that of PAQ, CPAQ and CMPAQ.
- In solutions, electronic absorption spectroscopy has also been used along with vibrational spectroscopy to deduce the structures and tautomeric equilibria for three azoquinolinol dyes.
- In solution PAQ exists predominantly in azo form in acidic as well as at alkaline pH. Hydroxyl group forms hydrogen bond with the ring nitrogen giving a predominant azo structure.
- In highly acidic solution CPAQ exists predominantly as hydrazone form whereas, at pH above 8 it exists as azo tautomer.
- CMPAQ is dominantly azoic in alkaline pH. As pH goes down the equilibrium shifts towards hydrazone form and at highly acidic solution CMPAQ exists mainly in hydrazone tautomer.
- For both CPAQ and CMPAQ intra-molecular hydrogen bonding involving the hydroxy group and carboxy (CPAQ) or carbomethoxy (CMPAQ) stabilizes the structures.

- In PAQ H-bonding is possible only at the quinolinol moiety forming a five membered ring, whereas in case of CPAQ and CMPAQ there will competition between six-membered H-bonding at the azo group and five membered H-bonding at quinolinol moiety.
- Binding of 5-(2'-carboxyphenyl)azoquinolin-8-ol (CPAQ) and RB has been studied with BSA as well as with Gelonin.
  - BSA has 6 independent binding sites for CPAQ, binding constant is 6.2×10^3 at physiological pH. Number of binding sites as well as binding constants of BSA for RB could not be calculated precisely.
  - Gelonin does not bind with CPAQ.
  - Gelonin binds RB. It is having 12 low affinity sites per molecule having binding constant of 8.9×10^4 and 2 high affinity binding sites, binding constant being 2.99×10^6.
- Assignments of the bound CPAQ are also presented. It is found that bound CPAQ exits exclusively in hydrazone form.
- Azo group nitrogen, adjacent to the phenyl ring probably participates in the formation of the CPAQ-BSA complex.

LIST OF PUBLICATIONS

I. In Journals

1. Structure of some arylazophenols and arylazonaphthols in solid state : A Resonance Raman study.
   P.K. Bajpai, Biswajit Pal and T.S. Basu Baul
   J.Raman Spectrosc. 26, 217 (1995).

2. Structural characterization of some quinolin-8-ol-containing azo dyes in solid and solution state as probed by Resonance Raman, FT-IR and Electronic Spectroscopic techniques.
   P.K. Bajpai, Biswajit Pal and T.S. Basu Baul
   J. Raman Spectrosc. 26, 351 (1995).

3. Vibrational studies on heterobifunctional crosslinking agents N-succinimidyl3-(2-pyridyldithio)propionate and N-succinimidyl 6-[3-(2-pyridyldithio)propionamido]hexanoate and theoretical elucidations.
   Biswajit Pal, P.K. Bajpai Jayati Sengupta and Vinod Singh
   J. Raman Spectrosc. 28 323, 1997.

4. Spectroscopic Characterization of A Protein - Gelonin: Assignments, Secondary Structure and Thermal Denaturation
   Biswajit Pal and P.K.Bajpai
   Indian J. Biochem. Biophys. (Communicated)

II. In Symposia/Conferences :

1. Resonance Raman study of some hydroxy azo dyes in solid state.
   Biswajit Pal, P.K. Bajpai and T.S. Basu Baul
   National Laser Symposium 1994, CAT, Indore, (1994).

2. Spectroscopic studies on heterobifunctional cross-linking agents N-succinimidyl 3-(2-pyridyldithio) propionate and N-succinimidyl 6-[3-(2-pyridyldithio)propionamido]hexanoate.
   Biswajit Pal, P.K. Bajpai and Vinod Singh
   National Laser Symposium 1995, I.R.D.E.,Dehra Dun,(1995).

3. Structure of some 5-(aryl)azo-8-quinolinols : A Resonance Raman Study.
   P.K. Bajpai and Biswajit Pal
   Workshop on Advanced Laser Spectroscopy, IIT, Kanpur, (1995).

4. Determination of Secondary Structure of a Protein - Gelonin
   P.K.Bajpai and Biswajit Pal
   International Seminar-cum-School on Macromolecular Crystallographic Data, SINP, Calcutta, (1995).

5. pH Induced Phase Transition in BSA - A Laser Raman Study
   P.K.Bajpai and Biswajit Pal
   National Laser Symposium 1996, BARC, Bombay, (1996).

6. Temperature Induced Denaturation of a Protein - Gelonin : An Infra Red and Diffused Reflectance Infrared Fourier Transform Study
   Biswajit Pal and P.K.Bajpai
   7th College on Biophysics, ICTP, Trieste, Italy, (1996).

7. Resonance Raman Study of 5(2'-carboxyphenyl)azoquinolin-8-ol in Protein Bound Form
   Biswajit Pal, P.K.Bajpai and T.S.Basu Baul
   National Laser Symposium 1997, CAT, Indore, (1997).